

# **DNA-mediated charge transport signaling within the cell**

Thesis by  
Michael Andrew Grodick

In partial fulfillment of the Requirements for the  
Degree of Doctor of Philosophy



California Institute of Technology  
Division of Chemistry and Chemical Engineering  
Pasadena, CA  
2016

(Defended July 1, 2015)

© 2015

Michael Andrew Grodick

All Rights Reserved

## **Acknowledgements**

Needless to say, I need to start out by thanking my adviser, Jackie Barton, for supporting me throughout my graduate career. Her enthusiasm for science is contagious and helped carry me through the most difficult parts of my education at Caltech. Jackie wants everyone to satisfy their full potential, to dream big, and to succeed. Not only was she an excellent mentor with regards to science, and many other aspects of my life. She always gave me advice on to how I could achieve a better work to life balance and was there for me whenever I needed advice or support. I cannot thank her enough and hope to work with her in the future.

I could not have asked for a better thesis committee. I think most everyone would agree that Harry Gray is one of the most influential scientists at Caltech. I believe that if Harry could have it his way, every student would be enabled to pursue any career that they choose and be successful during their careers. Doug Rees was always a positive force on my committee. During examinations it was clear that Doug wanted to help me succeed and to offer any advice that he could to help with my projects. Dianne Newman was the fourth member of my committee. Dianne was incredibly helpful with my projects as she invited me into her lab and introduced me to the people and resources necessary to learn new interdisciplinary techniques that proved vital to my project. She is constantly striving to improve the experience of not only the students in biology, but also students in labs from across the disciplines, bringing them together in programs like the Center for Environmental Microbial Interactions to jump-start collaborations and new projects based on interdisciplinary themes. Across the board, my committee was supportive and helpful.

I also have to thank all of my friends. During my time at Caltech, some of my best friends from college including Andrew Long, Saager Chekka, Jason Lawrie, Thatcher Houldin, and Alex Dodd kept in close contact with me be it by playing online games together, chatting, or visiting one another. It was important to have people outside of the Caltech community to remind me of what it is like to live outside the walls of Caltech.

I also had the opportunity at Caltech to make many new friends. Some of my closest friends include Seth and Anna Arnold, James Blakemore, and Adam Boynton who all formed the core of my wolf pack. I could almost always count on being able to spend time with at least one of these people on any given night that I felt like hanging out. This group of people helped me grow tremendously as a person as well, offering me advice that has truly impacted my life and who I am as a person. They also were always there to listen. I think it is safe to say that they know more about me than they care to know! Davide Lionetti, Emily Tsui, Kyle Horak, Sandy Suseno, and Guy Eduoard were the crew from the Agapie group that I hung out with extensively, especially during the first few years of my time at Caltech. They are incredibly hard workers and they know how to party just as hard. Ryan Henning, Jacob Kanady, Alex Sutherland, Peter Agbo, Joey Varghese, and Ashwin Ram represented the group of people I most liked to talk with about politics and issues that affect the world. None of them will hold back in an argument and this led to many passion-infused discussions where I almost always walked away learning something and questioning certain aspects of my views. When Andy Zhou joined the lab a few years ago, he and I nearly immediately formed a strong friendship. He is one of the few people I know who shares my extensive love of both games and sushi! Andy was yet another person who was always there for me. I have many other

friends that need to be mentioned including Aaron and Wes Sattler (they tend to be one unit), and some of my newer friends who I am very sad that I will not get to know better including Rebekah Silva, Kelsey Boyle, Sirius Han, and Tonia Ahmed. I am glad that I did not leave Caltech sooner because it has been a pleasure getting to know these people. Lastly, I count everyone in the lab as a friend. The Barton group has been a great place to work and hanging out with all of you was fun. I am sure that I have left out many other comrades from Caltech. You have all been great!!

I need to acknowledge and thank the Barton lab again, this time as co-workers and collaborators. Previous graduate students who helped me get started in the lab and showed me the ropes include Dr. Paul Lee, Dr. Wendy Mercer, Dr. Pamela Sontz, Dr. Eric Olmon, Dr. Tim Mui, Dr. Curtis Schneider, and Dr. Hang Song. I have also had the pleasure of collaborating on projects and manuscripts with Anna Arnold, Rebekah Silva, Catrina Pheaney, Ted Zwang, Helen Segal, Ariel Furst, and Natalie Muren in addition to Janani Comar and Sirius Han who were undergraduates that I mentored through the SURF program at Caltech. Collaborations can be a bit hectic to manage, especially when the people with whom you work are so talented and passionate, but I really enjoyed working with all of you in addition to everyone else in the Barton lab and learning side-by-side with everyone.

The staff at Caltech is really what makes Caltech run. Mo Renta is there for the lab and has been there for me at every turn. Mo absolutely has a colorful personality, which often leads to very interesting discussions! She has a tough, tough job and somehow manages to do it very well day in and day out. She is also incredibly forgiving and I am thankful she has had my back so many times. Amy Woodall-Ojeda is Mo's new

counterpart for Jackie in the chair office, and has been wonderful and is always pleasant to converse with in Crellin. Agnes Tong is an invaluable part of the CCE division. I have no idea how she finishes all of the tasks that are thrown her way and she does it with a smile on her face. Meanwhile, she is an amazing advocate for the graduate students and makes sure to watch out for all of us at every turn. Others in the division that help to manage everything from scheduling to running and repairing equipment to keeping the stock rooms running include Margot Hoyt, Anne Penney, Tom Dunn, Jeff Groseth, Mona Shangholi, Angelo Di Bilio, and Cora Carriedo. These people in addition to the maintenance and facilities staff have been integral to keeping everything running smoothly at Caltech during my time here.

I need to thank the many mentors that I have had in my life that helped lead me to Caltech and pursue a graduate education in Chemistry. Mr. Jasperse, Mr. VonEhr, Mr. Scholten, Mrs. Richards, and Mrs. Andre were the teachers that I count to be the most important during my time in elementary, middle, and high school. They taught me some of the most fundamental things about not only science, but also about life and learning. In college, Prof. Protasiewicz was an amazing mentor who helped to inform me about the possibilities and opportunities that existed beyond getting a chemistry degree, which helped me immensely in making the choice to go to graduate school, which he fully supported and encouraged. Dr. Xiaolong Wang and Dr. Naresh Nayyar were the most important academic advisers that I had and were the ones who taught me about how to conduct science and chemistry within a laboratory setting. Without all of these mentors, I would not have made it to Caltech.

Last and not least I need to thank my family. I have one of the most loving, supportive, and helpful families around. My mother and father are the most important people in my life. They taught me so much about the world. The importance of education was instilled in me by my parents at an early age. They also gave me countless opportunities to thrive whether it be related to education, traveling the world and learning about other cultures, or just plain having a good time. My siblings are all older than me and for that, I am so grateful! They were the trail blazers in the family and paved a path for me that was easy to travel. As role models, they all left large shoes to fill. They also taught me about friendship and how to succeed in life, just as they have all succeeded in life. The rest of my family including my aunts, uncles, grandparents, cousins, and everyone else are also wonderful! I actually look forward to family reunions, and many of you have played much more important roles in my life than you know. I love you all.

## Abstract

DNA possesses the curious ability to conduct charge longitudinally through the  $\pi$ -stacked base pairs that reside within the interior of the double helix. The rate of charge transport (CT) through DNA has a shallow distance dependence. DNA CT can occur over at least 34 nm, a very long molecular distance. Lastly, DNA CT is exquisitely sensitive to disruptions, such as DNA damage, that affect the dynamics of base-pair stacking. Many DNA repair and DNA-processing enzymes are being found to contain 4Fe-4S clusters. These co-factors have been found in glycosylases, helicases, helicase-nucleases, and even enzymes such as DNA polymerase, RNA polymerase, and primase across the phylogeny. The role of these clusters in these enzymes has remained elusive. Generally, iron-sulfur clusters serve redox roles in nature since, formally, the cluster can exist in multiple oxidation states that can be accessed within a biological context. Taken together, these facts were used as a foundation for the hypothesis that DNA-binding proteins with 4Fe-4S clusters utilize DNA-mediated CT as a means to signal one another to scan the genome as a first step in locating the subtle damage that occurs within a sea of undamaged bases within cells.

Herein we describe a role for 4Fe-4S clusters in DNA-mediated charge transport signaling among EndoIII, MutY, and DinG, which are from distinct repair pathways in *E. coli*. The DinG helicase is an ATP-dependent helicase that contains a 4Fe-4S cluster. To study the DNA-bound redox properties of DinG, DNA-modified electrochemistry was used to show that the 4Fe-4S cluster of DNA-bound DinG is redox-active at cellular potentials, and shares the 80 mV vs. NHE redox potential of EndoIII and MutY. ATP hydrolysis by DinG increases the DNA-mediated redox signal observed

electrochemically, likely reflecting better coupling of the 4Fe-4S cluster to DNA while DinG unwinds DNA, which could have interesting biological implications. Atomic force microscopy experiments demonstrate that DinG and EndoIII cooperate at long range using DNA charge transport to redistribute to regions of DNA damage. Genetics experiments, moreover, reveal that this DNA-mediated signaling among proteins also occurs within the cell and, remarkably, is required for cellular viability under conditions of stress. Knocking out DinG in CC104 cells leads to a decrease in MutY activity that is rescued by EndoIII D138A, but not EndoIII Y82A. DinG, thus, appears to help MutY find its substrate using DNA-mediated CT, but do MutY or EndoIII aid DinG in a similar way? The InvA strain of bacteria was used to observe DinG activity, since DinG activity is required within InvA to maintain normal growth. Silencing the gene encoding EndoIII in InvA results in a significant growth defect that is rescued by the overexpression of RNaseH, a protein that dismantles the substrate of DinG, R-loops. This establishes signaling between DinG and EndoIII. Furthermore, rescue of this growth defect by the expression of EndoIII D138A, the catalytically inactive but CT-proficient mutant of EndoIII, is also observed, but expression of EndoIII Y82A, which is CT-deficient but enzymatically active, does not rescue growth. These results provide strong evidence that DinG and EndoIII utilize DNA-mediated signaling to process DNA damage. This work thus expands the scope of DNA-mediated signaling within the cell, as it indicates that DNA-mediated signaling facilitates the activities of DNA repair enzymes across the genome, even for proteins from distinct repair pathways.

In separate work presented here, it is shown that the UvrC protein from *E. coli* contains a hitherto undiscovered 4Fe-4S cluster. A broad shoulder at 410 nm,

characteristic of 4Fe-4S clusters, is observed in the UV-visible absorbance spectrum of UvrC. Electron paramagnetic resonance spectroscopy of UvrC incubated with sodium dithionite, reveals a spectrum with the signature features of a reduced,  $[4\text{Fe-4S}]^{+1}$ , cluster. DNA-modified electrodes were used to show that UvrC has the same DNA-bound redox potential, of  $\sim 80$  mV vs. NHE, as EndoIII, DinG, and MutY. Again, this means that these proteins are capable of performing inter-protein electron transfer reactions. Does UvrC use DNA-mediated signaling to facilitate the repair of its substrates?

UvrC is part of the nucleotide excision repair (NER) pathway in *E. coli* and is the protein within the pathway that performs the chemistry required to repair bulky DNA lesions, such as cyclopyrimidine dimers, that form as a product of UV irradiation. We tested if UvrC utilizes DNA-mediated signaling to facilitate the efficient repair of UV-induced DNA damage products by helping UvrC locate DNA damage. The UV sensitivity of *E. coli* cells lacking DinG, a putative signaling partner of UvrC, was examined. Knocking out DinG in *E. coli* leads to a sensitivity of the cells to UV irradiation. A 5-10 fold reduction in the amount of cells that survive after irradiation with  $90 \text{ J/m}^2$  of UV light is observed. This is consistent with the hypothesis that UvrC and DinG are signaling partners, but is this signaling due to DNA-mediated CT? Complementing the knockout cells with EndoIII D138A, which can also serve as a DNA CT signaling partner, rescues cells lacking DinG from UV irradiation, while complementing the cells with EndoIII Y82A shows no rescue of viability. These results indicate that there is cross-talk between the NER pathway and DinG via DNA-mediated signaling. Perhaps more importantly, this work also establishes that DinG, EndoIII, MutY, and UvrC comprise a signaling network that seems to be unified by the ability of

these proteins to perform long range DNA-mediated CT signaling via their 4Fe-4S clusters.

## Table of Contents

Acknowledgements .....	iii
Abstract.....	vii
Table of Contents.....	xii
List of Figures.....	xiv
List of Tables .....	xvi
<b>Chapter 1. DNA Charge Transport within the Cell .....</b>	<b>1</b>
<b>Introduction .....</b>	<b>2</b>
<b>Platforms to Study the Characteristic Features of DNA CT.....</b>	<b>3</b>
<b>General Observations of DNA CT in Biological Systems .....</b>	<b>11</b>
<b>Prospectus.....</b>	<b>28</b>
<b>Chapter 2. DNA-Mediated Signaling by Proteins with 4Fe-4S Clusters is Necessary for Genomic Integrity .....</b>	<b>38</b>
<b>Introduction .....</b>	<b>39</b>
<b>Materials and Methods .....</b>	<b>41</b>
<b>Results and Discussion .....</b>	<b>62</b>
DNA binding activates DinG towards reduction and oxidation at cellular redox potentials .....	62
EndoIII and DinG use DNA CT to redistribute to sites of damage .....	62
DinG uses DNA-mediated CT to facilitate the repair of damage by MutY.....	67
The repair of R-loops by DinG relies on DNA-mediated signaling by EndoIII in InvA .....	69
<b>Conclusion .....</b>	<b>79</b>
<b>Chapter 3. UvrC contains a 4Fe-4S cluster that is utilized in DNA-mediated signaling .....</b>	<b>86</b>
<b>Introduction .....</b>	<b>87</b>
<b>Materials and Methods .....</b>	<b>90</b>
<b>Results and Discussion .....</b>	<b>99</b>
UvrC contains a 4Fe-4S cluster.....	99
UvrC is redox-active when bound to DNA and shares a redox potential with other DNA-processing enzymes that contain 4Fe-4S clusters .....	102
DNA-mediated signaling within <i>E. coli</i> is required for efficient repair by UvrC....	107
<b>Conclusion .....</b>	<b>113</b>
<b>Chapter 4. Summary and Perspectives.....</b>	<b>121</b>

<b>Appendix I. Multiplexed Electrochemistry of DNA-bound Metalloproteins .....</b>	<b>128</b>
<b>Introduction .....</b>	<b>129</b>
<b>Materials and Methods .....</b>	<b>132</b>
<b>Results.....</b>	<b>140</b>
<b>Discussion .....</b>	<b>156</b>
<b>Conclusion .....</b>	<b>164</b>

## List of Figures

### Chapter 1.

1.1 Measuring DNA CT with metal complexes .....	5
1.2 Measuring DNA CT in single molecules .....	7
1.3 Measuring DNA CT with DNA-modified electrodes.....	8
1.4 Initial experiments to probe DNA CT in biology.....	12
1.5 Electrochemistry of DNA glycosylases on DNA-modified electrodes .....	17
1.6 Model for the enhanced DNA lesion search efficiency of DNA repair proteins with 4Fe-4S by DNA CT signaling.....	19
1.7 AFM reveals that CT proficiency determines whether proteins localize near DNA mismatches.....	21

### Chapter 2.

2.1 SDS-PAGE gel for purification of DinG.....	48
2.2 Statistical data for the AFM experiments .....	53
2.3 Occupancy of DinG on long strands of DNA.....	55
2.4 Occupancy of either EndoIII and DinG or EndoIII Y82A and DinG on long strands of well-matched DNA .....	56
2.5 Electrochemistry of DinG on DNA-modified electrodes .....	63
2.6 AFM redistribution assay .....	65
2.7 Rescue of growth defect conferred by knocking out <i>nth</i> in InvA .....	72
2.8 Effect of <i>nth</i> deletion in InvA (InvA $\Delta nth$ ) .....	73
2.9 Scheme depicting how repair proteins may use DNA-mediated signaling to search for damage .....	74

### Chapter 3.

3.1 SDS-PAGE of MBP-UvrC purification .....	95
3.2 UV-visible absorbance spectrum of MBP-UvrC.....	101

<b>3.3</b> EPR spectrum of MBP-UvrC and dithionite .....	<b>103</b>
<b>3.4</b> EPR spectrum of MBP-UvrC .....	<b>104</b>
<b>3.5</b> Cyclic voltammetry of MBP-UvrC .....	<b>105</b>
<b>3.6</b> Model for redistribution of DNA repair proteins to sites of damage .....	<b>108</b>
<b>3.7</b> Diagram depicting signaling among DNA repair proteins containing 4Fe-4S clusters .....	<b>110</b>
<b>3.8</b> UV-sensitivity assay .....	<b>111</b>

## **Appendix I.**

<b>A1.1</b> Schematic depicting the versatility of multiplexed analysis for the investigation of metalloprotein electrochemistry .....	<b>131</b>
<b>A1.2</b> Enzymatic assay for EndoIII glycosylase activity .....	<b>137</b>
<b>A1.3</b> Consistency of DNA-modified electrodes .....	<b>142</b>
<b>A1.4</b> Cyclic voltammetry of EndoIII as a function of gasket thickness .....	<b>143</b>
<b>A1.5</b> The electrochemistry of EndoIII on DNA-modified electrodes was determined as a function of the underlying DNA film morphology .....	<b>145</b>
<b>A1.6</b> The degree of signal attenuation induced by a single perturbation to the $\pi$ -stack, for both closely and loosely packed DNA monolayers, was investigated.....	<b>147</b>
<b>A1.7</b> Kinetic analysis of the signal generated from EndoIII on differing DNA film morphologies .....	<b>149</b>
<b>A1.8</b> Signal accumulation of EndoIII as a function of time on both closely and loosely packed monolayers .....	<b>151</b>
<b>A1.9</b> Comparison of the electrochemical properties and stability of wild type EndoIII and a Y82A mutant.....	<b>153</b>
<b>A1.10</b> Electrochemical and stability comparison of a new family of electrostatic EndoIII mutations .....	<b>155</b>
<b>A1.11</b> Electrochemical stability of EndoIII mutants .....	<b>157</b>
<b>A1.12</b> Crystal structure of EndoIII with the location of mutations shown.....	<b>163</b>

## List of Tables

### Chapter 1.

1.1 DNA-processing enzymes containing 4Fe-4S clusters .....	26
---	----

### Chapter 2.

2.1 Oligonucleotides for electrochemistry substrates, gene replacements, sequencing, or colony PCR, and site-directed mutagenesis .....	42
2.2 Plasmids used for DinG experiments .....	44
2.3 Strains used in DinG experiments .....	45
2.4 MutY activity assay .....	68

### Chapter 3.

3.1 Oligonucleotides for electrochemistry substrates, gene replacements, sequencing, or colony PCR, and site-directed mutagenesis .....	91
3.2 Plasmids used for UvrC experiments .....	92

### Appendix I.

A1.1 Primer Sequences for site-directed mutagenesis .....	134
---	-----

*Chapter 1*

## **DNA Charge Transport within the Cell**

Adapted from: Grodick, M. A, Muren, N. B. & Barton, J. K. *Biochemistry* **54**, 962-973 (2015).

## Introduction

Our laboratory has focused on studies of DNA-mediated charge transport (CT). This chemistry offers a means to carry out redox chemistry at a distance and provides a sensitive reporter on the integrity of the intervening DNA. In photophysical, biochemical, and electrochemical experiments, general features of this chemistry have been elucidated. Perhaps uniquely, DNA CT can occur by transport through the base pair stack over long molecular distances. But importantly, this long distance redox chemistry can only occur if the DNA helix is well stacked; anything that interrupts that stacking turns off CT. Thus the chemistry offers a means to effect long range redox signaling as long as the integrity of the DNA duplex is intact. An array of reviews discussing the mechanistic details of DNA CT can be found in the literature.<sup>1-4</sup> The uniqueness of this chemistry thus begs the question: is DNA CT utilized within the cell?

Studies to probe how this chemistry may be utilized within the cell are now being explored. DNA CT chemistry is important to consider in the context of how DNA may be damaged under conditions of oxidative stress, and how that damage is sensed and repaired is described. Increasingly, proteins involved in DNA processing have been found to contain 4Fe-4S clusters, cofactors generally thought to carry out redox reactions within the cell. Moreover DNA CT can promote redox chemistry over long molecular distances, potentially providing a means for signaling across the genome. Furthermore, because DNA CT reports on the integrity of the DNA duplex, this signaling can reflect whether the intervening DNA is damaged and in need of repair, and whether DNA processing needs to begin, to be stalled, or to be increased. To begin, different experiments that have been used to elucidate DNA CT chemistry are discussed. What are

the characteristic features of DNA CT? Within that framework, experiments carried out on DNA-binding proteins to explore how this chemistry may be utilized are introduced. The experiments described are intended to illustrate DNA CT chemistry and particularly a role for proteins containing 4Fe-4S clusters in carrying out signaling using this chemistry. These studies thus present a framework for considering how DNA CT may be used for genomic signaling and how this framework was used as a basis for the work presented within this thesis.

## **Platforms to Study the Characteristic Features of DNA CT**

The conductivity of DNA arises most fundamentally from its continuous,  $\pi$ -stacked core of aromatic bases that extends down the helical axis. In fact, this conductivity was first predicted from early DNA structural studies which revealed striking similarities to sheets of graphite, both in  $\pi$ -stacking and interplanar spacing.<sup>5</sup> However, unlike graphite and other  $\pi$ -stacked solids, DNA is a dynamic, macromolecular array that functions in solution. This critical difference gives rise to several defining characteristics of DNA CT, and thus studies to probe this chemistry must be performed using platforms with aqueous conditions in which the dynamic motions of the DNA bases are unrestricted. In our laboratory we have established three such general platforms to study DNA CT in DNA duplexes from different vantage points: free in solution, tethered to electrode surfaces, and as single molecules.<sup>2</sup> Across these platforms several essential, conserved features of this chemistry have been observed: (i) electronic coupling of the donor and acceptor to the DNA  $\pi$ -stack is required; (ii) even slight disruptions to the DNA  $\pi$ -stack between the donor and acceptor inhibit DNA CT; and (iii) the distance

dependence of DNA CT is very shallow. Here the platforms and fundamental studies that revealed these characteristics and that are critical for DNA CT in biological systems are briefly summarized.

Given the need for aqueous conditions to make biologically relevant measurements of DNA CT, the first experiments to probe this chemistry were performed with free DNA duplexes in solution containing pendant redox donors and acceptors. In one such construct, the metallointercalators  $\text{Ru}(\text{phen})_2\text{dppz}^{2+}$  (phen = 1,10-phenanthroline, dppz = dipyrido[3,2-*a*:2',3'-*c*]phenazine) and  $\text{Rh}(\text{phi})_2\text{phen}^{3+}$  (phi = 9,10-phenanthrenequinone diimine) were covalently attached to either ends of a 15-mer DNA duplex as donor and acceptor handles, respectively (Figure 1.1).<sup>6</sup> Photoexcitation of the donor results in luminescence that is rapidly quenched by the acceptor via DNA CT. Importantly, coupling of the donor and acceptor to the DNA  $\pi$ -stack is essential for this chemistry to proceed; substitution of  $\text{Ru}(\text{phen})_2(\text{phen}')^{2+}$  (phen' = 5-amido-glutaric-acid-1,10-phenanthroline), a poor DNA intercalator, inhibits quenching.

Similar results were obtained with a more native construct in which fluorescence quenching of adenine base analogs by guanine allows for direct, base-to-base measurements of DNA CT.<sup>7</sup> In these experiments, for which the base analogs 2-aminopurine ( $\text{A}_2$ ) or 1, $\text{N}^6$ -ethenoadenine ( $\text{A}_e$ ) were incorporated into 12-mer DNA duplexes, quenching of  $\text{A}_2$  occurs far more rapidly and over longer distances than quenching of  $\text{A}_e$ . This result is consistent with the different structures of these analogs that allow for well integrated stacking of  $\text{A}_2$  into the DNA helix and poor stacking of  $\text{A}_e$ . Beyond the importance of electronic coupling to the  $\pi$ -stack to participate in DNA CT,

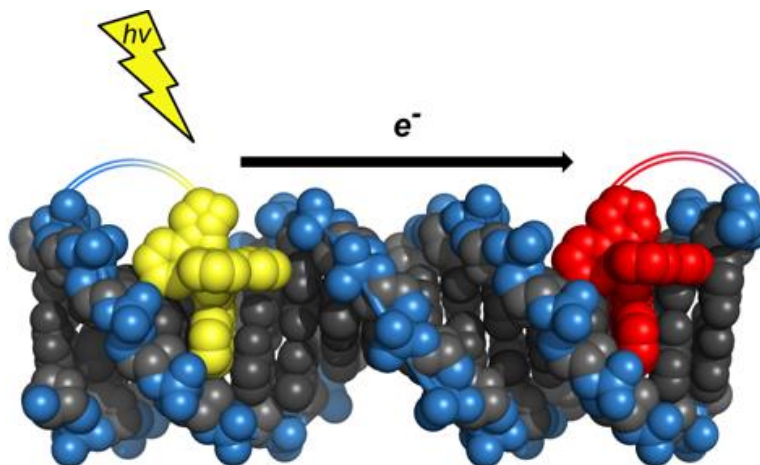


**Figure 1.1** Measuring DNA CT with metal complexes. Shown is a characteristic DNA assembly used to monitor DNA-mediated redox chemistry in solution, using metallointercalators to monitor luminescence quenching by electron transfer through the DNA base stack.<sup>6</sup>

solution-based platforms also provided the first indication of the exquisite sensitivity of this chemistry to perturbations along the  $\pi$ -stacked path; the introduction of even a single base mismatch between the donor and acceptor severely decreases the quenching yield.<sup>8</sup> Studies of base-base CT also taught us important lessons about the timescales and dynamics of DNA CT. DNA CT occurs on the picosecond timescale but is gated by the motions of the bases.<sup>9</sup>

In order to relate these observations more directly to DNA CT in biological systems, it was necessary to design platforms that allow ground state measurements of DNA CT, while still maintaining the DNA in an aqueous, buffered environment. In one such platform, a single DNA duplex is made to covalently span an etched gap in a carbon nanotube circuit.<sup>10</sup> Current flow through this device reports directly on DNA CT efficiency (Figure 1.2). By cycling the type of DNA incorporated into the device from well-matched DNA to DNA with a single base mismatch to well-matched DNA again, current flow is turned on, then off, and then on again, respectively. This ground state, single molecule platform provides more direct measurements of DNA CT and confirms the high sensitivity of this chemistry to even minor structural disruptions of the  $\pi$ -stack.

In a second ground state platform, DNA functionalized with an alkanethiol linker is allowed to self-assemble vertically as a film on a gold electrode surface (Figure 1.3). These DNA-modified electrodes can then be used to monitor DNA CT electrochemically between the electrode and a redox-active probe molecule bound at the distal end of the DNA.<sup>11,12</sup> Taking advantage of the inherent capacity of electrochemistry for multiplexing, 16-electrode chips to facilitate side-by-side analysis of multiple samples and controls were developed, thereby opening the door for even more complex

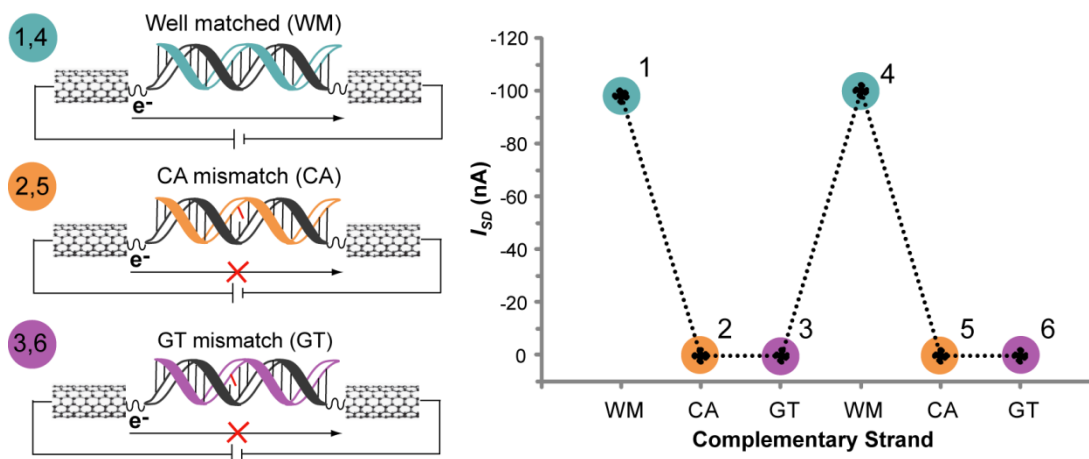


**Figure 1.2** Measuring DNA CT in single molecules. A single DNA duplex is made to covalently bridge a gap in an electronically wired, carbon nanotube device such that the measured current flow through the device reflects DNA CT efficiency.<sup>10</sup> To confirm that charge flow through the device is DNA-mediated and to illustrate the sensitivity of DNA CT to single base mismatches, an experiment was designed to allow the introduction of a single base mismatch through thermal dehybridization and rehybridization of the bridging duplex (left). One strand of the DNA duplex is covalently attached at either side of the gap (grey), while the other, noncovalent strand is cycled between a well-matched strand (blue) and strands with a single base mismatch (orange, purple) by sequential dehybridization, rinsing, and rehybridization. During this cycling between well-matched and mismatched duplexes, the source-drain current ( $I_{SD}$ ) for the device was measured at a constant gating voltage ( $V_G = -3V$ ) and plotted for each bridging duplex (right plot, where the colors and numbers of the duplexes in the left illustration correspond to those on the plot). This experiment clearly illustrates the high sensitivity of DNA CT to single base mismatches; DNA CT is inhibited when the device is bridged with a mismatched duplex and restored when the device is rehybridized with a well-matched duplex.

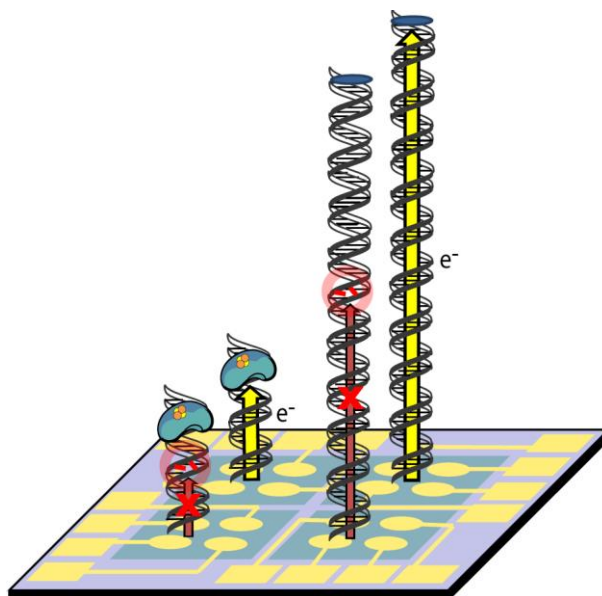


**Figure 1.3** Measuring DNA CT with DNA-modified electrodes. Schematic of a multiplex chip with four different DNAs in the four quadrants of the chip. Left side: mismatched (front) and well-matched (back) 17-mers with DNA-bound, redox-active protein containing a [4Fe-4S] cluster signified by the cluster of two orange and two yellow spheres. The protein binds the DNA, which is covalently attached by one end to the gold surface, and reduction of the cluster proceeds via DNA CT. Right side: well mismatched (front) and well-matched (back) 100-mers with a covalent, small molecule redox probe. The location of the mismatch in the 17-mer and 100-mer is circled in red. DNA CT to the redox-active protein or small molecule probe is significantly attenuated (red X) in the presence of a single base mismatch for both the 17-mer and 100-mer.<sup>13,14</sup>

investigations of DNA CT (Figure 1.3). Importantly, the same characteristics of DNA CT that are observed with free DNA in solution are observed with DNA-modified electrodes; electronic coupling of the redox probe to the DNA  $\pi$ -stack is essential to observe a DNA-mediated redox signal<sup>15</sup> and DNA CT is disrupted by a variety of biologically significant perturbations to the DNA  $\pi$ -stack, including intervening base mismatches,<sup>13–16</sup> base lesions,<sup>17</sup> and structural distortions caused by protein binding and activity.<sup>18,19</sup>

Critical for studying DNA CT in biological systems, DNA-modified electrodes also make it possible to measure the DNA-bound potentials of proteins with redox-active cofactors such as iron-sulfur clusters (Figure 1.3).<sup>20–25</sup> Like synthetic redox probes, DNA CT to DNA-bound proteins show the same coupling requirement to the  $\pi$ -stack<sup>22,23</sup> and the same sensitivity to intervening structural disturbances, such as base mismatches and lesions.<sup>20,24,25</sup> Thus DNA-modified electrodes allow for the identification and characterization of proteins that have the capacity to participate in DNA CT chemistry in living organisms.

In addition to illustrating these first two characteristics of DNA CT chemistry, these diverse platforms were also used to probe a third critical parameter for understanding the role of DNA CT in biology: *how far can DNA effectively conduct charge?* This distance dependence was first studied with free DNA in solution, using a covalently attached metallointercalator photooxidant that, upon irradiation, induces DNA-mediated, long-range guanine oxidation.<sup>26,27</sup> By biochemical sequencing, this damage is observed at the 5'-G of guanine doublets, the site of lowest oxidation potential. Importantly, and consistent with a DNA CT mechanism, the degree of coupling of the

photooxidant to the  $\pi$ -stack and the integrity of the intervening  $\pi$ -stack were found to be far greater determinants of oxidation yield than the distance of the oxidation site from the photooxidant. In fact, over the longest distance measured, 20 nm or 60 bp, the oxidation yield was unaffected by the separation distance.<sup>27</sup>

Using multiplexed, DNA-modified electrodes, ground state DNA CT to a distal, covalent redox probe was measured over an even longer distance of 34 nm or 100 bp (Figure 1.3).<sup>14</sup> For these experiments, the multiplexed chip platform was crucial for enabling the side-by-side comparison of DNA CT in short and long DNA duplexes. Remarkably, DNA CT over 34 nm yields the same redox signal size and the same signal attenuation from the incorporation of a single base mismatch as DNA CT in much shorter, 6 nm or 17 bp duplexes. Over both 34 nm and 6 nm, the rate of DNA CT is limited by the electron tunneling rate through the alkanethiol linker that attaches the DNA to the gold surface.<sup>14,28</sup> Thus, the distance dependence of DNA CT is very shallow, allowing efficient charge conduction by DNA over distances that challenge the physical limits of these *in vitro* platforms for measuring this chemistry. Indeed, we have not yet determined an upper limit in distance for DNA CT, only that over these 100 base pair distances CT is efficient and no decay in yield is observed. After establishing these conserved, structurally derived characteristics of DNA CT, including (i) required electronic coupling to the  $\pi$ -stack, (ii) high sensitivity to intervening structural perturbations of the  $\pi$ -stack, and (iii) a capacity to transport charge over very long distances, the clear next step was to utilize this foundation to consider a role for this chemistry in living cells.

## General Observations of DNA CT in Biological Systems

Initial experiments probed broadly the possibility that DNA CT might play a role in biological systems and sought to identify the cellular players that have the capacity to engage in this chemistry. *Can cellular DNA participate in DNA CT? Can DNA-binding proteins participate in DNA CT?* From this beginning point, the ways in which DNA CT may be exploited by these players were then probed, including the funneling of charge through cellular DNA to concentrate damage at distant sites throughout the genome, and the sending and receiving of DNA-mediated charge by DNA-binding proteins as a means to sense and respond to oxidative stress. These general observations set the stage for our current, extensive studies on whether DNA-bound proteins may use DNA CT to signal to each other across the genome in order to achieve more efficiently a variety of logistically challenging biological tasks.

The measurement of long-range oxidative damage to DNA *in vitro*<sup>26,27</sup> set the stage to investigate this phenomenon in cellular DNA (Figure 1.4). Reactive oxygen species pose a constant threat to the integrity of the genome, making it critical for cells to reduce the net impact of inevitable damage. One strategy is to promote the accumulation of holes at specific regions of low oxidation potential, namely tracts of multiple guanine bases, in order to concentrate damage and spare the majority of the DNA.<sup>29</sup> The possibility that DNA can facilitate such long-range funneling of damage via DNA CT was investigated in several native cellular environments, including isolated HeLa cell nuclei,<sup>30</sup> nucleosome core particles,<sup>31</sup> and mitochondria.<sup>32,33</sup> In these studies, oxidative damage was induced by photoexcited  $[\text{Rh}(\text{phi})_2(\text{bpy})]^{3+}$  (bpy = 2,2'-bipyridine), a DNA intercalator and potent photooxidant (Figure 1.4). A comparison of the binding sites of

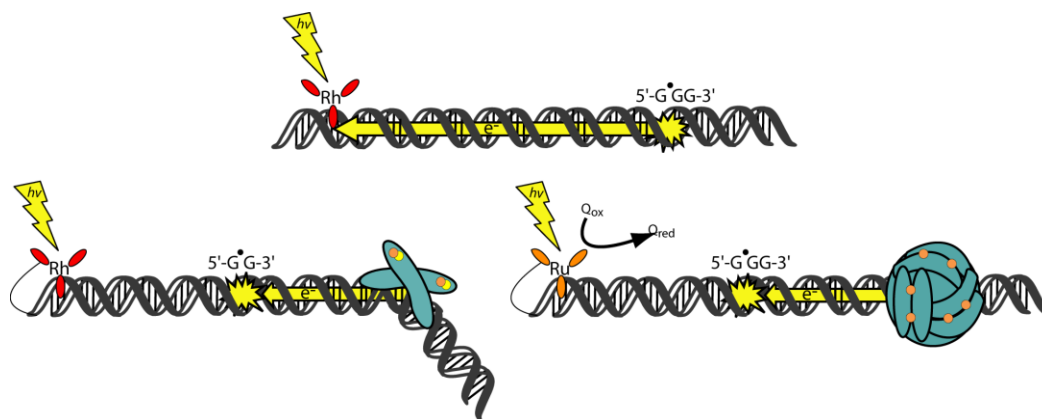


**Figure 1.4** Initial experiments to probe DNA CT in biology. Illustrated are some examples of experimental constructs used to evaluate the capabilities of different cellular players to participate in DNA CT, including cellular DNA (top) and proteins with redox-active cofactors (bottom left and right). Top: the capacity of cellular DNA to funnel damage over long distances in the genome via DNA CT was studied within its native environment inside a variety of organelles.<sup>29–33</sup> Damage is induced by a photoexcited, intercalated metal complex and the appearance of damage at the 5'-guanine of distant guanine repeat sites supports that DNA CT facilitates this transport of electrons over such long distances. Bottom Left: SoxR, an oxidative stress response transcription factor binds DNA as a dimer, with each monomer containing a [2Fe-2S] cluster signified by a cluster of one orange and one yellow sphere. SoxR is activated by oxidative DNA damage from a distance, and induced by a covalent, photoexcited metal complex.<sup>34</sup> Bottom Right: Dps, a 12-subunit protein that binds DNA as a spherical dodecamer, contains 12 intersubunit ferroxidase sites that, in the depicted experiment, are occupied by 1 Fe<sup>2+</sup> each (12 Fe<sup>2+</sup>/ Dps; each bound Fe<sup>2+</sup> is represented by a single orange sphere). Dps uses ferroxidase activity to protect DNA from reactive oxygen species and can neutralize guanine radicals from a distance when they are formed by a photoexcited metal complex.<sup>35</sup>

the metal complex with the locations of guanine damage showed significant separation, necessitating some form of controlled charge migration. Additionally, damage was observed specifically at the 5'-guanine of guanine repeat sites, a hallmark of DNA CT. Thus, these studies verified that long-range DNA CT can indeed take place in a complex and congested native organelle environment and can divert DNA damage to distant reservoirs in the genome.<sup>36</sup>

Given the confirmation that cellular DNA can facilitate DNA CT across long distances, the next step was to determine whether DNA-binding proteins can access, and potentially exploit, this chemistry. A logical starting point was to consider redox-active proteins that protect the cell against oxidative stress and thus must be able to sense and respond to oxidative threats. The first such protein investigated was SoxR, a bacterial transcription factor that, when activated, induces the transcription of a battery of genes involved in the oxidative stress response (Figure 1.4).<sup>37</sup> SoxR generally remains bound to DNA as a dimer in the cell and each monomer contains a [2Fe-2S] cluster that critically allows it to sense and respond to oxidative stress; oxidation of the cluster results in an up to 100-fold increase in transcription of its stress response genes.<sup>38</sup> But how is the cluster oxidized? Electrochemistry of SoxR bound to DNA-modified electrodes revealed that redox activity of the [2Fe-2S] clusters can be accessed by DNA CT. Additionally, the potential of the cluster shifts by positive ~500 mV upon DNA-binding, thereby modulating the capacity of SoxR to function as an oxidative stress sensor.<sup>39</sup> To investigate whether SoxR can be activated by oxidative DNA damage from a distance, the DNA intercalating photooxidant [Rh(phi)<sub>2</sub>(bpy)]<sup>3+</sup> was covalently attached to a DNA duplex, 80 bp from the SoxR binding site (Figure 1.4). Upon photoexcitation of the

metal complex, which injects electron holes into the DNA and generates distant guanine radicals, transcription of SoxR-regulated genes is activated.<sup>34</sup> This result indicates that SoxR can utilize DNA CT to sense oxidative damage efficiently across long molecular distances in the genome and activate the appropriate protective response.

Recent studies were conducted on bacterial Dps and human p53, other DNA-binding redox-active proteins that are also involved in responding to oxidative stress. Dps, a bacterial mini-ferritin which uses ferroxidase activity to protect DNA in pathogenic bacteria from reactive oxygen species, was studied to determine if it can wield this capability from a distance, via DNA CT (Figure 1.4). DNA-bound, ferrous iron-loaded Dps, but not apo-Dps or ferric iron-loaded Dps, was observed to neutralize distant guanine radicals formed by a distally bound, covalent photooxidant, confirming its potential to use DNA CT for cellular protection.<sup>35</sup> Similarly, human p53, a transcription factor that decides the fate of human cells under stressful cellular conditions, was found to respond to distal hole injection into DNA by a covalent anthraquinone photooxidant.<sup>40,41</sup> Specifically, oxidation of multiple cysteine residues to disulfide bonds within p53 causes dissociation from specific DNA promoter sequences. Importantly, p53 binding sites with lower oxidation potential (i.e. sites with guanine doublets and triplets) show more dissociation of p53 in response to the oxidative insult.<sup>41</sup> Thus, the redox sensitivities of p53-binding sites combined with long-range DNA CT provide an efficient mechanism for p53 to regulate the expression of specific genes in response to a genome-wide report of oxidative stress.

Collectively, these examples demonstrate that diverse DNA-binding proteins with a variety of redox-active cofactors have the ability to take advantage of DNA CT

chemistry in order to achieve more efficiently a variety of challenging cellular tasks. This work has fueled more in-depth studies into perhaps the most intriguing and powerful question that arises from these initial observations of DNA CT in biological systems: *Do DNA-bound proteins use DNA CT to signal to each other?*

### **Signaling among DNA repair glycosylases containing 4Fe-4S clusters**

A striking number of DNA-processing enzymes in both prokaryotes and eukaryotes have been found to contain 4Fe-4S clusters. This iron co-factor was first associated with DNA repair enzymes when a 4Fe-4S cluster was discovered in *E. coli* Endonuclease III (EndoIII), a DNA glycosylase from the base excision repair (BER) pathway.<sup>42-44</sup> Other BER enzymes, such as *E. coli* MutY and homologous BER enzymes from other organisms, were also shown to contain 4Fe-4S clusters.<sup>45,46</sup> The 4Fe-4S cluster in these enzymes resides near the DNA binding interface and the clusters do not play a redox role in catalysis. Originally, the role of these iron-sulfur clusters was thought to be solely structural. While iron-sulfur clusters often serve a redox role in other classes of enzymes, a redox role for the clusters in the DNA glycosylases was first rejected, since for EndoIII the reduction potential of the  $[4\text{Fe-4S}]^{2+/1+}$  couple was found to be  $< -400$  mV vs. NHE based on measurements using redox mediators.<sup>43,44</sup> Additionally, while the cluster in MutY is required for DNA binding, the overall structure of MutY is not affected by the absence of the cluster.<sup>46</sup>

Our laboratory hypothesized instead that the 4Fe-4S clusters in these proteins are used for DNA-mediated redox signaling.<sup>20,22,23,47</sup> Importantly, measurements of redox characteristics of the cluster were required when bound to the DNA polyanion, where the

repair protein carries out its function. DNA-modified electrodes were thus used to probe the redox characteristics of the 4Fe-4S cluster in DNA glycosylases. The first important observations made were that the 4Fe-4S cofactors in DNA glycosylases can be reduced or oxidized via long range DNA CT and binding to DNA shifts the reduction potential of the 4Fe-4S cluster.<sup>20,21</sup> Cyclic voltammetry on DNA-modified gold electrodes shows a reversible redox signal at a midpoint potential of ~80 mV vs. NHE (Figure 1.5). This electrochemical signal is dependent on the DNA bases being well stacked. By introducing a single abasic site in the DNA substrate, the electrochemical signal is significantly attenuated, consistent with the redox pathway from the electrode to the cluster being through the DNA  $\pi$ -stack. Thus, the 4Fe-4S cluster of the protein appears to be well-coupled electronically into the DNA base stack.

An array of EndoIII mutants have been studied electrochemically on DNA-modified electrodes.<sup>22,23,48</sup> Interestingly, all of the mutants examined so far have the same DNA-bound redox potential, though for many of the mutant enzymes, an increased or decreased signal intensity as measured by cyclic voltammetry is observed, indicating the electronic coupling of the mutant enzymes to the DNA base stack has changed (Figure 1.5). Of particular interest is the CT-deficient EndoIII Y82A mutant, which has a significantly lower electrochemical signal on DNA-modified electrodes compared to wild-type (WT) EndoIII, though it maintains enzymatic activity comparable to that of the WT enzyme.<sup>22,48</sup>

Direct electrochemical measurements of EndoIII on highly oriented pyrolytic graphite (HOPG) with and without DNA revealed that upon binding to DNA, the redox potential of the  $[4\text{Fe-4S}]^{3+/2+}$  couple shifts negatively by ~200 mV.<sup>21</sup> The protein is thus

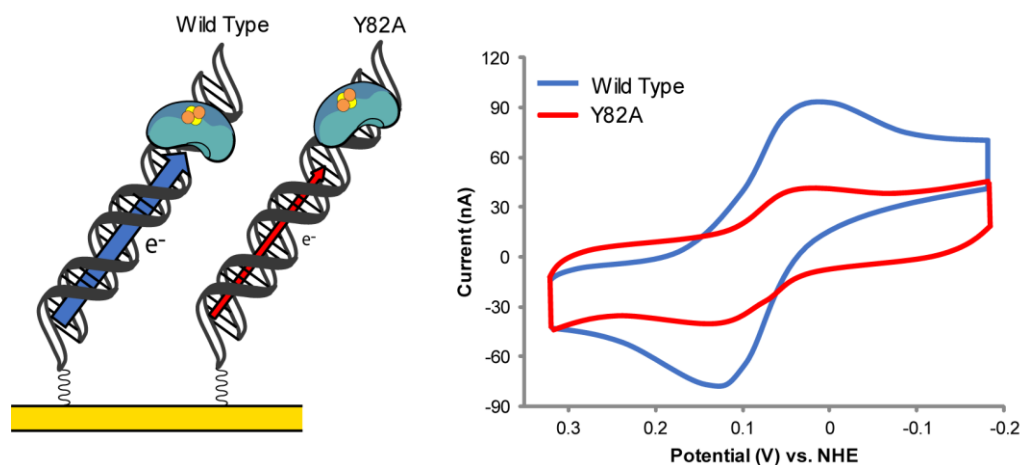


**Figure 1.5** Electrochemistry of DNA glycosylases on DNA-modified electrodes. Both single and multiplexed DNA-modified gold electrodes have been used to study the electrochemical characteristics of DNA glycosylases containing [4Fe-4S] clusters. In these experiments, the protein is bound to the DNA, which is attached to the gold electrode surface, and the cluster is reduced via DNA CT (left). Cyclic voltammetry has been used to determine that the midpoint redox potential of these enzymes is around 80 mV vs. NHE.<sup>20,22,48</sup> and to establish that EndoIII Y82A is deficient in its ability to perform DNA-mediated CT (right). The intensity of the electrochemical signal of EndoIII Y82A is much lower than that of WT EndoIII, depicted by the red and blue arrows, respectively, in the illustration (left). The redox-active [4Fe-4S] clusters in the proteins are signified here by clusters of two orange and two yellow spheres.

activated towards oxidation upon binding to DNA. The earlier studies suggesting Endo III to be redox-inactive under physiological conditions still hold true, but not if the protein is bound to DNA. This shift in potential moreover corresponds to a three orders of magnitude higher affinity for DNA when the 4Fe-4S cluster is in the 3+ oxidation state relative to the 2+ oxidation state.<sup>21</sup> The increase in the binding affinity of the protein for DNA in the oxidized form versus the reduced form is understandable given that higher oxidation states should be preferentially stabilized when the 4Fe-4S cluster is in the vicinity of the polyanionic DNA backbone.

The role of MutY and EndoIII is to prevent oxidized bases from causing mutagenesis, by MutY excising bases that are mispaired with oxidized bases, or EndoIII directly excising oxidized bases, prior to replication. A question that has yet to be definitively answered is how these enzymes, thought to be at low copy number within cells, can locate and fix such subtle damage scattered across the 4.6 megabase genome of *E. coli* before the organism divides. The copy number of MutY is estimated to be ~30.<sup>49</sup> We have proposed that DNA CT may be used by MutY, EndoIII, and other DNA-processing enzymes containing 4Fe-4S clusters as a means to both scan the genome for damage and locate the damage as a first step in DNA repair.<sup>22,23,47,50</sup>

Our model for how DNA repair proteins with 4Fe-4S clusters use DNA-mediated CT as a means of signaling to locate and repair damage, illustrated in Figure 1.6, is based upon many of the redox characteristics discussed above.<sup>22</sup> When a DNA glycosylase is freely diffusing in solution, its 4Fe-4S cluster is expected to be in the 2+ oxidation state. Upon binding to DNA, the redox potential of the protein shifts and the 4Fe-4S cluster may be oxidized by reactive oxygen species, other endogenous chemicals, or guanine

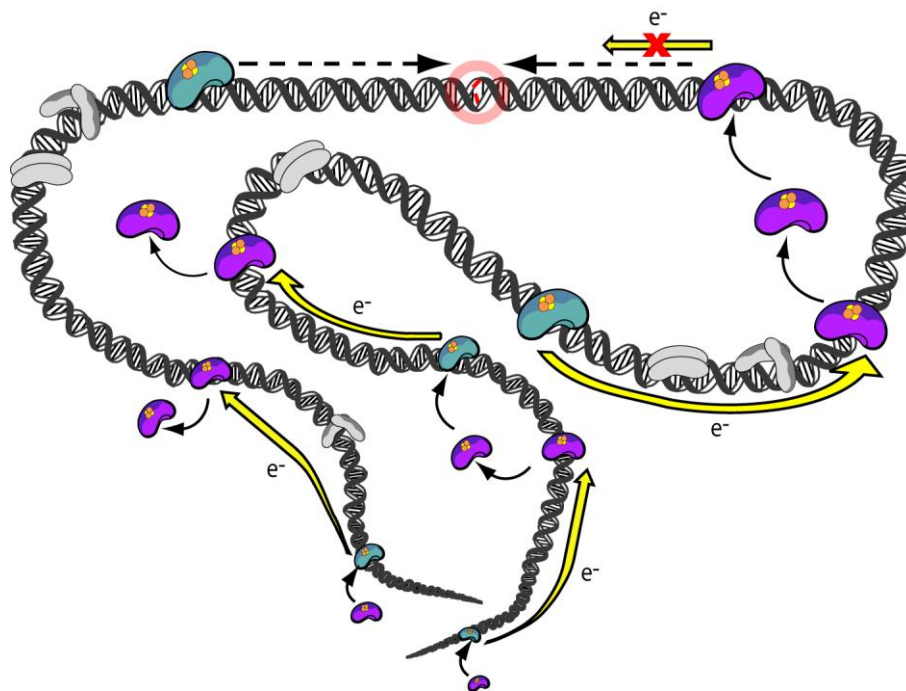


**Figure 1.6** Model for the enhanced DNA lesion search efficiency of DNA repair proteins with 4Fe-4S by DNA CT signaling. Repair proteins with 4Fe-4S clusters, such as MutY and EndoIII, may use DNA CT to effectively scan long stretches of genomic DNA for damage as illustrated (from bottom to top).<sup>22,23,47,50</sup> In the cytoplasm, the 4Fe-4S cluster of repair proteins is in the 2+ oxidation state (purple), but the cluster is oxidized to the 3+ state (turquoise) upon DNA binding if an electron can be transferred to a distally bound protein (receptor) via DNA CT (yellow arrows). Importantly, the intervening DNA must be free of damage for this transfer to occur. Successful electron transfer reduces the cluster of the receptor protein from the 3+ to 2+ oxidation state which decreases its binding affinity for DNA and promotes its dissociation. This protein, diffusing freely in the cytoplasm, can then bind at a different DNA location and repeat this use of DNA CT to scan another segment of the genome. If, however, the protein binds a location where there is damage intervening it and a potential receptor protein, electron transfer cannot occur and the potential receptor protein remains tightly bound to the DNA with its cluster in the 3+ oxidation state. The bound proteins (either in the 3+ or 2+ state) which are now localized in the vicinity of the damage, can then process along the DNA (dashed black arrow) to efficiently find and repair the damage. The redox-active [4Fe-4S] clusters in the proteins are signified here by clusters of two orange and two yellow spheres.

radicals from a distance.<sup>51,52</sup> If a second DNA glycosylase binds at a sufficient distance relative to the first glycosylase to participate in a DNA-mediated redox reaction and the DNA between the two proteins is undamaged, then the second glycosylase could transfer an electron through the DNA base stack to reduce the distally bound protein. Once in the reduced form, this protein would have a lower binding affinity, would dissociate from DNA, and take advantage of 3-D diffusion to search the genome elsewhere. Importantly, this electron transfer event between the two glycosylases would represent an effective scanning of the DNA integrity between the two proteins. This scanning process would continue until the proteins bind near sites of damage. Since DNA CT through the damaged DNA would be attenuated, any oxidized protein would stay bound in the vicinity of the lesion, diffuse one-dimensionally to the lesion, and process the lesion according to previously described mechanisms.<sup>53-56</sup> DNA CT thus offers a mechanism for DNA glycosylases that contain 4Fe-4S clusters to use DNA-mediated signaling *as a first step* in the search for damage, using DNA CT to scan the genome and concentrate the repair proteins in the vicinity of damage.

An experiment using atomic force microscopy (AFM) was used to visualize protein-DNA complexes in order to test directly if EndoIII redistributes onto DNA that contains damage.<sup>22,23</sup> In this experiment, EndoIII was incubated with mixtures of DNA, one DNA containing a single C:A mismatch, which attenuates DNA CT but is not a substrate for EndoIII, the other DNA being fully matched and undamaged (Figure 1.7). The well-matched DNA and mismatched DNA can be distinguished in the AFM given their different lengths. The short strands (~1.9 kbps) are well-matched, while the long strands (~3.8 kbps) contain a single C:A mismatch near the center of the strand. After

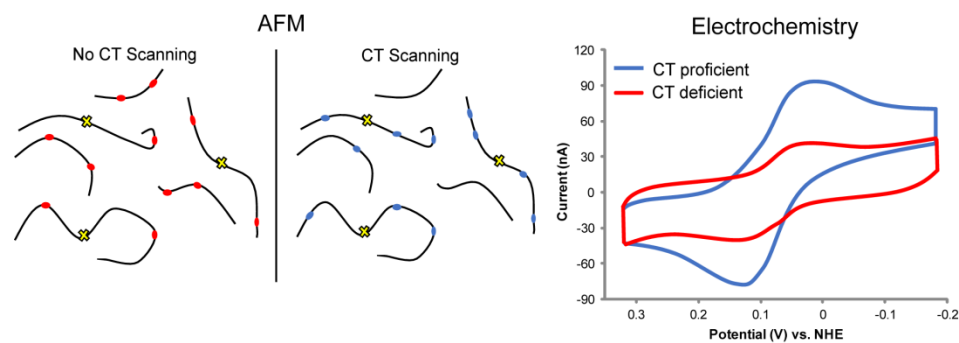


**Figure 1.7** AFM reveals that CT proficiency determines whether proteins localize near DNA mismatches. When wild-type, CT-proficient EndoIII, or SaXPD (blue in left diagram and CV on right) are independently incubated with mixtures of long strands of DNA (3.8 kbps) containing a mismatch (yellow X) and well-matched short strands of DNA (1.9 kbps), a redistribution of the enzymes to the mismatched strand of DNA is observed (right).<sup>22,47,50</sup> This is consistent with DNA-mediated charge transport promoting redistribution to the site that attenuates DNA CT. This redistribution to the damaged strand is not observed for the CT-deficient EndoIII Y82A or SaXPD L325V mutants (red in diagram and in CV on right), nor is it observed when CT-deficient mutants are mixed with SaXPD.

incubation, what is found is that the proteins do in fact redistribute to the long mismatched strands of DNA. Even though there is only a single base mismatch in 3800 base pairs, the binding density of the protein is found to be higher on the mismatched strand; as a control, where there is no mismatch in the long strands of DNA, the protein density is the same on both the well-matched and mismatched strands of DNA. Interestingly, a role for DNA CT in this experiment was also tested. As discussed previously, EndoIII Y82A is a mutant of EndoIII that is CT-deficient as assessed electrochemically, but has enzymatic activity comparable to that of WT EndoIII;<sup>22,48</sup> when EndoIII Y82A is incubated with the mixtures of mismatched and well-matched DNA, there is no observed redistribution. Adding hydrogen peroxide to the protein-DNA mixtures during incubation increases the extent of redistribution, suggesting that oxidative stress may further drive redistribution to sites of damage.<sup>23</sup> Indeed, in subsequent experiments using various mutants of EndoIII, a direct correlation between the proficiency in carrying out DNA CT and the ability to redistribute onto the damaged strand was found. These results strongly indicate that DNA-mediated redox signaling can be used by DNA glycosylases to drive redistribution to the vicinity of DNA damage. But does this cooperative signaling occur within a cell?

As predicted by the model, which is supported by the AFM results, if EndoIII and MutY use DNA-mediated redox signaling as a first step to locate damage, then the activity within cells of one of the glycosylases should be affected by the presence or absence of the other. A genetic experiment was used to show that this indeed appears to be the case. A *lac*<sup>+</sup> reversion assay using the CC104 strain of bacteria was used to measure the activity of MutY upon silencing the gene encoding EndoIII, *nth*.<sup>22,57,58</sup>

Within the CC104 strain of bacteria, MutY prevents GC:TA transversions within the *lacZ* gene by removing adenines placed opposite the oxidized lesion, 8-oxoG. Cells in which the GC:TA transversion has occurred, termed *lac*<sup>+</sup> revertants, can grow on media that contains lactose as the sole carbon source, providing a readout of MutY activity. When the *nth* gene was inactivated within CC104, the number of *lac*<sup>+</sup> revertants increased 1.5 to 2-fold reflecting a decrease in MutY activity.<sup>22</sup> This result is consistent with signaling between EndoIII and MutY. Moreover, mutants of EndoIII were expressed off of complementation plasmids in CC104  $\Delta$ *nth* to provide evidence that this signaling occurs via DNA-mediated CT. When the CC104  $\Delta$ *nth* cells are complemented with EndoIII Y82A, the CT-deficient mutant, there is no rescue of MutY activity. However, when the cells are complemented with EndoIII D138A, which is catalytically inactive but CT-proficient, MutY activity is restored. These results in combination with the results from AFM suggest that DNA glycosylases utilize DNA-mediated redox signaling as a first step in locating DNA damage efficiently within cells.

### **Signaling enzymatic activity of SaXPD, a DNA Helicase with a 4Fe-4S Cluster**

The evidence that DNA glycosylases may use 4Fe-4S clusters to participate in DNA CT in order to localize to sites of damage in cells is intriguing, but importantly, other DNA-processing enzymes have also been shown to contain 4Fe-4S clusters. For example, XPD is an ATP-dependent helicase from the nucleotide excision repair pathway that has also been implicated in transcription-coupled repair.<sup>59,60</sup> In eukaryotes XPD is part of the TFIIH complex, which is vital for both nucleotide excision repair and transcription. Mutations in XPD in humans can lead to Xeroderma Pigmentosum and

Cockayne's syndrome. Recently, XPD along with an entire family of helicases were predicted to contain 4Fe-4S clusters.<sup>60,61</sup> In 2008, three separate crystal structures were published for XPD from three different species, confirming the presence of the 4Fe-4S cluster in XPD. One structure was for XPD from *S. acidocaldarius*,<sup>59</sup> one from *S. tokodaii*,<sup>62</sup> and one from *T. acidophilum*.<sup>63</sup> Two of the crystal structures contained the intact 4Fe-4S cluster when crystallized, while the third did not. Of particular note is the observation that the global structure of XPD from *S. tokodaii* was not perturbed even though it did not contain the 4Fe-4S cluster.

The XPD protein from *S. acidocaldarius* (SaXPD) was electrochemically characterized on DNA-modified electrodes. Here, unlike in previous studies where a DNA duplex was utilized, the substrate on the self-assembled DNA monolayers was a 20-mer double-stranded duplex with a 9-mer 5' to 3' single-stranded overhang, which is a substrate that can be unwound by helicases. Strikingly, the DNA-bound midpoint redox potential of SaXPD was found to be ~80 mV vs. NHE, the same DNA-bound potential measured for the glycosylases MutY and EndoIII from *E. coli*.<sup>20,25</sup> Moreover, since the substrate on the surface of the electrode is a substrate that SaXPD can unwind, the effect of adding ATP to the solution was studied. Upon adding ATP, the current intensity rises by 10-20%, and at a rate comparable to the rate of ATP hydrolysis for SaXPD. Adding ATP $\gamma$ S led to no increase in the signal, indicating the effect is driven by the hydrolysis of ATP. This DNA-modified electrochemical assay therefore reports on the enzymatic activity of SaXPD and likely reflects better coupling of the 4Fe-4S cluster to the electrode during a helicase reaction. This could have important implications for the function of XPD and coordination of nucleotide excision repair within the cell. If during

enzymatic activity the efficiency of DNA-mediated electronic signaling is increased, this could be used as a means for XPD to communicate its activity to proteins downstream of XPD that contain 4Fe-4S clusters.

Since SaXPD shares a midpoint redox potential with MutY and EndoIII, chemically XPD could shuttle electrons to and from MutY and EndoIII *in vitro*. AFM was used to test directly if SaXPD can thus use DNA CT to signal to EndoIII and to localize to sites of DNA damage (Figure 1.7). When SaXPD is incubated with samples of well-matched DNA and DNA containing a mismatch, the protein preferentially binds to strands of DNA with damage,<sup>47</sup> analogous to the effect observed for *E. coli* EndoIII.<sup>22</sup> Again, a mismatch is not a substrate for XPD. SaXPD L325V is a mutant that was found to be deficient in DNA CT electrochemically, and here too, as found with EndoIII mutants, deficient in CT signaling, the L325V mutant of SaXPD is unable to redistribute to sites of damage. Significantly, when mixtures of EndoIII and SaXPD are mixed with the DNAs, the proteins redistribute to sites of damage, but when the mutants SaXPD L325V or EndoIII Y82A are swapped for their WT counterparts in the mixtures, redistribution is no longer observed. These results provide evidence that EndoIII and SaXPD can signal one another via DNA CT to localize to sites of damage.<sup>47</sup> Indeed, even though EndoIII and SaXPD are from different organisms, even different kingdoms, the fact that they contain 4Fe-4S clusters that share a similar redox potential and can electrochemically couple to the DNA  $\pi$ -stack allows them to use DNA CT as a means of signaling, cooperating from a distance to find sites of DNA damage.

Importantly, SaXPD is part of a family of helicases that contain 4Fe-4S clusters (Table 1.1). The *E. coli* homolog of SaXPD, DinG, is one of the major focuses of this

**Table 1.1** DNA-processing enzymes containing 4Fe-4S clusters

Enzyme <sup>a</sup>	Domains <sup>b</sup>	Enzymatic Activity
MutY, EndoIII, UDG	A, B, E	glycosylase, BER
AddAB	B	helicase-nuclease, RR <sup>c</sup>
Dna2	A,E	helicase-nuclease, replication, RR
Exonuclease V	E	5'-exonuclease, replication and repair
Primase	A, E	RNA polymerase, replication
RNA polymerase	A, E	RNA polymerase, transcription
Rad3/XPD	A, E	helicase, NER transcription
FancJ, ChlR1, DOG-1, RTEL	E	helicases, multiple pathways
DinG	B	helicase, R-loop maturation
DNA polymerases $\alpha$ , $\delta$ , $\epsilon$	E	DNA polymerase, replication

<sup>a</sup>This list is not comprehensive, but represents a sampling of the many enzymes found recently to contain 4Fe-4S clusters.<sup>60,61,67,68</sup> <sup>b</sup>For domains B = bacteria, A = archaea, E = eukarya, and <sup>c</sup>RR = recombination repair

thesis. DinG is a damage-inducible, ATP-dependent helicase from *E. coli* that also contains a 4Fe-4S cluster and shares significant homology to SaXPD.<sup>64-66</sup> DinG, like XPD, unwinds DNA with a 5' to 3' polarity. Most substrates that contain a 5' to 3' overhang of at least 15 base pairs can be unwound by DinG, though DinG cannot unwind double-stranded DNA (dsDNA). Uniquely, DinG can, however, unwind R-loops, which are RNA-DNA hybrids that form within a bubble. R-loops have been shown to be one of the target substrates of DinG *in vivo*.<sup>69</sup> Similar to EndoIII, the redox potential of the [4Fe-4S]<sup>2+/1+</sup> couple when not bound to DNA was found to be ~-400 mV vs. NHE using titrations with redox mediators.<sup>65</sup> Since DinG is from a genetically tractable organism, the important question of whether or not DNA-mediated CT signaling occurs between repair enzymes containing 4Fe-4S clusters from different DNA repair pathways *in vivo* within cells could be examined.

## Prospectus

DNA CT chemistry offers a means to carry out redox chemistry at a distance and in a fashion that depends upon the integrity of the intervening base pair stack. We have seen how this chemistry may be utilized as a sensor of oxidative stress, both in funneling damage and in oxidizing DNA-bound protein sensors. We have also seen how proteins containing 4Fe-4S clusters may signal one another using DNA CT chemistry and how specifically this signaling may be used as a first step in efficiently redistributing repair proteins to sites of DNA lesions for repair. The association of 4Fe-4S clusters, common redox cofactors in biology, with proteins involved in DNA repair, is being found with increasing frequency and has apparently been preserved in higher organisms that carry out still more complex modes of repair. Utilizing DNA CT with these redox cofactors provides a role for these clusters in the repair proteins along with a mechanism to understand how the cell achieves the high level of efficient repair we require. Indeed, given findings of 4Fe-4S clusters now in proteins involved in all aspects of DNA processing, it is tempting to suggest that here too these redox cofactors may be present to carry out DNA CT. Thus DNA CT could provide a general means of signaling among DNA-bound proteins across the genome.

Work presented in this thesis focuses on studying DNA-mediated signaling amongst DNA repair enzymes that contain 4Fe-4S clusters and how DNA CT chemistry can be utilized as a means to facilitate the cooperative and efficient repair of the genome within the cell. Until the discovery that the *E. coli* helicase DinG contained a 4Fe-4S cluster, studies focused on how DNA CT in *E. coli* may be utilized by MutY and EndoIII, the only DNA-processing enzymes within *E. coli* known at the time to contain 4Fe-4S

clusters, for cooperative signaling. Additionally, most of the EndoIII and MutY experiments as discussed above were performed *in vitro*. In Chapter 2 of the thesis, DNA-bound DinG is shown electrochemically to share the redox potential of DNA-bound EndoIII and MutY. The AFM redistribution assay was used to show that EndoIII and DinG redistribute to sites of damage that attenuate DNA CT. Finally, genetics experiments strongly indicate that DNA-mediated CT signaling is used as a means of coordinating the activity of MutY, EndoIII, and DinG within the cell. In Chapter 3, it is shown spectroscopically that *E. coli* UvrC appears to contain a native 4Fe-4S cluster. Furthermore, initial genetics experiments designed to explore interactions between UvrC and other DNA repair proteins with 4Fe-4S clusters within the cell reveal that DNA-mediated CT signaling appears to be used as a general mechanism that cells use to facilitate the necessarily efficient repair of the genome. DNA CT thus appears to provide a chemical mechanism that nature uses to mediate redox reactions at a distance in order to coordinate DNA repair.

## References

1. Genereux, J. C. & Barton, J. K. Mechanisms for DNA Charge Transport. *Chem. Rev.* **110**, 1642–1662 (2010).
2. Muren, N. B., Olmon, E. D. & Barton, J. K. Solution, surface, and single molecule platforms for the study of DNA-mediated charge transport. *Phys. Chem. Chem. Phys.* **14**, 13754–13771 (2012).
3. Sontz, P. A., Muren, N. B. & Barton, J. K. DNA Charge Transport for Sensing and Signaling. *Acc. Chem. Res.* **45**, 1792–1800 (2012).
4. Genereux, J. C., Boal, A. K. & Barton, J. K. DNA-Mediated Charge Transport in Redox Sensing and Signaling. *J. Am. Chem. Soc.* **132**, 891–905 (2010).
5. Eley, D. D. & Spivey, D. I. Semiconductivity of organic substances. Part 9.—Nucleic acid in the dry state. *Trans. Faraday Soc.* **58**, 411–415 (1962).
6. Murphy, C. J. *et al.* Long-range photoinduced electron transfer through a DNA helix. *Science* **262**, 1025–1029 (1993).
7. Kelley, S. O. & Barton, J. K. Electron Transfer Between Bases in Double Helical DNA. *Science* **283**, 375–381 (1999).
8. Kelley, S. O., Holmlin, R. E., Stemp, E. D. A. & Barton, J. K. Photoinduced Electron Transfer in Ethidium-Modified DNA Duplexes: Dependence on Distance and Base Stacking. *J. Am. Chem. Soc.* **119**, 9861–9870 (1997).
9. O'Neill, M. A., Becker, H.-C., Wan, C., Barton, J. K. & Zewail, A. H. Ultrafast Dynamics in DNA-Mediated Electron Transfer: Base Gating and the Role of Temperature. *Angew. Chem. Int. Ed.* **42**, 5896–5900 (2003).

10. Guo, X., Gorodetsky, A. A., Hone, J., Barton, J. K. & Nuckolls, C. Conductivity of a single DNA duplex bridging a carbon nanotube gap. *Nat. Nanotechnol.* **3**, 163–167 (2008).
11. Drummond, T. G., Hill, M. G. & Barton, J. K. Electrochemical DNA sensors. *Nat. Biotechnol.* **21**, 1192–1199 (2003).
12. Gorodetsky, A. A., Buzzeo, M. C. & Barton, J. K. DNA-Mediated Electrochemistry. *Bioconjug. Chem.* **19**, 2285–2296 (2008).
13. Slinker, J. D., Muren, N. B., Gorodetsky, A. A. & Barton, J. K. Multiplexed DNA-Modified Electrodes. *J. Am. Chem. Soc.* **132**, 2769–2774 (2010).
14. Slinker, J. D., Muren, N. B., Renfrew, S. E. & Barton, J. K. DNA charge transport over 34 nm. *Nat. Chem.* **3**, 228–233 (2011).
15. Kelley, S. O., Boon, E. M., Barton, J. K., Jackson, N. M. & Hill, M. G. Single-base mismatch detection based on charge transduction through DNA. *Nucleic Acids Res.* **27**, 4830–4837 (1999).
16. Boon, E. M., Ceres, D. M., Drummond, T. G., Hill, M. G. & Barton, J. K. Mutation detection by electrocatalysis at DNA-modified electrodes. *Nat. Biotechnol.* **18**, 1096–1100 (2000).
17. Boal, A. K. & Barton, J. K. Electrochemical Detection of Lesions in DNA. *Bioconjug. Chem.* **16**, 312–321 (2005).
18. Boon, E. M., Salas, J. E. & Barton, J. K. An electrical probe of protein–DNA interactions on DNA-modified surfaces. *Nat. Biotechnol.* **20**, 282–286 (2002).

19. Furst, A. L., Muren, N. B., Hill, M. G. & Barton, J. K. Label-free electrochemical detection of human methyltransferase from tumors. *Proc. Natl. Acad. Sci.* **111**, 14985–14989 (2014).
20. Boal, A. K. *et al.* DNA-Bound Redox Activity of DNA Repair Glycosylases Containing [4Fe-4S] Clusters†. *Biochemistry* **44**, 8397–8407 (2005).
21. Gorodetsky, A. A., Boal, A. K. & Barton, J. K. Direct Electrochemistry of Endonuclease III in the Presence and Absence of DNA. *J. Am. Chem. Soc.* **128**, 12082–12083 (2006).
22. Boal, A. K. *et al.* Redox signaling between DNA repair proteins for efficient lesion detection. *Proc. Natl. Acad. Sci.* **106**, 15237–15242 (2009).
23. Romano, C. A., Sontz, P. A. & Barton, J. K. Mutants of the Base Excision Repair Glycosylase, Endonuclease III: DNA Charge Transport as a First Step in Lesion Detection. *Biochemistry* **50**, 6133–6145 (2011).
24. DeRosa, M. C., Sancar, A. & Barton, J. K. Electrically monitoring DNA repair by photolyase. *Proc. Natl. Acad. Sci. U. S. A.* **102**, 10788–10792 (2005).
25. Mui, T. P., Fuss, J. O., Ishida, J. P., Tainer, J. A. & Barton, J. K. ATP-Stimulated, DNA-Mediated Redox Signaling by XPD, a DNA Repair and Transcription Helicase. *J. Am. Chem. Soc.* **133**, 16378–16381 (2011).
26. Hall, D. B., Holmlin, R. E. & Barton, J. K. Oxidative DNA damage through long-range electron transfer. *Nature* **382**, 731–735 (1996).
27. Núñez, M. E., Hall, D. B. & Barton, J. K. Long-range oxidative damage to DNA: Effects of distance and sequence. *Chem. Biol.* **6**, 85–97 (1999).

28. Drummond, T. G., Hill, M. G. & Barton, J. K. Electron Transfer Rates in DNA Films as a Function of Tether Length. *J. Am. Chem. Soc.* **126**, 15010–15011 (2004).
29. Merino, E. J., Boal, A. K. & Barton, J. K. Biological contexts for DNA charge transport chemistry. *Curr. Opin. Chem. Biol.* **12**, 229–237 (2008).
30. Núñez, M. E., Holmquist, G. P. & Barton, J. K. Evidence for DNA Charge Transport in the Nucleus†. *Biochemistry* **40**, 12465–12471 (2001).
31. Núñez, M. E., Noyes, K. T. & Barton, J. K. Oxidative Charge Transport through DNA in Nucleosome Core Particles. *Chem. Biol.* **9**, 403–415 (2002).
32. Merino, E. J. & Barton, J. K. DNA Oxidation by Charge Transport in Mitochondria†. *Biochemistry* **47**, 1511–1517 (2008).
33. Merino, E. J., Davis, M. L. & Barton, J. K. Common Mitochondrial DNA Mutations Generated through DNA-Mediated Charge Transport†. *Biochemistry* **48**, 660–666 (2009).
34. Lee, P. E., Demple, B. & Barton, J. K. DNA-mediated redox signaling for transcriptional activation of SoxR. *Proc. Natl. Acad. Sci. U. S. A.* **106**, 13164–13168 (2009).
35. Arnold, A. R. & Barton, J. K. DNA Protection by the Bacterial Ferritin Dps via DNA Charge Transport. *J. Am. Chem. Soc.* **135**, 15726–15729 (2013).
36. Friedman, K. A. & Heller, A. Guanosine Distribution and Oxidation Resistance in Eight Eukaryotic Genomes. *J. Am. Chem. Soc.* **126**, 2368–2371 (2004).
37. Pomposiello, P. J., Bennik, M. H. J. & Demple, B. Genome-Wide Transcriptional Profiling of the *Escherichia coli* Responses to Superoxide Stress and Sodium Salicylate. *J. Bacteriol.* **183**, 3890–3902 (2001).

38. Ding, H., Hidalgo, E. & Dimple, B. The Redox State of the [2Fe-2S] Clusters in SoxR Protein Regulates Its Activity as a Transcription Factor. *J. Biol. Chem.* **271**, 33173–33175 (1996).
39. Gorodetsky, A. A. *et al.* DNA binding shifts the redox potential of the transcription factor SoxR. *Proc. Natl. Acad. Sci.* **105**, 3684–3689 (2008).
40. Augustyn, K. E., Merino, E. J. & Barton, J. K. A role for DNA-mediated charge transport in regulating p53: Oxidation of the DNA-bound protein from a distance. *Proc. Natl. Acad. Sci.* **104**, 18907–18912 (2007).
41. Schaefer, K. N. & Barton, J. K. DNA-Mediated Oxidation of p53. *Biochemistry* **53**, 3467–3475 (2014).
42. Kuo, C. F. *et al.* Atomic structure of the DNA repair [4Fe-4S] enzyme endonuclease III. *Science* **258**, 434–440 (1992).
43. Fu, W., O’Handley, S., Cunningham, R. P. & Johnson, M. K. The role of the iron-sulfur cluster in Escherichia coli endonuclease III. A resonance Raman study. *J. Biol. Chem.* **267**, 16135–16137 (1992).
44. Cunningham, R. P. *et al.* Endonuclease III is an iron-sulfur protein. *Biochemistry* **28**, 4450–4455 (1989).
45. Hinks, J. A. *et al.* An Iron-Sulfur Cluster in the Family 4 Uracil-DNA Glycosylases. *J. Biol. Chem.* **277**, 16936–16940 (2002).
46. Porello, S. L., Cannon, M. J. & David, S. S. A Substrate Recognition Role for the [4Fe-4S]<sub>2</sub><sup>+</sup> Cluster of the DNA Repair Glycosylase MutY. *Biochemistry* **37**, 6465–6475 (1998).

47. Sontz, P. A., Mui, T. P., Fuss, J. O., Tainer, J. A. & Barton, J. K. DNA charge transport as a first step in coordinating the detection of lesions by repair proteins. *Proc. Natl. Acad. Sci.* **109**, 1856–1861 (2012).
48. Pheeny, C. G., Arnold, A. R., Grodick, M. A. & Barton, J. K. Multiplexed Electrochemistry of DNA-Bound Metalloproteins. *J. Am. Chem. Soc.* **135**, 11869–11878 (2013).
49. Demple, B. & Harrison, L. Repair of Oxidative Damage to DNA: Enzymology and Biology. *Annu. Rev. Biochem.* **63**, 915–948 (1994).
50. Grodick, M. A., Segal, H. M., Zwang, T. J. & Barton, J. K. DNA-Mediated Signaling by Proteins with 4Fe–4S Clusters Is Necessary for Genomic Integrity. *J. Am. Chem. Soc.* **136**, 6470–6478 (2014).
51. Yavin, E. *et al.* Protein–DNA charge transport: Redox activation of a DNA repair protein by guanine radical. *Proc. Natl. Acad. Sci. U. S. A.* **102**, 3546–3551 (2005).
52. Lin, J.-C., Singh, R. R. P. & Cox, D. L. Theoretical Study of DNA Damage Recognition via Electron Transfer from the [4Fe-4S] Complex of MutY. *Biophys. J.* **95**, 3259–3268 (2008).
53. Friedman, J. I. & Stivers, J. T. Detection of Damaged DNA Bases by DNA Glycosylase Enzymes. *Biochemistry* **49**, 4957–4967 (2010).
54. Blainey, P. C., Oijen, A. M. van, Banerjee, A., Verdine, G. L. & Xie, X. S. A base-excision DNA-repair protein finds intrahelical lesion bases by fast sliding in contact with DNA. *Proc. Natl. Acad. Sci.* **103**, 5752–5757 (2006).

55. Fromme, J. C., Banerjee, A., Huang, S. J. & Verdine, G. L. Structural basis for removal of adenine mispaired with 8-oxoguanine by MutY adenine DNA glycosylase. *Nature* **427**, 652–656 (2004).
56. Nelson, S. R., Dunn, A. R., Kathe, S. D., Warshaw, D. M. & Wallace, S. S. Two glycosylase families diffusively scan DNA using a wedge residue to probe for and identify oxidatively damaged bases. *Proc. Natl. Acad. Sci.* **111**, E2091–E2099 (2014).
57. Cupples, C. G. & Miller, J. H. A set of lacZ mutations in Escherichia coli that allow rapid detection of each of the six base substitutions. *Proc. Natl. Acad. Sci.* **86**, 5345–5349 (1989).
58. Michaels, M. L., Cruz, C., Grollman, A. P. & Miller, J. H. Evidence that MutY and MutM combine to prevent mutations by an oxidatively damaged form of guanine in DNA. *Proc. Natl. Acad. Sci.* **89**, 7022–7025 (1992).
59. Fan, L. *et al.* XPD Helicase Structures and Activities: Insights into the Cancer and Aging Phenotypes from XPD Mutations. *Cell* **133**, 789–800 (2008).
60. Rudolf, J., Makrantonis, V., Ingledew, W. J., Stark, M. J. R. & White, M. F. The DNA Repair Helicases XPD and FancJ Have Essential Iron-Sulfur Domains. *Mol. Cell* **23**, 801–808 (2006).
61. Wu, Y., Suhasini, A. N. & Jr, R. M. B. Welcome the Family of FANCDJ-like Helicases to the Block of Genome Stability Maintenance Proteins. *Cell. Mol. Life Sci.* **66**, 1209–1222 (2008).
62. Liu, H. *et al.* Structure of the DNA Repair Helicase XPD. *Cell* **133**, 801–812 (2008).

63. Wolski, S. C. *et al.* Crystal Structure of the FeS Cluster–Containing Nucleotide Excision Repair Helicase XPD. *PLoS Biol* **6**, e149 (2008).
64. Voloshin, O. N., Vanevski, F., Khil, P. P. & Camerini-Otero, R. D. Characterization of the DNA Damage-inducible Helicase DinG from *Escherichia coli*. *J. Biol. Chem.* **278**, 28284–28293 (2003).
65. Ren, B., Duan, X. & Ding, H. Redox Control of the DNA Damage-inducible Protein DinG Helicase Activity via Its Iron-Sulfur Cluster. *J. Biol. Chem.* **284**, 4829–4835 (2009).
66. Voloshin, O. N. & Camerini-Otero, R. D. The DinG Protein from *Escherichia coli* Is a Structure-specific Helicase. *J. Biol. Chem.* **282**, 18437–18447 (2007).
67. White, M. F. & Dillingham, M. S. Iron-sulphur clusters in nucleic acid processing enzymes. *Curr. Opin. Struct. Biol.* **22**, 94–100 (2012).
68. Wu, Y. & Brosh, R. M. DNA helicase and helicase–nuclease enzymes with a conserved iron–sulfur cluster. *Nucleic Acids Res.* **40**, 4247–4260 (2012).
69. Boubakri, H., Septenville, A. L. de, Viguera, E. & Michel, B. The helicases DinG, Rep and UvrD cooperate to promote replication across transcription units in vivo. *EMBO J.* **29**, 145–157 (2010).

*Chapter 2*

## **DNA-Mediated Signaling by Proteins with 4Fe-4S clusters is Necessary for Genomic Integrity**

Adapted from: Grodick, M. A, Segal, H. M., Zwang, T. J. & Barton, J. K. *J. Am. Chem. Soc.* **136**, 6470-6478 (2014).

M. A. Grodick performed the electrochemical experiments and analysis in addition to the R-loop growth experiment and analysis. M. A. Grodick and H. M. Segal performed the *lac*<sup>+</sup> reversion assay and analysis. T. J. Zwang performed the atomic force microscopy experiment and analysis.

## Introduction

Iron-sulfur clusters are increasingly being found in proteins that are tasked with maintaining the fidelity of the genome.<sup>1-3</sup> These clusters were first observed in DNA-binding proteins in the base excision repair (BER) glycosylase, Endonuclease III (EndoIII).<sup>4</sup> More recently, 4Fe-4S clusters have been found in a range of DNA repair and DNA-processing enzymes including helicases, DNA polymerases, RNA polymerases, DNA helicase-nucleases, and DNA primases from across the phylogeny.<sup>2,4-13</sup> Many of the enzymes that have been shown to contain these clusters are genetically linked to human diseases, such as early onset breast cancer and Fanconi's anemia, yet the proteins perform immensely different functions. The clusters do not participate in catalysis in these proteins,<sup>2,3,5</sup> though DNA binding may be affected by perturbing the cluster.<sup>14</sup> Recently, studies focusing on the biogenesis of iron-sulfur clusters have revealed that disruption of iron-sulfur cluster assembly proteins in eukaryotic cells leads to nuclear genomic instability and defects in DNA metabolism, replication, and repair.<sup>15-17</sup> The ubiquity of these complex cofactors suggests an essential and shared role for their presence in DNA processing enzymes.

We have considered that the 4Fe-4S clusters in DNA repair enzymes may serve as redox cofactors, much as 4Fe-4S clusters do in other enzymes within the cell.<sup>1,18</sup> Most of our work has focused on *E. coli* EndoIII, where the 4Fe-4S cluster was first found. Although a redox role for the cluster was considered,<sup>4</sup> the 4Fe-4S cluster in EndoIII is redox-inactive at typical cellular potentials. We showed, however, that DNA binding shifts the redox potential of the cluster -200 mV to 80 mV vs. the normal hydrogen electrode (NHE), moving the 3+/2+ redox couple into the physiological regime.<sup>19</sup> Strikingly, we

have now seen that 4Fe-4S clusters in other repair proteins share this DNA-bound potential of ~80 mV versus NHE.<sup>20,21</sup> We have proposed that these clusters are utilized for DNA-mediated charge transport (CT) chemistry as a first step in the search for DNA lesions to repair.<sup>18,22</sup> Indeed we have explored how EndoIII and another BER glycosylase with a 4Fe-4S cluster, MutY, may use DNA CT cooperatively as a first step in repair.<sup>22</sup> Here we explore how DNA CT may be utilized more generally in *E. coli* for inter-protein signaling between repair pathways to maintain the integrity of the genome.

The chemistry of DNA CT offers a powerful tool to probe the integrity of duplex DNA. It has now been well documented that DNA can conduct charge through the  $\pi$ -stacked base pairs within the helix.<sup>23</sup> Subtle perturbations to the DNA base stack, including the presence of base pair mismatches, abasic sites, or even DNA lesions, such as those that are substrates for DNA glycosylases, attenuate DNA CT.<sup>18,24</sup> Protein binding can also interrupt DNA CT if it disrupts base stacking, as seen with enzymes that flip DNA bases out of the helix.<sup>25</sup> This CT chemistry has been used to develop electrochemical sensors that detect base lesions, mismatches, and DNA-binding proteins on DNA-modified electrodes.<sup>18,25-27</sup> Charge can be transported through DNA over long molecular distances, and the distance dependence of CT is quite shallow.<sup>23</sup> In fact, charge can be efficiently transported through at least 100 base pairs, and over this distance the rate is still limited by transport through the linker rather than the DNA base stack.<sup>28,29</sup> Given that DNA CT can occur over long molecular distances and can be modulated by DNA-binding proteins, does DNA-mediated CT play a general role within the cell?

Recently DinG, a DNA damage response helicase from *E. coli*, was shown to contain a 4Fe-4S cluster.<sup>30</sup> DinG is part of the SOS response, which is activated by DNA

damaging agents and cellular stressors. DinG shares homology with the nucleotide excision repair protein XPD as well as with a host of Superfamily 2 helicases from archaea and eukaryotes that are linked to human disease and share a conserved 4Fe-4S domain.<sup>5</sup> DinG unwinds DNA that has single-stranded overhangs with a 5' to 3' polarity.<sup>31</sup> DNA-RNA hybrid duplexes that form within a DNA bubble, termed R-loops, represent a unique substrate that DinG has been shown to unwind *in vitro*.<sup>32</sup> Importantly, DinG is required to unwind R-loops *in vivo* in order to resolve stalled replication forks and thus to maintain the integrity of the genome.<sup>33</sup> Here we examine the DNA-bound redox properties of DinG and explore more generally crosstalk among redox-active DNA-processing enzymes in *E. coli* via 4Fe-4S clusters.

## **Materials and Methods**

### *DNA, plasmids, and Strains used in these experiments*

The DNA including substrates and PCR primers used within the DinG experiments are presented below in Table 2.1, the plasmids in Table 2.2, and the strains in Table 2.3.

**Table 2.1** Oligonucleotides for electrochemistry substrates, gene replacements, sequencing or colony PCR, and site-directed mutagenesis

Designation and use	Sequence (5' to 3') (bases highlighted in red yield the point mutation after SDM)
Primer for cloning <i>dinG</i> forward	GGTTTTCCCATGGCATTAAACCGCC
Primer for cloning <i>dinG</i> reverse	CATCATTAAGCTTCCGACGGCGT
pET28b- <i>dinG</i> insert sequencing forward 1	T7 promoter primer
pET28b- <i>dinG</i> insert sequencing forward 2 (within gene)	ACTGACGCCGAACAATCAGGA
pET28b- <i>dinG</i> insert sequencing reverse 1	T7 terminator primer
pET28b- <i>dinG</i> insert sequencing reverse 2 (within gene)	TTCGGCAAATGACTGTAAGCCCAC
Substrate for electrochemistry – 20-mer thiolated modified strand	HS-C6-GTGCTGCAACGTGTCTGCGC (annealed with either the well-matched complement or abasic complement to yield the substrate used in experiments)
Substrate for electrochemistry – 35-mer complementary strand for well-matched substrate	AGACTGCAGACGAGAGCGCAGACACG TTGCAGCAC
Substrate for electrochemistry – 35-mer complementary strand for abasic substrate	AGACTGCAGACGAGAGCGCAGACACG TTGCA_CAC (“_” represents an abasic site)
AFM substrates	3.8 kb long strands and 1.6 or 2.2 kb shorts strands were prepared as described previously <sup>30</sup> (22, 35)
$\Delta$ <i>dinG</i> ::cm <sup>R</sup> , forward primer	CCGAAAAATGCCACAATATTGGCTGTT TATACAGTATTTTCAGGTTTTCTCGTGTA GGCTGGAGCTGCTTC
$\Delta$ <i>dinG</i> ::cm <sup>R</sup> , reverse primer	CCGAAAAATGCCACAATATTGGCTGTT TATACAGTATTTTCAGGTTTTCTCGTGTA GGCTGGAGCTGCTTC
$\Delta$ <i>dinG</i> ::cm <sup>R</sup> , sequencing forward	GATGGTGTCTTGCATGACGTG
$\Delta$ <i>dinG</i> ::cm <sup>R</sup> , sequencing reverse	TCAATACGCCGCCCAACTCA
SDM reverse primer for generation of pBBR1-MCS4 <i>nth</i> Y82A	CGATTGGGCTTGCTAACAGCAAAGCAG AAAATATCATCAAAACCTGC

SDM forward primer for generation of pBBR1-MCS4 <i>nth</i> D138A	CTATTCGTGTCGCCACGCACATTTTCCG CGTTTGTAATC
SDM reverse primer for generation of pBBR1-MCS4 <i>nth</i> D138A	CGGAAAATGTGCGTGGCGACAGCAAT AGTCGGCCAGC
pBBR1MCS-4- <i>nth</i> sequencing forward	GGTGCTGATGCCGCTGGCGATTCAG
pBBR1MCS-4- <i>nth</i> sequencing reverse	TGTGCTGCAAGGCGATTAAGTTGG
Genomic <i>nth</i> region check forward 1	GAGATCCGCATTCCCATTTA
Genomic <i>nth</i> region check reverse 1	GGCTTAACGGCGATATGTTC
InvA check 1 from (33)*	CCAGTCATTTGGCGAAAG
InvA check 2 from (33)*	GGCGTAATAGCGAAGAGG

\*Used together as primers in PCR to amplify a ~4250 bp product if *rrnA* is inverted

**Table 2.2** Plasmids used for DinG experiments

<b>Plasmid Designation</b>	<b>Description</b>	<b>Source, reference, or method to construct</b>
pBBR1MCS-4 or p(empty)	pBBR1MCS-4, a vector for the constitutive expression of genes placed in the MCS (multiple cloning site)	(22)
pBBR1MCS-4- <i>nth</i> or p(WT EndoIII)	pBBR1MCS-4 carrying the <i>nth</i> gene in the MCS, constitutively expresses WT EndoIII	(22)
pBBR1MCS-4- <i>nth</i> D138A or p(EndoIII D138A)	pBBR1-MCS4 carrying the <i>nth</i> D138A gene in the MCS, constitutively expresses EndoIII D138A	Site-directed mutagenesis of pBBR1MCS-4- <i>nth</i> using SDM primers listed in Table 2.3.
pBBR1MCS-4- <i>nth</i> Y82A or p(EndoIII Y82A)	pBBR322-MCS4 carrying the <i>nth</i> Y82A gene in the MCS, constitutively expresses EndoIII Y82A	Site-directed mutagenesis of pBBR1MCS-4- <i>nth</i> using Y82A forward and reverse primers listed in Table 2.2
pET-28b- <i>dinG</i>	Overexpresses DinG in presence of IPTG	Insertion of <i>dinG</i> amplicon into pET-28b(+) (Novagen) as described above (30)
pEM-Ap <sup>R</sup> or p(RNaseH)	pACYC184 derived vector carrying the <i>rnh</i> <sup>+</sup> gene and an Ap <sup>R</sup> gene, overexpresses RNaseH	Gift from Dr. Bénédicte Michel (Le centre de la Recherche Scientifique, Gif-sur-Yvette, France) (33)

**Table 2.3** Strains used in DinG experiments

Strain	Genotype designation	Source, reference, or method to construct
<b>Lac<sup>+</sup> forward reversion assay, a GC:TA transversion assay to probe MutY activity</b>		
CC104	F128-(CSH104) <i>lacI373, lacZ574, ara-600, Δ(gpt-lac)5, λ, relA1, spoT1, thiE1</i>	(22)
CC104 <i>ΔdinG</i>	CC104 <i>ΔdinG::cm<sup>R</sup></i>	Inactivation of <i>dinG</i> by replacement with <i>cm<sup>R</sup></i> using pKD3 and pKD46 (CGSC & 7)
<b>InvA <i>Δnth</i> R-loop assay to probe DinG activity</b>		
JW1625-1	F-, <i>Δ(araD-araB)567, ΔlacZ4787(::rrnB-3), λ, Δnth-782::kan, rph-1, Δ(rhaD-rhaB)568, hsdR514</i>	Obtained from Coli Genetic Stock Center (Yale University, New Haven, CT)
BW16847	F-, <i>Δ(codB-lacI)3, ΔphoA532, pdxH15(Am), purR106::Tn10, Δ(phnP-phnD)3330(phnC?)</i>	Obtained from Coli Genetic Stock Center (Yale University, New Haven, CT)
InvA	MG1655 <i>ΔlacZ ΔattB::spcR Inv (attL15-cm<sup>R</sup> attR75-kan<sup>R</sup>)</i>	Gift from Dr. Bénédicte Michel at the Centre de Génétique Moléculaire (CNRS) (33)
MG001	BW16847 <i>Δnth::kan<sup>R</sup></i>	BW16847 * P1 JW1625-1
InvA <i>Δnth</i>	InvA <i>Δnth::kan<sup>R</sup>, pdxH15(Am), purR106::Tn10</i>	MG001 * P1 InvA and colony PCR to find colonies with the <i>Δnth::kan<sup>R</sup></i> locus
InvA <i>ΔpurR</i>	InvA <i>purR106::Tn10</i>	MG001 * P1 InvA and colony PCR to find colonies without the <i>Δnth::kan<sup>R</sup></i> locus

### *Expression and Purification of DinG.*

The *dinG* gene was amplified from *E. coli* using previously published primers and was inserted into a pET-28 b (+) vector (Novagen) using standard molecular cloning techniques (Table 2.1).<sup>30</sup> An Expand High Fidelity PCR system (Roche) was used to amplify the *dinG* gene from the *E. coli* genome. The restriction enzymes used to restrict the *dinG* gene insert and the pET-28b(+) vector were NcoI-HF (New England Biolabs) and HindIII (New England Biolabs). The restricted vector was then treated with Antarctic phosphatase (New England Biolabs). To ligate the restricted gene insert and vector, T4 DNA Ligase (New England Biolabs) was used. The ligation reaction mixture was then transformed into NovaBlue Singles competent cells (Novagen). The plasmid DNA was purified using a Miniprep kit (Qiagen) and plasmids with molecular weights that matched the expected size of the desired construct were isolated. After the vector was isolated, the cloned *dinG* gene was sequenced (Laragen) using the primers listed in Table 2.1. An aliquot of BL21(DE3) competent cells (Invitrogen) was then transformed with the pET28b-*dinG* vector. The constructed pET28b-*dinG* vector encodes for DinG with a C-terminal hexahistidine affinity tag under control of the T7 promoter. In BL21(DE3) cells, expression of DinG is driven by the addition of Isopropyl  $\beta$ -D-1-thiogalactopyranoside (IPTG).

To express DinG, six liters of LB, which had been inoculated with an overnight culture of BL21(DE3) cells harboring the pET28b-*dinG* vector, were shaken at 37 °C. After the cultures reached an O.D. of ~0.6-0.8, enough IPTG (Research Products International Corp.) was added to bring the concentration of IPTG in each flask to 150  $\mu$ M. The flasks were then returned to the incubator, which had been cooled to ~22 °C. After

~16 hours of IPTG induction at ~22° C, the cells were collected by centrifugation at 5,500 rpm for 15 minutes. The cell pellets were frozen at -80 °C.

To purify DinG, the cell pellets were resuspended in 300 mL buffer A (20 mM Tris-HCl, 8.0 pH at 4 °C, 0.5 M NaCl, and 20% glycerol) with added DNaseI from bovine pancreas (10 kU, Sigma), RNase (Roche), and Complete Protease Inhibitor Cocktail Tablets (Roche). The cells were lysed using microfluidization. The lysate was centrifuged at 12,000 rpm for 45 minutes, and the supernatant from the cell lysate was filtered and loaded onto a 5 mL Histrap HP (GE healthcare) nickel-affinity column that had been equilibrated with buffer A. The column was then connected to an ÄKTA FPLC (fast protein liquid chromatography, GE healthcare) and was washed with 3-5 column volumes (CV) of buffer A. The protein was eluted using a linear gradient from 0-20% buffer B (20 mM Tris-HCl, 8.0 pH at 4 °C, 0.5 M NaCl, 500 mM imidazole, and 20% glycerol) over 10 CV, followed by a linear gradient from 20-30% buffer B over 10 CV. Fractions containing the desired protein, which were yellow and eluted at ~150 mM imidazole, were desalted into buffer C using a Hiprep 26/10 desalting column (GE healthcare). The collected protein was then concentrated down to 10-13 mL using an Amicon Ultra-15 centrifugal filter unit (Millipore) and loaded onto a Hiload Superdex 200 26/600 pg (GE healthcare) that had been equilibrated with buffer C. The protein eluted after ~180 mL of buffer C (20 mM Tris-HCl, 8.0 pH at 25 °C, 0.5 M NaCl, and 20% glycerol) had passed over the column. The purity of the protein was confirmed using SDS-PAGE (Figure 2.1). Using an extinction coefficient at 278 nm of  $80,435 \text{ M}^{-1} \text{ cm}^{-1}$  for DinG as previously estimated, and an extinction coefficient at 410 nm of  $\sim 17,000 \text{ M}^{-1} \text{ cm}^{-1}$ , characteristic of [4Fe-4S] clusters coordinated by four cysteines, the

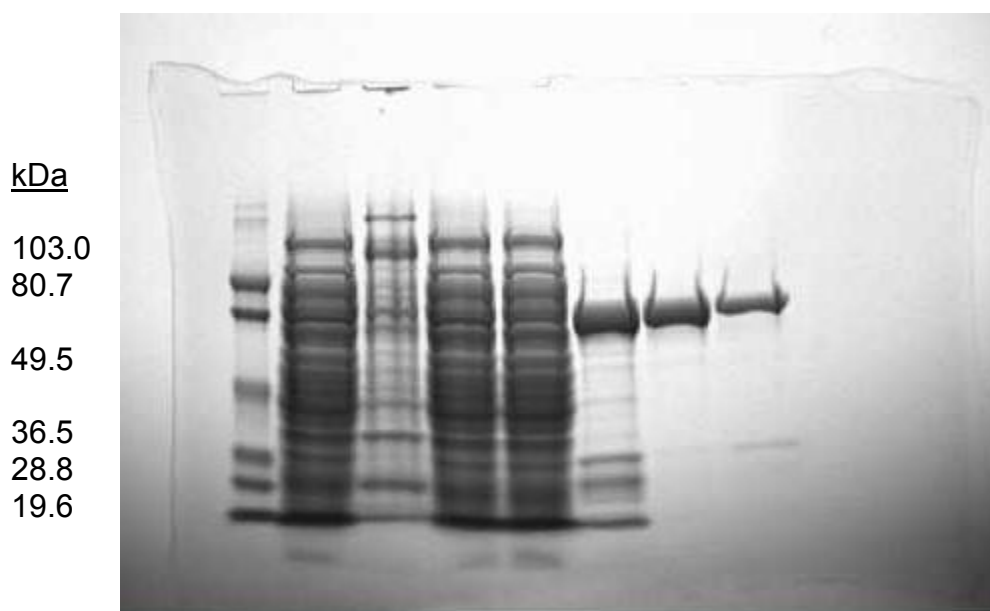


**Figure 2.1** SDS-PAGE gel for purification of DinG. Lanes are referred to as 1 to 8 from left to right. The lanes contain an SDS-PAGE weight standard-low range (Biorad) (lane 1), the supernatant from the cell lysate (lane 2), the pellet from the cell lysate (lane 3), the filtered cell lysate (lane 4), the the Histrap HP column flow-through (lane 5), the collected fractions from the Histrap HP column (lane 6), the collected fractions from the Superdex 200 column (lane 7), and a 10x dilution of the stored protein after thawing (lane 8). Corresponding molecular weights for each of the six bands in the weight standard lane are designated to the left of the image.

cluster-loading of the protein was routinely >80%.<sup>30</sup> A helicase activity assay for DinG, modified from previously published procedures, was used to show that the protein is active after purification.<sup>30,32</sup>

#### *DNA-modified DinG Electrochemistry*

The DNA substrate used for the electrochemical characterization of DinG was either a well-matched 20-mer DNA oligomer with a 15-mer 5' to 3' single-stranded overhang or the same substrate with the exception of an abasic site being placed on the complementary strand four base pairs from the bottom of the duplex (Table 2.1). A 20-mer strand of DNA with a terminal thiol and 6-carbon linker at the 5' end of the strand was annealed to a 35-mer unmodified strand of DNA to yield the electrochemical substrate. The electrochemical substrate was designed to be competent to unwind by DinG in a helicase reaction. Single-stranded DNA stimulates the ATPase activity of DinG, which requires at least a 15-mer single-stranded 5' to 3' overhang in order to unwind DNA substrates *in vitro*.<sup>32</sup> In the electrochemical cell, the DNA substrate is covalently tethered to the gold surface via a gold-thiol bond.

The thiol-modified strand was synthesized on a 3400 Applied Biosystems DNA synthesizer using standard phosphoramidite chemistry. The complementary strands were purchased from IDT. All phosphoramidites, including the terminal phosphoramidite containing a 6-carbon disulfide linker were purchased from Glen Research. The thiol-modified and complementary strands were purified by HPLC using an analytical C-18 column (Agilent). DNA strands were characterized by MALDI mass-spectroscopy. The

DNA was quantified by UV-Visible absorbance and equimolar amounts were annealed yielding the duplex substrate.

To prepare DNA-modified single electrodes, a 50  $\mu\text{M}$  solution of the DNA substrate (5  $\mu\text{M}$  phosphate, 50 mM NaCl, pH  $\sim$  7.0) was incubated overnight at ambient temperature on a bare gold on mica surface (Agilent) in an electrochemical cell with a capacity of 50  $\mu\text{L}$ . Following incubation with the DNA solution, the surface was rinsed and backfilled by incubating the electrode with 1 mM 6-mercapto-1-hexanol (5% glycerol, 100 mM NaCl, 1 mM EDTA, 20 mM Pi, pH  $\sim$  7.5) for 45 minutes at room temperature. Multiplex chip electrodes were prepared as described previously.<sup>29,34</sup> The well-matched electrochemistry substrate was used for all single electrode experiments. For experiments with multiplex chip electrodes, the well-matched and abasic-site substrates were laid down side-by-side in separate quadrants on a single chip.<sup>29,34</sup>

After backfilling, the DNA-modified electrodes were rinsed with the electrochemistry buffer (4 mM spermidine, 4 mM  $\text{MgCl}_2$ , 0.25 mM EDTA, 20% glycerol, 250 mM NaCl, 20 mM tris-HCl, pH  $\sim$ 8.5). Protein concentration was measured by UV-Visible absorbance using an extinction coefficient at 410 nm of  $17,000 \text{ M}^{-1} \text{ cm}^{-1}$ .<sup>22</sup> An aliquot of 20  $\mu\text{M}$  DinG was flash-thawed by incubating it in a room temperature water-bath. The protein's buffer was exchanged for the electrochemistry buffer by diluting the protein 2-fold into 2x spermidine buffer (8 mM spermidine, 8 mM  $\text{MgCl}_2$ , 1 mM EDTA, 20 mM tris-HCl, pH  $\sim$ 9.0).

Electrochemical measurements were made using a CHI620D Electrochemical Analyzer. For cyclic voltammetry, sweeps within a window from -0.4 V vs. Ag/AgCl to 0.1 or 0.2 V were carried out at a scan rate of 50 mV/s for several hours. For

electrochemistry measurements on single electrodes with ATP, 1 mM ATP, or 1 mM ATP $\gamma$ S (Sigma) was added after the electrochemical signal grew into an appreciable size (>20 nA). Cyclic voltammetry was then used to scan the electrode over several hours.

#### *Atomic Force Microscopy Redistribution (AFM) Assay*

AFM experiments were performed using a protocol similar to that reported previously with the following modifications.<sup>22,35</sup> The long and short strands of DNA have an identical sequence as they were both amplified off of the pUC19 plasmid with primers containing a 2' *O*-methyl residue to generate 1.8 and 2.2 kb strands of DNA with 14-mer single-stranded overhangs, so that the two could be subsequently ligated. For well-matched long strands of DNA, the two PCR products were annealed with complementary 14 bp overhangs. For the mismatched long strands of DNA, the strands were annealed in the same way except one of the PCR products contained a 14 bp overhang with a single base changed to yield a C:A mismatch upon the annealing of the 2 strands. Prior to deposition, the protein and DNA solution was incubated at 4 °C for 2 hours. The sample was then deposited (5–10  $\mu$ L) onto a freshly cleaved mica surface for 2 min, rinsed with 2 mL of water, and dried under argon. The concentration of DinG was 60 nM for AFM experiments with DinG. For AFM experiments with mixtures of DinG and EndoIII or DinG and EndoIII Y82A, the concentration of each protein was 30 nM.

Images of protein and DNA mixtures that had been deposited on dry mica surfaces were gathered using a Bruker Dimension Icon AFM (Beckman Institute MMRC). Images were captured in air with scan areas of  $2 \times 2 \mu\text{m}^2$  or  $3 \times 3 \mu\text{m}^2$  in soft tapping mode, and a scan rate of 3.00 Hz. RFESPA silicon AFM probes with reflective aluminum backing

(Bruker), with a spring constant of 3 N/m and a resonance frequency of 69-81 kHz, were used for gathering images.

Bruker nanoscope analysis software was used to measure general DNA contour lengths and height profiles of the proteins. For each dataset, images from at least three independently prepared surfaces were analyzed. At least 50 images were analyzed for both the mismatched DNA-protein samples and the well-matched samples. The binding density ratio,  $r$ , is defined as the ratio of the density of proteins bound on the long strands of DNA divided by the density of proteins bound on the short strands of DNA. The density of proteins on each strand is found by dividing the number of proteins by the length of the DNA strands, 3.8 kb pairs for the long strand and 1.9 kb pairs, which is the average length of the short strands, for short strands. Error represents SEM ( $n \geq 3$ ) for each experiment. Distinguishable strands and bound proteins were counted by hand. In order to control for bias, for each experiment, images were randomly assigned identification numbers. The images were then scored blindly. The number of long strands, proteins on long strands, short strands, and proteins on short strands was collected for each image.

An alternative way to calculate the binding density ratio is to treat each individual image as a sample, to plot them as a histogram (Figure 2.2) and to find the mean of the normal distribution. Using this methodology, instead of treating each surface as an individual experiment, a binding density ratio of  $1.61 \pm 0.08$  is found for DinG with mismatched DNA. A binding density ratio of  $1.40 \pm 0.05$  is found for DinG mixed with EndoIII and mismatched DNA. Finally a binding density ratio of  $0.91 \pm 0.04$  is found for DinG mixed with EndoIII Y82A.

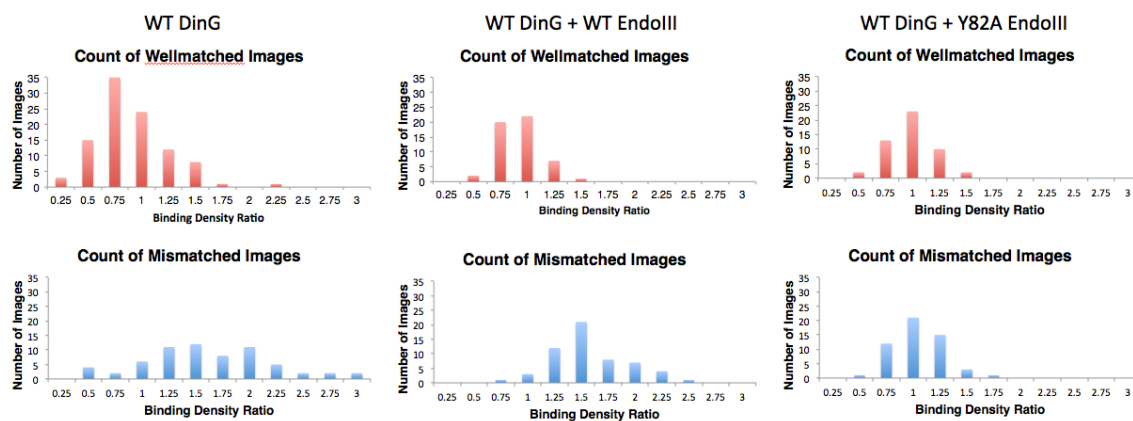


**Figure 2.2** Statistical data for the AFM experiments. Histograms showing the distribution of binding density ratios within the population of sample images. The value on the x-axis is the upper range of a .25 unit wide separation, meaning that the column plotted above “1” is the number of images with a binding density ratio between 0.75 and 1.

Because the AFM images are snapshots of the system near equilibrium, the number of bound proteins on strands reflects the apparent non-specific binding affinity of the proteins for DNA. As such, another way to analyze the data would be to qualitatively analyze the apparent binding affinity of each protein in the different experiments by visualizing the occupancy of the DNA, i.e., the percent of DNA with a minimum of 1, 2, 3, or 4 proteins on a strand of DNA. Since DNA-binding proteins with 4Fe-4S clusters have a lower DNA binding affinity when the cluster is in the reduced vs. oxidized (19), in a collection of proteins, some reduced and some oxidized, CT between proteins should affect the overall effective binding affinity for DNA. Conversely, if only one protein is bound to DNA, its affinity would not be affected by DNA CT. This was observed for mixtures of DNA and DinG (Figure 2.3), which also indicates that DinG does not preferentially bind a mismatch. The same was observed for mixtures of DinG with WT EndoIII, or with EndoIII Y82A; the percent of long, well-matched strands with one protein bound is the same for DinG/EndoIII and DinG/Y82A mixtures (Figure 2.4). If more than one protein is bound to a given strand, however, each subsequent protein that binds has a probability to transport charge through the DNA and promote another protein's dissociation, in a way that parallels anti-cooperative binding. If a mismatch is present, which attenuates CT, however, this anti-cooperative effect would be lessened as it would if EndoIII Y82A is substituted for EndoIII, decreasing the concentration of signaling partners. This is precisely what is observed (Figures 2.3 and 2.4). The percentage of long strands with a minimum of 2, 3, or 4 bound DinG proteins is lower for DinG when there is no mismatch than when there is a mismatch.

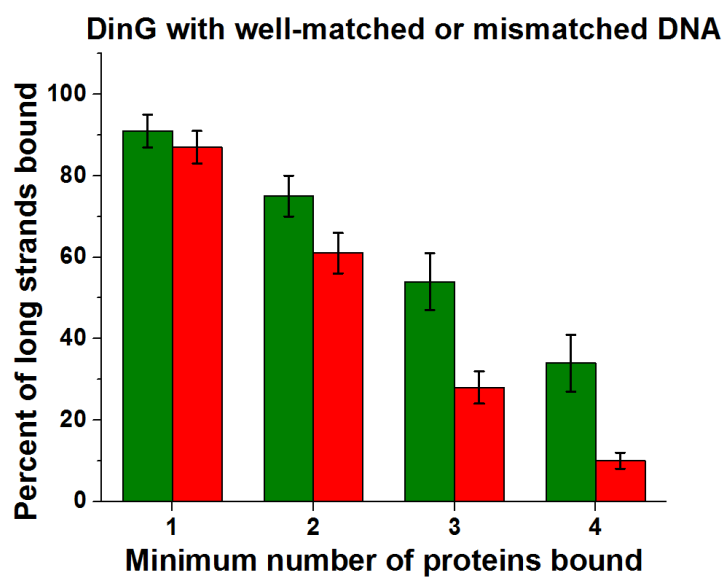


**Figure 2.3** Occupancy of DinG on long strands of DNA. The percent of long strands of either well-matched (green) or mismatched (red) DNA is plotted against the minimum number of proteins bound to a strand.

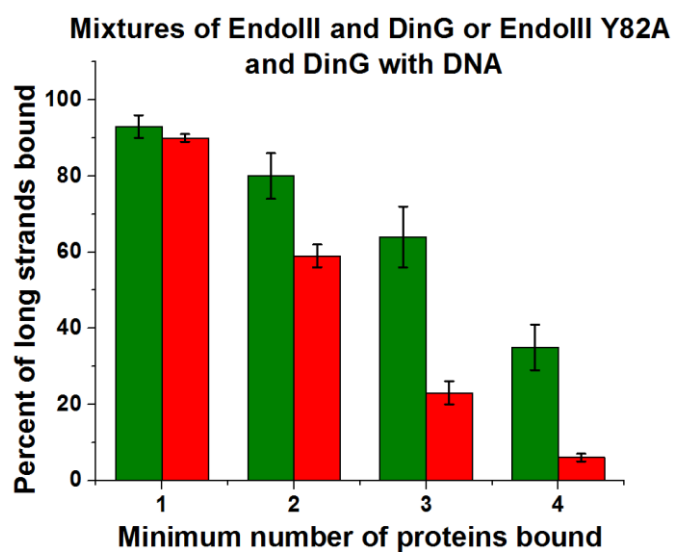


**Figure 2.4** Occupancy of either EndoIII and DinG or EndoIII Y82A and DinG on long strands of well-matched DNA. The percent of well-matched long strands of either EndoIII and DinG (green) or EndoIII Y82A (red) DNA is plotted against the minimum number of proteins bound to a strand.

When DinG is mixed with EndoIII compared to EndoIII Y82A, an anti-cooperative effect is once again observed. There is a decreased percentage of long strands of DNA bound with a minimum of 2, 3, or 4 proteins for DinG and EndoIII compared to DinG and EndoIII Y82A. This observation, especially when considered in conjunction with their similar population of single-bound-protein-DNA complexes, further supports the ability of DinG and EndoIII to cooperate using DNA-mediated CT.

*MutY activity assay (CC104 lac<sup>+</sup> forward reversion assay)*

The method used to inactivate *dinG* on the genome within the CC104 strain was adapted from a previously published procedure.<sup>36</sup> The FRT-flanked chloramphenicol acetyltransferase gene, *cat*, from pKD3 was amplified by PCR using the  $\Delta$ *dinG*::cm<sup>R</sup> forward primer and  $\Delta$ *dinG*::cm<sup>R</sup> reverse primer (Table 2.1). Following inactivation of *dinG* in the CC104 strain, colony PCR with the  $\Delta$ *dinG*::cm<sup>R</sup> forward and reverse sequencing primers (Table 2.1) was performed to confirm *dinG* had been replaced by *cat*. All PCR products were sequenced to confirm that the chromosomal gene disruption was successful (Laragen).

All mutant EndoIII plasmids, which were derived from pBBR1MCS-4,<sup>37</sup> were generated using a QuikChange II Site Directed Mutagenesis kit (Agilent). The pBBR1MCS-4, pBBR1MCS-4-*nth*, pBBR1MCS-4-*nth* D138A, and pBBR1MCS-4-*nth* Y82A plasmids encode and constitutively express no protein, WT EndoIII, EndoIII D138A, and EndoIII Y82A, respectively. The pBBR1MCS-4 derived plasmids are referred to as p(empty), p(WT EndoIII), p(EndoIII D138A), and p(EndoIII Y82A), respectively, throughout the text as indicated in Table 2.2. The p(WT EndoIII) plasmid

that was used as the template for the site-directed mutagenesis reactions was previously constructed in our laboratory.<sup>22</sup> The primers outlined in Table 2.1 were used to make the p(EndoIII Y82A) and p(EndoIII D138A) mutant plasmids. The isolated plasmids were sequenced (Laragen) using the forward and reverse pBBR1MCS-4-*nth* sequencing primers (Table 2.1) to verify that the desired mutation had been made in the *nth* gene.

The MutY activity assay was adapted from a previously published procedure.<sup>22,38</sup> The CC104 or CC104  $\Delta$ *dinG::cm<sup>R</sup>* strains were transformed by electroporation with the p(EndoIII D138A), p(empty), and p(EndoIII Y82A) plasmids (Table 2.2). Following transformation, the cells were recovered in 1 mL LB for 2 hours. The cells were spread on LB ampicillin (100  $\mu$ g/mL) agar plates and incubated for 16 hours, after which a single transformant was restreaked onto a fresh LB ampicillin (100  $\mu$ g/mL) agar plate. These plates were incubated at 37°C for 12 hours.

One colony from each strain was used to inoculate a 1 mL LB ampicillin (100  $\mu$ g/mL) culture. These cultures were incubated with shaking at 37°C for 16 hours. Next, 250  $\mu$ L of each culture was spread onto NCE lactose (0.2% w/v) ampicillin (40  $\mu$ g/mL) agar plates, and incubated at 37°C. The number of colony-forming units, representing *lac*<sup>+</sup> revertants, was counted after 48 hours. Differences for growth between strains was monitored by evaluating the number of colony forming units on NCE glucose (0.2% w/v) ampicillin (40  $\mu$ g/mL) agar plates. Note that we assay for MutY activity rather than EndoIII since the frequency of spontaneous GC:TA transversions associated with 8-oxoG:A repair by MutY is far greater than the pyrimidine lesions repaired by EndoIII.

*InvA Anth growth assay*

The genomic *nth* gene, encoding EndoIII, was knocked out of the InvA strain using P1 phage transduction.<sup>39</sup> The P1 *vir* phage was obtained from the Coli Genetic Stock Center (Yale). To amplify the concentration of the phage, an overlay plate method was used to infect a fresh culture of MG1655 cells. Briefly, 100 microliters of an overnight culture of MG1655 cells was added to 4 mL of LB overlay (5 mM CaCl<sub>2</sub>, 0.4% agar, LB, at 50 °C) and spread onto a pre-warmed LB plate. 1.5 microliters of P1 *vir* phage was added to the center of the overlay. The overlay was then grown up overnight. Where the phage had been aliquoted, a large semi-transparent viral plaque arose. By core-sampling the resulting plaque, enough P1 *vir* phage could be used to infect a donor strain, in this case, JW1625-1. As such, 400 microliters of an overnight culture of JW1625-1 cells was added to 20 mL of LB overlay (0.4% agar, 5 mM CaCl<sub>2</sub>, and LB, at 50 °C). Using a pipettor, the plaque from the MG1655 overlay was sucked up by stabbing it with a 200 microliter pipet tip and dispensed into the 20 mL of LB overlay + JW1625-1, vortexed, and poured this into an empty petri dish. The next day, the petri dish with the LB overlay had dozens of spots that represented viral plaques. The contents of the plate were scooped into a 30 mL centrifuge tube, 500 microliters of chloroform were added, the tube was vortexed, and spun down at 3k rpm for 5 minutes in floor centrifuge. The supernatant was decanted off into a 15 mL falcon tube and stored at 4 °C, yielding JW1625-1 P1 lysate.

Now, the P1 lysate from JW1625-1 was ready to be used to transduce the *nth::kan<sup>R</sup>* marker into the BW16847. A 5 mL culture of BW16847 cells was grown up overnight. 1.5 mL of this culture was spun down and resuspended in 750 microliters of P1 salts (10 mM calcium chloride, and 5 mM magnesium sulfate). Aliquots of 100 microliters of cells were

made. To these aliquots, various amount of P1 lysate were added (100 microliters, 10 microliters, and 1 microliter). The phage was allowed to adsorb for 30 minutes. Next, 1 mL of LB broth and 200 microliters of 1 M sodium citrate were added to each aliquot. Additionally 100 microliters of cells without p1 lysate added were prepared alongside these with the added LB. These cultures were shaken at 37 degrees Celsius for 1 hour. Next, each culture was spun down, resuspended in LB, and spread onto LB + tetracycline (15 µg/mL) + kanamycin (50 µg/mL) + 5 mM sodium citrate. A single colony that arose on these plates was restreaked onto fresh LB + tetracycline (15 µg/mL) + kanamycin (50 µg/mL) + 5 mM sodium citrate plates two times in succession.

Next, a P1 lysate for the newly generated strain, termed MG001 in Table 2.3, was prepared using the same methods that were used to obtain the JW1625-1 lysate. This lysate was used to infect cells from the InvA strain using the same methods used to obtain the MG001 strain. After infection, the infected cells were spread onto LB + tetracycline (15 µg/mL) + kanamycin (50 µg/mL) + 5 mM sodium citrate. Single colonies that arose on these plates were restreaked onto fresh LB + tetracycline (15 µg/mL) + kanamycin (50 µg/mL) + 5 mM sodium citrate plates two times in succession. Colony PCR using a GoTaq PCR kit (Promega) and using the forward and reverse genomic *nth* region check primers listed in Table 2.3. Since the kan<sup>R</sup> and *nth* genes have different sizes, separation of the PCR products on a 1.4% agarose gel, followed by visualization, can be used to check which colonies have the new *nth::kan<sup>R</sup>* marker within the InvA genetic background. Note that in addition to the Tn10 transposon, a mutation in the *pdxH* gene was also carried into the InvA background.

One of the hits from the P1 phage transduction contained the *nth* knockout in InvA (InvA  $\Delta nth$ ). Plasmids that constitutively express various mutants of EndoIII were prepared as outlined in the MutY activity assay section above. The EndoIII plasmids p(WT EndoIII), p(EndoIII D138A), p(EndoIII Y82A), and p(empty), in addition to an RNaseH overexpression plasmid (Table 2.2) designated p(RNaseH), were transformed into the InvA  $\Delta nth$  strain using standard electroporation techniques. Colony PCR using the InvA check 1 and check 2 primers (Table 2.1) was used to verify that InvA-derived strains still contained the inverted *rrnA* operon after these genetic manipulations and transformations. Colony PCR with the genomic *nth* check primers (Table 2.1) was used to verify that the *nth* gene was knocked out of each putative  $\Delta nth$  strain.

Growth curves of the InvA  $\Delta nth$  strain in addition to InvA  $\Delta nth$  transformed with p(WT EndoIII), p(EndoIII Y82A), p(EndoIII D138A), p(empty), or p(RNaseH) were used to assess the effect of knocking out the *nth* gene from the InvA background. Single colonies from LB ampicillin (100  $\mu\text{g}/\text{mL}$ ) or LB plates for each of the strains were used to inoculate separate cultures of LB, LB ampicillin (100  $\mu\text{g}/\text{mL}$ ), MM (M9 + 0.2% glucose),<sup>40</sup> or MM ampicillin (100  $\mu\text{g}/\text{mL}$ ). Cell growth was then monitored through measurement of the optical density at 600 nm for each of the cultures over time in LB or MM.

## Results and Discussion

### DNA binding activates DinG towards reduction and oxidation at cellular redox potentials

DNA-modified electrodes were utilized to explore the DNA-bound redox chemistry of DinG. Cyclic voltammetry of the protein on gold electrodes modified with a 20-mer duplexed DNA oligomer appended with a 15-base 5' single-stranded overhang displays a reversible redox potential for DinG of 80 mV vs. NHE (Figure 2.5). This DNA-bound potential differs from the midpoint redox potential of  $\sim -390$  mV vs. NHE assigned to the  $[4\text{Fe-4S}]^{2+/1+}$  couple of the cluster observed in the absence of DNA as measured by titrations with redox mediators.<sup>30</sup> Cyclic voltammetry of DinG on multiplexed electrodes reveals that a single abasic site placed in the DNA duplex attenuates the current by  $12 \pm 3\%$ , consistent with the signal being DNA-mediated.<sup>23,34</sup> Moreover, upon addition of ATP to DinG bound to DNA-modified electrodes, the reductive and oxidative peak currents markedly increase; ATP $\gamma$ S, which is poorly hydrolyzed, does not yield a significant increase in current (Figure 2.5). Thus, it appears that the ATPase activity of DinG can be monitored electrically, even though ATP hydrolysis is a redox-independent process. It is interesting to consider that this electronic signaling of activity may be used within a biological context.

### EndoIII and DinG use DNA CT to redistribute to sites of DNA damage

Given that DinG displays a DNA-bound potential similar to that of EndoIII of  $\sim 80$  mV vs. NHE, we sought to test whether EndoIII and DinG can signal to one another via DNA CT *in vitro* to aid one another in finding lesions that disrupt CT.

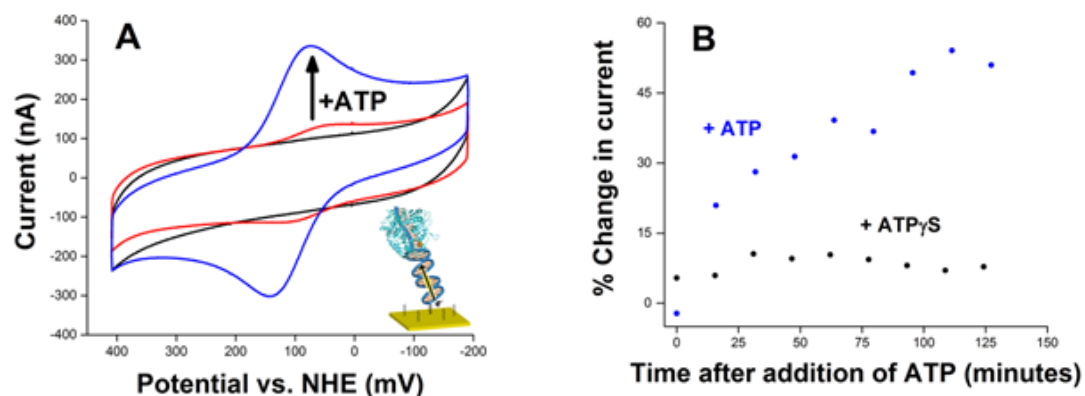


**Figure 2.5** Electrochemistry of DinG on DNA-modified electrodes. (A) Cyclic voltammogram of 10  $\mu$ M DinG (red), DinG after the addition of 5 mM ATP (blue), and buffer only (black) after incubation for three hours. Inset: Cartoon representation of a protein bound to DNA on a DNA-modified electrode. (B) Percent change in current after the addition of 1 mM ATP (blue) or 1 mM ATP <sub>$\gamma$</sub> S (black). Percent change in current is the percent increase in the measured current compared to the predicted current, based on the linear growth of the signal with respect to time for the incubation of DinG before the addition of ATP.

It is noteworthy that both repair proteins are involved in finding lesions that interrupt DNA CT. Using atomic force microscopy (AFM), we examined whether the DinG helicase would redistribute onto 3.8 kilobase (kb) DNA strands containing a single base mismatch, which interrupts DNA CT, rather than remaining bound to well-matched DNA strands. Our model for how repair proteins utilize DNA CT predicts such a redistribution as a first step in repair (*vide infra*), and this assay provides direct support for the model. If proteins of similar potential carry out DNA CT on well matched DNA strands and dissociate from DNA upon reduction, they should preferentially redistribute onto DNA strands where DNA CT is inhibited by an intervening mismatch. Note that, while a single base mismatch inhibits DNA CT, it is not a substrate for either DinG or EndoIII binding. We have utilized this AFM assay previously to test EndoIII redistribution as a first step in finding damage.<sup>22</sup> We have also utilized this assay to test CT signaling between EndoIII and *S. acidocaldarius* XPD (SaXPD), which also contains a 4Fe-4S cluster with a DNA-bound potential of ~ 80 mV vs. NHE, in locating DNA damage;<sup>21,35</sup> these proteins are present in completely distinct organisms, but based on their shared DNA-bound potential, are able to signal one another using DNA CT.

In this AFM assay, DNA-protein mixtures are deposited onto a dry mica surface on which single molecules of both free and protein-bound DNA can be visualized.<sup>22,35</sup> Duplexes of DNA that contain a single C:A mismatch located in the middle of the strand are mixed with fully matched DNA. These strands can be distinguished in the AFM by their difference in length: the mismatched strands are ~3.8 kb pairs long while the matched strands on average contain ~1.9 kb pairs (Figure 2.6). They share DNA sequence since the 3.8 kb strands are prepared by ligation of the two shorter strands.<sup>22,35</sup>

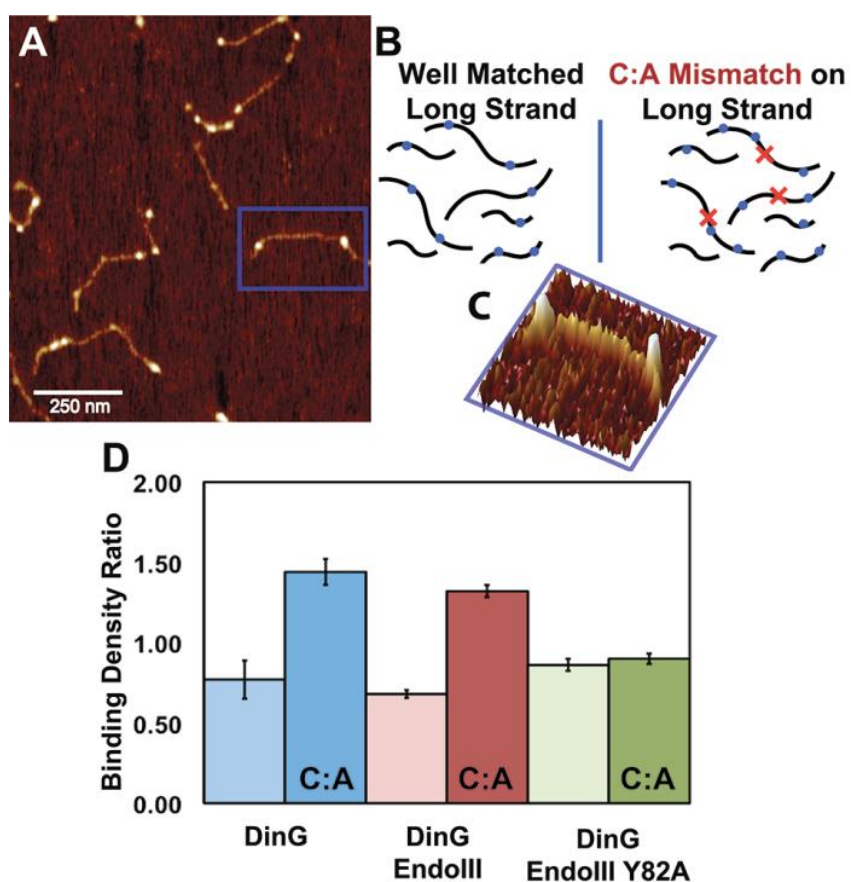


**Figure 2.6** AFM redistribution assay. (A) A flattened image (Bruker nanoscope analysis software) for tapping-mode AFM topography of DinG-bound DNA adsorbed on mica. (B) Schematic representation of the redistribution assay. At equilibrium, repair proteins (blue) are preferentially localized on strands of DNA (black) with a C:A mismatch (red X). (C) 3-dimensional rendering of the blue-bordered region of the AFM image in A that shows a strand of DNA bound by two DinG proteins. (D) Measured binding density ratios, the density of proteins on long strands divided by the density of proteins on short strands, for proteins bound to mixtures of long and short strands of DNA with and without a mismatch (C:A) in the middle of the long strand. Three separate mixtures of protein and DNA were deposited onto individual surfaces and at least fifty images were analyzed for each DinG (blue), a mixture of DinG and EndoIII (red), and a mixture of DinG and a CT-deficient mutant, Y82A EndoIII (green).  $\pm$  SEM using a single image as a data point.

For mixtures of mismatched long strands and well-matched short strands that are incubated with DinG alone, we find an average of  $2.60 \pm 0.22$  proteins bound per mismatched strand compared to  $0.90 \pm 0.17$  proteins per well-matched strand. Calculating the binding density ratio of each independent trial ( $n \geq 3$  for each experiment) and correcting for the lengths of the strands leads to a binding density ratio of  $1.44 \pm 0.08$  (SEM) favoring the mismatched strand. Thus, even though DinG does not bind preferentially to a mismatch, DNA CT by DinG favors its redistribution onto the strand containing the single base mismatch.

Signaling between EndoIII and DinG was also tested by AFM. In 1:1 mixtures of DinG and wild-type (WT) EndoIII, a binding density ratio of  $1.32 \pm 0.04$  favoring the mismatched strand is observed (Figure 2.6). But does this redistribution depend upon DNA CT? In 1:1 mixtures of DinG and EndoIII Y82A, a mutant protein that is defective in DNA-mediated CT,<sup>22,35</sup> a binding density ratio of  $0.90 \pm 0.03$  is found (Figure 2.6); there is no preference for the mismatched strand. This binding density ratio is comparable to what is observed for DinG alone when both strands are fully matched (Figure 2.6); when the proteins cannot carry out DNA CT, they cannot redistribute onto the strand containing the lesion. Since DinG can redistribute in the absence of EndoIII, and DinG and EndoIII can redistribute when mixed only if EndoIII is effective in signaling by DNA CT, these observations support the need for effective signaling between EndoIII and DinG in finding the damaged strand. We have seen comparable results earlier in mixtures of SaXPD and EndoIII.<sup>35</sup>

It should be noted that protein loadings on the 3.8 kb strands are on the order of two proteins per strand under these experimental conditions. Therefore, assuming that DinG

and EndoIII are signaling one another, for approximately half of the strands signaling must occur between DinG and EndoIII rather than just between DinG partners or between EndoIII partners. Moreover, given a loading of about two proteins per strand, these results are consistent with DNA CT occurring over kilobase distances. It is also important to note that these proteins show no evidence of co-localizing at DNA mismatch sites by AFM. Overall, these data demonstrate that DinG and EndoIII can use DNA-mediated CT at long range to cooperate with one another to localize to regions of damage.

### **DinG uses DNA-mediated CT to facilitate the repair of DNA damage by MutY**

To begin to probe DNA-mediated signaling within the cell, a *lac*<sup>+</sup> forward reversion assay reporting on GC:TA transversions that reflects MutY activity within the CC104 strain of *E. coli* was utilized.<sup>38</sup> The CC104 strain reports on GC to TA transversions, which are prevented by MutY excising adenines improperly placed opposite an 8-oxodG lesion, in the *lacZ* gene. Cells in which this transversion process has occurred form colonies on plates containing lactose as the sole carbon source and are termed *lac*<sup>+</sup> revertants. Using this strain, changes in MutY activity can be assessed upon genetically knocking out DinG. If DinG and MutY cooperate in finding DNA lesions that attenuate CT, eliminating DinG from the cell should lead to a decrease in MutY activity and a corresponding increase in *lac*<sup>+</sup> revertants. We and others had earlier seen an effect of knocking out EndoIII on MutY activity in this assay.<sup>22,41</sup> When *dinG* is knocked out of the CC104 strain (CC104  $\Delta$ *dinG*), we find that the number of revertants increases 60% compared to WT CC104 (Table 2.4). While the effect is not high, it is notable given that

#### **Table 2.4 MutY activity assay (CC104 *lac*<sup>+</sup> forward reversion assay)**

Strain	Plasmid <sup>1</sup>	Number of <i>lac</i> <sup>+</sup> Revertants <sup>2</sup>	Relative to CC104 <sup>3</sup>
CC104	p(empty)	4.6 ± 0.4	1
CC104 $\Delta$ <i>dinG</i>	p(empty)	7.5 ± 0.7	1.6*
CC104	p(EndoIII D138A)	8.5 ± 1.1	1
CC104 $\Delta$ <i>dinG</i>	p(EndoIII D138A)	6.7 ± 0.6	0.8*
CC104	p(EndoIII Y82A)	3.4 ± 0.3	1
CC104 $\Delta$ <i>dinG</i>	p(EndoIII Y82A)	5.8 ± 0.8	1.7*

<sup>1</sup> See Table S2 for full plasmid designation

<sup>2</sup> Values for *lac*<sup>+</sup> revertants per 10<sup>9</sup> cells are reported for at least three independent trials (N ≥ 20). ± SEM

<sup>3</sup> Relative to CC104 is defined as the ratio of *lac*<sup>+</sup> revertants for the CC104 *dinG* knockout strain to the number of *lac*<sup>+</sup> revertants for the wild type CC104 strain containing the same plasmid as the CC104 *dinG* knockout strain

\* (p < 0.01)

knocking out MutY itself gives a maximum of 10-15 fold increase in revertant count under similar conditions.<sup>22</sup> It should also be noted that EndoIII and DinG do not have overlapping substrate specificity with MutY. A deletion of the *nth* gene from CC104 in combination with a deletion of the *mutY* gene resulted in the same number of revertants as that of the *mutY* deletion alone.<sup>22</sup> If the effect on MutY activity stems from lowering the concentration of DNA-bound 4Fe-4S proteins that cooperatively signal with MutY, then complementing the cells with a plasmid that expresses a mutant of EndoIII that contains a 4Fe-4S cluster, but is enzymatically inactive, p(EndoIII D138A) (Table 2.4),<sup>22,42</sup> should rescue MutY activity. Indeed, expression of EndoIII D138A restores the activity of MutY in CC104  $\Delta$ *dinG*; the number of revertants found is comparable to WT CC104. However, complementing with a plasmid that expresses an EndoIII mutant, p(EndoIII Y82A), which is defective in DNA CT but nonetheless contains a 4Fe-4S cluster and is enzymatically active,<sup>22</sup> does not rescue MutY activity (Table 2.4). It should be noted that rescue with DinG was not explored, since overexpression of DinG using plasmids was previously observed to be toxic to cells.<sup>33</sup> While these data may not indicate dramatic effects, they are statistically significant and fully consistent with our model. These data thus suggest that MutY, EndoIII, and DinG may be capable of signaling one another via DNA-mediated CT to coordinate their activity in cells.

### **The repair of R-loops by DinG relies on DNA-mediated signaling by EndoIII in *InvA***

Perhaps more interesting to consider is the possibility of signaling in the reverse sense, with a BER protein signaling to DinG to aid DinG in finding its lesions, and here dramatic effects on survival are observed. Does EndoIII signaling aid DinG in locating R-

loops, a substrate of DinG, in *E. coli*? R-loops are RNA:DNA hybrids that perturb duplex base stacking and would be expected to attenuate DNA CT, so that, based on the AFM results, DNA-mediated signaling could help DinG in its first step of finding its substrate. Here we took advantage of a strain, InvA, where the repair of R-loops by DinG is critical for cell survival. In the InvA strain, by inverting a frequently transcribed *rrnA* operon, the incidence of R-loop formation in cells is increased,<sup>33</sup> as a result, replication forks stalling when they collide head-on with the transcription machinery are necessarily amplified in the InvA strain. Resolving stalled replication forks is vital to preventing significantly deleterious DNA damage and thus to survival.<sup>33,43</sup> In previous work it has been shown that within the InvA strain, the repair of R-loops by DinG was shown to be essential to maintain viability; deletion of *dinG* yielded a significant plating defect. Rescue by overexpression of RNaseH is a hallmark of R-loop dependent phenotypes, as RNaseH endonucleolytically degrades RNA within an RNA:DNA hybrid, but not free RNA.<sup>33</sup> Complementing the InvA  $\Delta$ *dinG* strain with a plasmid encoding RNaseH thus rescued activity.<sup>33</sup> Growth assays to test DinG activity using InvA are particularly advantageous in testing signaling with other proteins since the growth defect is dramatic; knocking out signaling partners should similarly yield clearly discernible effects.

To test signaling between EndoIII and DinG, we prepared an EndoIII knockout in the InvA strain (InvA  $\Delta$ *nth*). If signaling with EndoIII is essential for DinG to effectively repair R-loops, consistent with our model, we would expect to observe effects on cell viability upon knocking out the *nth* gene in InvA. After incubation in LB for several hours, growth of the InvA  $\Delta$ *nth* strain is indeed compromised compared to the InvA parent strain (Figure 2.7). If the strains are instead grown under nutrient deprivation in minimal media,

cellular viability is completely lost (Figure 2.8). The growth curves for InvA  $\Delta nth$  alongside InvA or InvA  $\Delta nth$  strains with transformed plasmids that express various EndoIII mutants and RNaseH are shown in Figure 2.7. If the growth defect for InvA  $\Delta nth$  is the result of the ineffective repair of R-loops, as was seen for the InvA  $\Delta dinG$  phenotype, complementation with a plasmid that overexpresses RNaseH, p(RNaseH), should restore activity, which is observed. This result indicates signaling between EndoIII and DinG but does not elucidate the mechanism of signaling. The cooperative signaling effect is not due to the enzymatic activity of EndoIII. The p(EndoIII D138A) plasmid, which expresses the EndoIII mutant lacking glycosylase activity but containing a 4Fe-4S cluster, also rescues the InvA  $\Delta nth$  strain. But is this cooperative signaling the result of long range DNA CT among 4Fe-4S proteins? While expressing WT EndoIII restores activity in InvA  $\Delta nth$ , complementation with the CT-defective, but enzymatically proficient p(EndoIII Y82A) plasmid does not. These results strongly correlate with the results from the AFM and reversion assays, and it appears that EndoIII signals to DinG via DNA CT to help DinG locate and process R-loops.

Our model for how DNA repair proteins with 4Fe-4S clusters use DNA-mediated CT as a first step in locating lesions to repair is depicted in Figure 2.9. Critical to the model is the fact that the DNA binding affinity of a protein that has a 4Fe-4S cluster is dependent on the oxidation state of the cluster. For these proteins, the shift in reduction potential upon DNA binding necessitates a lower DNA binding affinity of at least three orders of magnitude for a 200 mV shift when in the reduced form (2+) compared to the

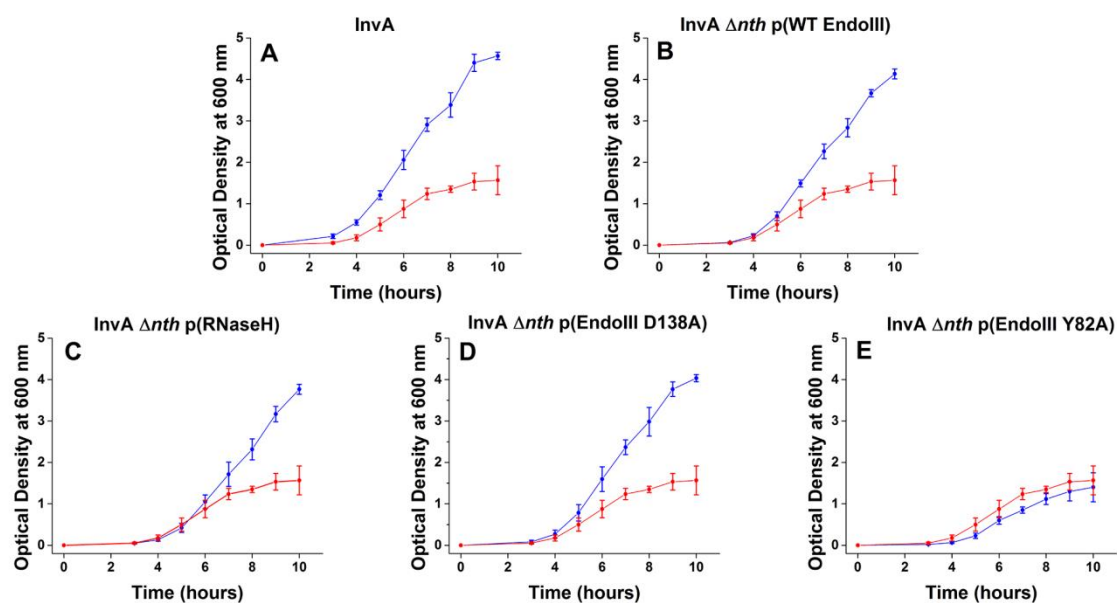


**Figure 2.7** Rescue of growth defect conferred by knocking out *nth* in *InvA*. Cultures of LB were inoculated with single colonies of each strain and growth was monitored by optical density at 600 nm over time. Strains of *InvA*  $\Delta nth$  grew comparably to *InvA*  $\Delta nth$  transformed with p(empty) showing that the effect is not due to the presence of the plasmid. Data were recorded for at least three independent trials. (A) Growth of *InvA* WT (blue) or *InvA*  $\Delta nth$  transformed with p(empty) (red)  $\pm$  SEM. (B) Growth of *InvA*  $\Delta nth$  transformed with p(WT EndoIII) (blue) or p(empty) (red)  $\pm$  SEM. (C) Growth of *InvA*  $\Delta nth$  transformed with p(RNaseH) (blue) or p(empty) (red)  $\pm$  SEM. (D) Growth of *InvA*  $\Delta nth$  transformed with p(EndoIII D138A) (blue) or p(empty) (red)  $\pm$  SEM. (E) Growth of *InvA*  $\Delta nth$  transformed with p(EndoIII Y82A) (black) or p(empty) (red)  $\pm$  SEM.

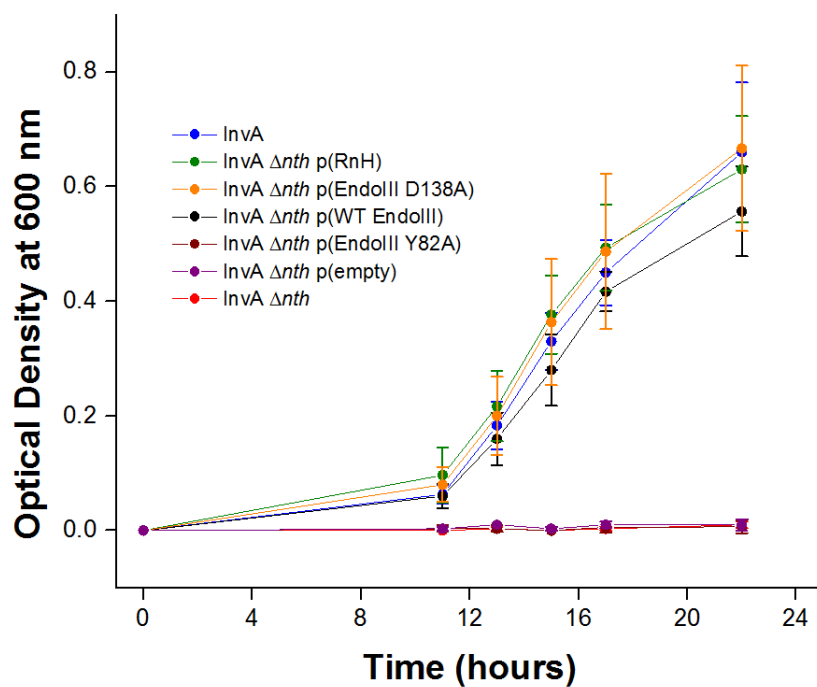


**Figure 2.8** Effect of *nth* deletion in InvA (InvA  $\Delta nth$ ). Cultures of MM (M9 + 0.2% glucose) or MM + ampicillin (100  $\mu\text{g}/\text{mL}$ ) were inoculated with single colonies of the InvA parent strain (blue), InvA  $\Delta nth$  p(RNaseH) (green), InvA  $\Delta nth$  p(EndoIII D138A) (orange), InvA  $\Delta nth$  p(WT EndoIII) (black), InvA  $\Delta nth$  p(EndoIII Y82A) (brown), InvA  $\Delta nth$  p(empty) (purple), or InvA  $\Delta nth$  (red). Growth was monitored over time  $\pm$  SEM.

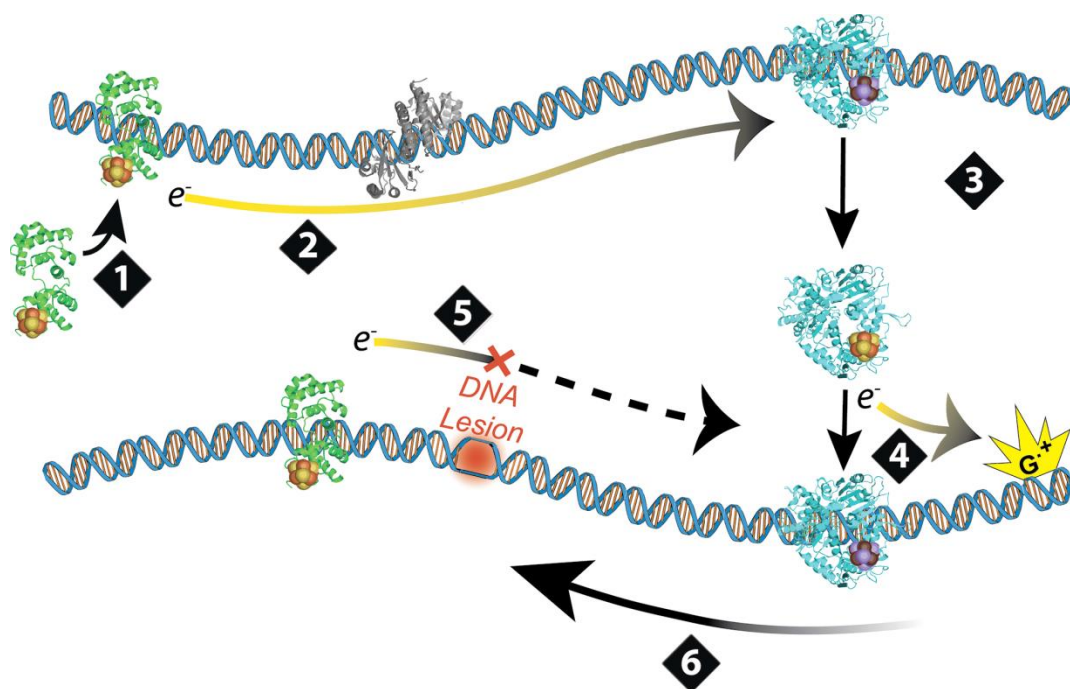


**Figure 2.9** Scheme depicting how repair proteins may use DNA-mediated signaling to search for damage. The model describes how DNA CT can drive the redistribution of the repair proteins into the vicinity of damage. [1] A protein with a reduced (orange-yellow) iron-sulfur cluster binds to DNA. [2] This protein's iron-sulfur cluster is oxidized (purple-brown) by another DNA-bound redox-active protein. This oxidation can occur over long distances and through other DNA-bound proteins (grey) so long as the  $\pi$ -orbital stacking of bases between the reductant and oxidant is unperturbed. [3] Reduction promotes the repair protein's dissociation from DNA. [4] The repair protein binds to an alternate DNA site where it is oxidized either by a guanine radical or another protein. [5] DNA lesions between proteins inhibit electron transport, so protein dissociation is not promoted. [6] Proteins that are now in close proximity to the lesion are able to move processively towards the damage for repair.

oxidized form (3+).<sup>19</sup> Figure 2.5 shows that the DNA-bound potential is significantly shifted from that reported in the absence of DNA.<sup>30</sup> Therefore, as illustrated in Figure 2.9, 4Fe-4S clusters in these proteins when they are freely diffusing are expected to be in the 2+ state. Upon binding to DNA, however, the proteins are activated towards oxidation. A given protein already bound to DNA in the oxidized form, perhaps oxidized from a distance by a guanine radical generated under oxidative stress,<sup>44</sup> could thus be reduced in a DNA-mediated fashion by another distinct redox-active protein that binds within CT distance of the first protein. Reducing this second protein would promote its dissociation from DNA. This inter-protein signaling requires an undamaged path between the two proteins; intervening DNA damage prevents the protein from receiving reducing equivalents so that its dissociation is not promoted. Effectively, this electron transfer event signals the repair protein to dissociate from undamaged regions and search for damage elsewhere in the genome. If there is an intervening damage product that blocks CT, however, then the repair protein stays bound in the vicinity of damage, and the protein can move on a slower timescale to the local site in need of repair. This process would lead to the redistribution of repair proteins in the vicinity of damage through an efficient scanning of the genome by proteins of similar redox potential. In essence, these proteins inform one another about the integrity of DNA by using DNA as a medium through which they transmit electronically encoded information. Because this signaling occurs over long distances, this mechanism would significantly reduce the time required to scan the genome, allowing for enzymes to repair the genome on biological timescales. Indeed, even when CT distances of only 100 bases, that which we have documented, are permitted in our model, a significant reduction in search time to scan the *E. coli* genome can be predicted.<sup>22</sup> Importantly, other models

have been investigated for how BER enzymes similar to MutY and EndoIII can scan the genome and locate their substrates. For example, it has been shown that one-dimensional sliding along DNA can be fast enough for glycosylases to come into contact with bases in the genome on the order of seconds.<sup>45-47</sup> Models for one-dimensional sliding do not, however, take into account protein traffic along the genome. It is important to note that DNA-mediated CT is not interrupted by intervening bound proteins as long as the proteins do not perturb the base pair stack. Thus sliding, hopping, and DNA CT models taken together offer an appealing means to explain how the search process may be optimized under the realistic conditions of the cell.

Data from DNA-modified electrochemistry experiments show that the DNA-bound reduction potential of DinG is remarkably similar to that for EndoIII, MutY, and SaXPD.<sup>19-</sup><sup>21</sup> As such, DinG is competent to shuttle electrons through DNA to or from EndoIII or MutY via its 4Fe-4S cluster, as would be required by the model proposed for the redistribution of these proteins to sites of damage. As with EndoIII and MutY, we consider the redox potential of DinG to correspond to the  $[4\text{Fe-4S}]^{3+/2+}$  couple that is now accessible due to the negative potential shift associated with binding to the DNA polyanion.<sup>19</sup> The ATP-dependent increase in current intensity observed for DinG on electrodes is consistent with previous results for SaXPD, except that the signal increase is nearly an order of magnitude higher than that observed for the thermophilic SaXPD.<sup>21</sup> This substantial difference in signal increase is understandable based upon the significantly lower rate of ATP hydrolysis of SaXPD versus DinG at ambient temperature. It is interesting to consider that the increase in signal intensity could be a general characteristic of these DNA enzymes that contain redox-active clusters, where they signal not only their presence, but also their

activity. For DinG, there could be signaling to upstream proteins that DinG is in the process of unwinding its substrate.

The atomic force microscopy experiments, moreover, support signaling between EndoIII and DinG *in vitro*. Based on the model, we expect the redistribution of proteins that use DNA-mediated CT signaling onto strands containing a single base mismatch and away from fully matched duplex DNA, which is the observed result. Proteins that are defective in DNA CT, furthermore, do not relocate to the mismatched strand, as predicted by our model. Since R-loops disrupt DNA CT, it would be expected that this chemistry could be used within a cell as a first step to drive the redistribution of DinG into the vicinity of R-loops as well; a binding preference of DinG for the R-loop would lead to subsequent localization.

Importantly, the genetics experiments point to a role for DNA-mediated signaling by DinG and other proteins with 4Fe-4S clusters within the cell. Based on the hypothesis that any DNA-processing enzymes with 4Fe-4S clusters of similar potential can cooperate, we would expect signaling between EndoIII and DinG, but also signaling between MutY and DinG. The *lac*<sup>+</sup> forward reversion assay demonstrates that DinG does indeed help MutY find and process its substrate, since knocking out DinG results in an increase in mutagenesis associated with a decrease in MutY activity. Moreover, expressing an enzymatically deficient mutant of EndoIII still rescues activity, while a CT-deficient mutant does not. Interestingly, this mutagenesis is suppressed by expression of EndoIII, despite the fact that EndoIII does not repair the same lesions as MutY.<sup>22</sup> It is remarkable to consider that an effect caused by knocking out a helicase can be reversed by expressing a separate DNA glycosylase, EndoIII. What they have in common is the 4Fe-4S cluster.

These results provide genetic evidence that the effect of knocking out DinG is due to DinG aiding MutY in processing its target lesion via DNA-mediated CT.

It is critical in the context of this model to demonstrate not only that DinG affects the activity of base excision repair enzymes with 4Fe-4S clusters, but also that base excision repair enzymes affect the activity of DinG. Within the *InvA* strain, R-loop formation is significantly amplified and the repair of R-loops becomes essential for cell viability under certain conditions. The fact that DinG is critically important in the *InvA* strain is understandable. But we find that by knocking out even EndoIII in *InvA*, a dramatic growth defect in LB and a complete loss of cellular viability under low nutrient conditions are observed. Since RNaseH can compensate for a loss of DinG activity by degrading R-loops, overexpression of RNaseH restoring normal growth confirms that the observed growth defect is due to EndoIII aiding DinG in processing R-loops. Just as was seen in the *lac*<sup>+</sup> forward reversion assay, expression of the enzymatically inactive but CT-proficient EndoIII D138A can also restore normal growth. Expressing EndoIII Y82A, which is CT-deficient, however, does not rescue growth. Therefore, it is not the loss of glycolytic activity of EndoIII that is suppressing growth in an EndoIII knockout in *InvA*, but the loss of the ability of EndoIII to carry out DNA-mediated CT chemistry.

## Conclusion

Overall these results provide substantial evidence, using both AFM and genetics experiments, that *E. coli* enzymes from distinct repair pathways signal one another from a distance through DNA as long as the proteins remain competent to carry out DNA-mediated CT, as measured electrochemically. The AFM experiments show that a single base mismatch in a 3.8 kb duplex is sufficient to promote the redistribution of the 4Fe-4S proteins to damaged DNA, driven by long range signaling. The genetics experiments emphasize that cooperative signaling for repair within the cell requires the ability of the proteins with 4Fe-4S clusters to carry out DNA CT, not their primary enzymatic activity. Signaling through DNA CT is fast (ps),<sup>48</sup> can occur over long molecular distances, and allows for the binding of many intervening proteins, as long as their distortion of the DNA duplex is minimal. As such, DNA CT provides a mechanism for efficient signal transduction on biological timescales, as the cell requires. Our proposed redistribution model is one way in which proteins may use DNA CT to efficiently scan the genome as a first step in finding lesions to repair and to prepare the genome for replication. The utilization of DNA CT by enzymes to maintain cellular viability and genomic integrity represents a novel role for 4Fe-4S clusters in DNA-processing enzymes. A growing body of evidence is emerging that highlights the importance of iron-sulfur clusters in enzymes that are involved in nearly every aspect of DNA metabolism. The results here provide a basis for understanding the ubiquity of 4Fe-4S clusters in proteins that maintain the integrity of the genome throughout the phylogeny.

## References

1. Genereux, J. C., Boal, A. K. & Barton, J. K. DNA-Mediated Charge Transport in Redox Sensing and Signaling. *J. Am. Chem. Soc.* **132**, 891–905 (2010).
2. Wu, Y. & Brosh, R. M. DNA helicase and helicase–nuclease enzymes with a conserved iron–sulfur cluster. *Nucleic Acids Res.* **40**, 4247–4260 (2012).
3. White, M. F. & Dillingham, M. S. Iron-sulphur clusters in nucleic acid processing enzymes. *Curr. Opin. Struct. Biol.* **22**, 94–100 (2012).
4. Cunningham, R. P. *et al.* Endonuclease III is an iron-sulfur protein. *Biochemistry* **28**, 4450–4455 (1989).
5. Wu, Y., Suhasini, A. N. & Jr, R. M. B. Welcome the Family of FANCI-like Helicases to the Block of Genome Stability Maintenance Proteins. *Cell. Mol. Life Sci.* **66**, 1209–1222 (2008).
6. Weiner, B. E. *et al.* An Iron-Sulfur Cluster in the C-terminal Domain of the p58 Subunit of Human DNA Primase. *J. Biol. Chem.* **282**, 33444–33451 (2007).
7. Netz, D. J. A. *et al.* Eukaryotic DNA polymerases require an iron-sulfur cluster for the formation of active complexes. *Nat. Chem. Biol.* **8**, 125–132 (2012).
8. Yeeles, J. T. P., Cammack, R. & Dillingham, M. S. An Iron-Sulfur Cluster Is Essential for the Binding of Broken DNA by AddAB-type Helicase-Nucleases. *J. Biol. Chem.* **284**, 7746–7755 (2009).
9. Saikrishnan, K. *et al.* Insights into Chi recognition from the structure of an AddAB-type helicase–nuclease complex. *EMBO J.* **31**, 1568–1578 (2012).

10. Pokharel, S. & Campbell, J. L. Cross talk between the nuclease and helicase activities of Dna2: role of an essential iron–sulfur cluster domain. *Nucleic Acids Res.* **40**, 7821–7830 (2012).
11. Liu, H. *et al.* Structure of the DNA Repair Helicase XPD. *Cell* **133**, 801–812 (2008).
12. Fan, L. *et al.* XPD Helicase Structures and Activities: Insights into the Cancer and Aging Phenotypes from XPD Mutations. *Cell* **133**, 789–800 (2008).
13. Wolski, S. C. *et al.* Crystal Structure of the FeS Cluster–Containing Nucleotide Excision Repair Helicase XPD. *PLoS Biol* **6**, e149 (2008).
14. Porello, S. L., Cannon, M. J. & David, S. S. A Substrate Recognition Role for the [4Fe-4S]<sub>2</sub><sup>+</sup> Cluster of the DNA Repair Glycosylase MutY. *Biochemistry* **37**, 6465–6475 (1998).
15. Veatch, J. R., McMurray, M. A., Nelson, Z. W. & Gottschling, D. E. Mitochondrial Dysfunction Leads to Nuclear Genome Instability via an Iron-Sulfur Cluster Defect. *Cell* **137**, 1247–1258 (2009).
16. Stehling, O. *et al.* MMS19 Assembles Iron-Sulfur Proteins Required for DNA Metabolism and Genomic Integrity. *Science* **337**, 195–199 (2012).
17. Gari, K. *et al.* MMS19 Links Cytoplasmic Iron-Sulfur Cluster Assembly to DNA Metabolism. *Science* **337**, 243–245 (2012).
18. Sontz, P. A., Muren, N. B. & Barton, J. K. DNA Charge Transport for Sensing and Signaling. *Acc. Chem. Res.* **45**, 1792–1800 (2012).
19. Gorodetsky, A. A., Boal, A. K. & Barton, J. K. Direct Electrochemistry of Endonuclease III in the Presence and Absence of DNA. *J. Am. Chem. Soc.* **128**, 12082–12083 (2006).

20. Boal, A. K. *et al.* DNA-Bound Redox Activity of DNA Repair Glycosylases Containing [4Fe-4S] Clusters†. *Biochemistry* **44**, 8397–8407 (2005).
21. Mui, T. P., Fuss, J. O., Ishida, J. P., Tainer, J. A. & Barton, J. K. ATP-Stimulated, DNA-Mediated Redox Signaling by XPD, a DNA Repair and Transcription Helicase. *J. Am. Chem. Soc.* **133**, 16378–16381 (2011).
22. Boal, A. K. *et al.* Redox signaling between DNA repair proteins for efficient lesion detection. *Proc. Natl. Acad. Sci.* **106**, 15237–15242 (2009).
23. Genereux, J. C. & Barton, J. K. Mechanisms for DNA Charge Transport. *Chem. Rev.* **110**, 1642–1662 (2010).
24. Boal, A. K. & Barton, J. K. Electrochemical Detection of Lesions in DNA. *Bioconjug. Chem.* **16**, 312–321 (2005).
25. Boon, E. M., Salas, J. E. & Barton, J. K. An electrical probe of protein–DNA interactions on DNA-modified surfaces. *Nat. Biotechnol.* **20**, 282–286 (2002).
26. Kelley, S. O., Jackson, N. M., Hill, M. G. & Barton, J. K. Long-Range Electron Transfer through DNA Films. *Angew. Chem. Int. Ed.* **38**, 941–945 (1999).
27. Gorodetsky, A. A., Buzzeo, M. C. & Barton, J. K. DNA-Mediated Electrochemistry. *Bioconjug. Chem.* **19**, 2285–2296 (2008).
28. Núñez, M. E., Hall, D. B. & Barton, J. K. Long-range oxidative damage to DNA: Effects of distance and sequence. *Chem. Biol.* **6**, 85–97 (1999).
29. Slinker, J. D., Muren, N. B., Renfrew, S. E. & Barton, J. K. DNA charge transport over 34 nm. *Nat. Chem.* **3**, 228–233 (2011).

30. Ren, B., Duan, X. & Ding, H. Redox Control of the DNA Damage-inducible Protein DinG Helicase Activity via Its Iron-Sulfur Cluster. *J. Biol. Chem.* **284**, 4829–4835 (2009).
31. Voloshin, O. N., Vanevski, F., Khil, P. P. & Camerini-Otero, R. D. Characterization of the DNA Damage-inducible Helicase DinG from *Escherichia coli*. *J. Biol. Chem.* **278**, 28284–28293 (2003).
32. Voloshin, O. N. & Camerini-Otero, R. D. The DinG Protein from *Escherichia coli* Is a Structure-specific Helicase. *J. Biol. Chem.* **282**, 18437–18447 (2007).
33. Boubakri, H., Septenville, A. L. de, Viguera, E. & Michel, B. The helicases DinG, Rep and UvrD cooperate to promote replication across transcription units in vivo. *EMBO J.* **29**, 145–157 (2010).
34. Pheaney, C. G., Arnold, A. R., Grodick, M. A. & Barton, J. K. Multiplexed Electrochemistry of DNA-Bound Metalloproteins. *J. Am. Chem. Soc.* **135**, 11869–11878 (2013).
35. Sontz, P. A., Mui, T. P., Fuss, J. O., Tainer, J. A. & Barton, J. K. DNA charge transport as a first step in coordinating the detection of lesions by repair proteins. *Proc. Natl. Acad. Sci.* **109**, 1856–1861 (2012).
36. Datsenko, K. A. & Wanner, B. L. One-step inactivation of chromosomal genes in *Escherichia coli* K-12 using PCR products. *Proc. Natl. Acad. Sci.* **97**, 6640–6645 (2000).
37. Kovach, M. E. *et al.* Four new derivatives of the broad-host-range cloning vector pBBR1MCS, carrying different antibiotic-resistance cassettes. *Gene* **166**, 175–176 (1995).

38. Cupples, C. G. & Miller, J. H. A set of lacZ mutations in *Escherichia coli* that allow rapid detection of each of the six base substitutions. *Proc. Natl. Acad. Sci.* **86**, 5345–5349 (1989).
39. *Current Protocols in Molecular Biology*.  
<<http://onlinelibrary.wiley.com/book/10.1002/0471142727/toc>>
40. Miller, J. H. *A Short Course in Bacterial Genetics: A Laboratory Manual and Handbook for Escherichia Coli and Related Bacteria*. (CSHL Press, 1992).
41. Tano, K., Iwamatsu, Y., Yasuhira, S., Utsumi, H. & Takimoto, K. Increased Base Change Mutations at G:C Pairs in *Escherichia coli* Deficient in Endonuclease III and VIII. *J. Radiat. Res. (Tokyo)* **42**, 409–413 (2001).
42. Thayer, M. M., Ahern, H., Xing, D., Cunningham, R. P. & Tainer, J. A. Novel DNA binding motifs in the DNA repair enzyme endonuclease III crystal structure. *EMBO J.* **14**, 4108–4120 (1995).
43. Aguilera, A. & García-Muse, T. R Loops: From Transcription Byproducts to Threats to Genome Stability. *Mol. Cell* **46**, 115–124 (2012).
44. Yavin, E. *et al.* Protein–DNA charge transport: Redox activation of a DNA repair protein by guanine radical. *Proc. Natl. Acad. Sci. U. S. A.* **102**, 3546–3551 (2005).
45. Blainey, P. C., Oijen, A. M. van, Banerjee, A., Verdine, G. L. & Xie, X. S. A base-excision DNA-repair protein finds intrahelical lesion bases by fast sliding in contact with DNA. *Proc. Natl. Acad. Sci.* **103**, 5752–5757 (2006).
46. Dunn, A. R., Kad, N. M., Nelson, S. R., Warshaw, D. M. & Wallace, S. S. Single Qdot-labeled glycosylase molecules use a wedge amino acid to probe for lesions while scanning along DNA. *Nucleic Acids Res.* **39**, 7487–7498 (2011).

47. Wallace, S. S. DNA glycosylases search for and remove oxidized DNA bases. *Environ. Mol. Mutagen.* **54**, 691–704 (2013).
48. Wan, C. *et al.* Femtosecond dynamics of DNA-mediated electron transfer. *Proc. Natl. Acad. Sci.* **96**, 6014–6019 (1999).

*Chapter 3*

**UvrC contains a 4Fe-4S cluster that is utilized in DNA-mediated signaling**

## Introduction

Maintaining the fidelity of the genome is one of the most important demands an organism must satisfy in order to sustain life. This task is a difficult one considering the constant assault on DNA by both endogenous and exogenous reactive chemicals in addition to radiation. A vast network of proteins is thus maintained by the cell to help prevent, recognize, and repair damage to DNA. In recent years, it has been revealed that many DNA-processing enzymes in organisms from bacteria to man contain 4Fe-4S clusters.<sup>1-3</sup> These iron-sulfur clusters have been found in glycosylases such as Endonuclease III (EndoIII) and MutY, helicase-nucleases such as Dna2 and AddAB, and helicases such as DinG and XPD across the phylogeny.<sup>4-12</sup> They have even been found in enzymes as fundamental as DNA polymerases, DNA primase, and RNA polymerase.<sup>13-17</sup> The roles of these 4Fe-4S clusters are still being uncovered, though in eukaryotes, dysfunction of the iron-sulfur cluster biogenesis machinery has now been linked to several types of genomic instability.<sup>18,19</sup> The clusters do not participate in catalysis, though the local structure is perturbed upon removing the cluster via oxidation or mutagenesis, as would be expected.<sup>9,12</sup> Work in our lab has focused on examining a redox role for these clusters when bound to DNA and how the iron-sulfur clusters in these proteins can participate in long range redox signaling.<sup>20</sup>

DNA CT provides an excellent mechanism to interrogate the integrity of DNA. DNA CT, the chemistry through which DNA can transport electrons or holes through the stacked bases of the DNA helix, has many interesting characteristics that may be relevant inside of cells.<sup>21</sup> First, DNA CT can occur over long molecular distances, up to 34 nm, and

the rate of electron transfer seems to decay shallowly over distances on the molecular scale.<sup>22</sup> DNA CT is also very fast, and has been observed over timescales as short as picoseconds.<sup>23</sup> Perhaps most importantly, DNA CT is sensitive to perturbations to the base stack. DNA base mismatches, damaged bases, and the binding of proteins that significantly kink the DNA or flip bases out of the helix all attenuate DNA CT.<sup>22,24-30</sup> We have hypothesized that 4Fe-4S clusters are used by proteins in DNA-mediated charge transport (CT) signaling to facilitate the search and repair process by nucleic-acid processing enzymes containing 4Fe-4S clusters.

A combination of electrochemical, biochemical, and genetics experiments within cells previously have shown that DNA repair enzymes with 4Fe-4S clusters can use the chemistry of DNA CT as a means of signaling to coordinate their activity within cells. Using DNA-modified electrodes, it was found that EndoIII, MutY, DinG, afUDG, and SaXPD, all of which are DNA repair proteins with 4Fe-4S clusters, share a DNA-bound potential of 80 mV vs. NHE.<sup>24-26</sup> Because these proteins share a redox potential, they in theory can shuttle electrons between one another as a form of signaling. We have explored the theory that these proteins utilize DNA CT to localize to sites of damage within the genome as a first step in the detection of lesions in a variety of contexts.<sup>25,27-29</sup> Experiments have provided strong evidence that EndoIII, DinG, and MutY utilize DNA-mediated CT as a means of signaling to redistribute to sites of damage *in vitro*. Furthermore, genetics experiments revealed that EndoIII, DinG, and MutY all depend upon one another as DNA CT signaling partners in order to carry out their activity within cells.<sup>25,27</sup> EndoIII, DinG, and MutY comprised the DNA-processing enzymes within *E. coli* known to contain 4Fe-

4S clusters. We predicted that UvrC, a nucleotide excision repair (NER) protein, contains a native 4Fe-4S cluster.

UvrC is part of the NER, which is responsible for repairing an array of damage including UV-induced pyrimidine dimer photoproducts, in addition to many bulky lesions and base modifications.<sup>30,31</sup> Many steps in the prokaryotic NER pathway are still being studied. What is known is that UvrA and UvrB associate in solution to form a heterotrimer or heterotetramer. UvrA and UvrB are considered to then bind and translocate together along DNA, seemingly to locate damage.<sup>31-33</sup> Upon UvrA and UvrB locating damage, UvrA dissociates and the DNA wraps around UvrB at the site of damage, forming the UvrB-DNA pre-incision complex.<sup>34-37</sup> At this point, UvrC localizes to the site of damage, and performs an incision of the DNA upstream and downstream of the site of damage.<sup>38,39</sup> UvrD then unwinds the damaged strand of DNA, polymerase I fills in the gap with undamaged bases, and ligase seals the phosphate backbone.<sup>40</sup> Of central importance to the work we present here is that it is unknown how UvrC, which performs the chemistry necessary to repair damaged DNA, locates UvrB bound at the site of damage. Both UvrA and UvrB are upregulated under conditions of stress as they are part of the SOS response. The copy number of UvrA is approximated to rise from ~20 copies to 200 copies and UvrB from ~200 copies per cell up to ~1000 copies.<sup>30</sup> This makes sense considering these proteins are required to find damaged DNA. UvrC, however, is found at an incredibly low copy number of ~10 copies within the cell.<sup>30,39</sup> This means that the rate limiting step, which is also the step required for the chemistry leading to repair, is almost certainly UvrC finding the UvrB-DNA pre-incision complex. We explored if UvrC contains a 4Fe-4S cluster, and

also if it may utilize DNA-mediated CT chemistry as a means of signaling in order to aid in its search for damage.

We present spectroscopic and electrochemical evidence that *E. coli* UvrC contains a 4Fe-4S cluster that is redox-active when bound to DNA. Using genetics experiments, we show that UvrC depends upon DNA-mediated signaling in order to function *in vivo*. By knocking out a DNA-mediated signaling partner, cells are more susceptible to UV damage, but this repair defect can be rescued by complementing the cells with a different signaling partner that is catalytically inactive but CT-proficient. Our results indicate that, despite serving different functions within the cell, DinG, MutY, EndoIII, and UvrC comprise a signaling network within *E. coli*.

## Materials and Methods

### *DNA, plasmids, and Strains used in these experiments*

The DNA including substrates and PCR primers used for the UvrC experiments are presented below in Table 3.1 and the plasmids used are listed in Table 3.2.

### *Expression and Purification of UvrC.*

The *uvrC* gene was amplified from *E. coli* using the primers listed in Table 3.1 and was inserted into a pBad-His<sub>6</sub>-MBP vector using the Gibson Assembly method. The pBad His<sub>6</sub> MBP TEV LIC cloning vector (8C) was a gift from Scott Gradia (Addgene plasmid #37503). An Expand High Fidelity PCR system (Roche) was used to amplify the *uvrC* gene, with ~40 base pairs (bp) of DNA that is homologous to the site of integration into the plasmid added to each end of gene insert, from the *E. coli* genome.

**Table 3.1** Oligonucleotides for electrochemistry substrates, gene replacements, sequencing or colony PCR, and site-directed mutagenesis

Designation and use	Sequence (5' to 3') (bases highlighted in red yield the point mutation after SDM)
Primer for cloning <i>uvrC</i> forward	GGTTTTCCCATGGCATTAAACCGCC
Primer for cloning <i>uvrC</i> reverse	CATCATTAAGCTTCCGACGGCGT
pBad-His <sub>6</sub> -MBP- <i>uvrC</i> sequencing primer 1 (within <i>mbp</i> gene)	GGTCGTCAGACTGTTCGATGAAGCC
pBad-His <sub>6</sub> -MBP- <i>uvrC</i> sequencing primer 2 (within <i>uvrC</i> gene)	TCAGCAGGTCGAGTATGTGC
pBad-His <sub>6</sub> -MBP- <i>uvrC</i> sequencing primer 3 (within <i>uvrC</i> gene)	GCTCAAAGAACAGCGTTTCC
pBad-His <sub>6</sub> -MBP- <i>uvrC</i> sequencing primer 4	GATTTAATCTGTATCAGG
Substrate for electrochemistry – 20-mer thiolated modified strand	HS-C6-GTGCTGCAACGTGTCTGCGC (annealed with either the well-matched complement or abasic complement to yield the substrate used in experiments)
Substrate for electrochemistry – 20-mer complementary strand for well-matched substrate	GCGCAGACACGTTGCAGCAC
Substrate for electrochemistry – 20-mer complementary strand for abasic substrate	GCGCAGACACGTTGCA_CAC (“_” represents an abasic site)
pBBR1MCS-4- <i>nth</i> sequencing forward	GGTGCTGATGCCGCTGGCGATTCAG
pBBR1MCS-4- <i>nth</i> sequencing reverse	TGTGCTGCAAGGCGATTAAGTTGG

**Table 3.2** Plasmids used for UvrC experiments

<b>Plasmid Designation</b>	<b>Description</b>	<b>Source, reference, or method to construct</b>
pBBR1MCS-4 or p(empty)	pBBR1MCS-4, a vector for the constitutive expression of genes placed in the MCS (multiple cloning site)	(34)
pBBR1MCS-4- <i>nth</i> or p(WT EndoIII)	pBBR1MCS-4 carrying the <i>nth</i> gene in the MCS, constitutively expresses WT EndoIII	(34)
pBBR1MCS-4- <i>nth</i> D138A or p(EndoIII D138A)	pBBR1-MCS4 carrying the <i>nth</i> D138A gene in the MCS, constitutively expresses EndoIII D138A	(34)
pBBR1MCS-4- <i>nth</i> Y82A or p(EndoIII Y82A)	pBBR322-MCS4 carrying the <i>nth</i> Y82A gene in the MCS, constitutively expresses EndoIII Y82A	(34)
pBad-His <sub>6</sub> -MBP- <i>uvrC</i>	Overexpresses UvrC in presence of L-arabinose	Insertion of <i>uvrC</i> gene into pBad vector (Addgene) constructed for this work.

The pBad-His<sub>6</sub>-MBP vector was restricted with HF-BamHI and HF-SspI (NEB). Next the vector was assembled by adding ~100 ng of the restricted vector and ~100 ng of the *uvrC* gene insert to Gibson Assembly master mix (NEB). After the reaction finished (~1 hour), the reaction solution was diluted 3-fold in water. Two microliters of the reaction mixture were added to an aliquot of electrocompetent TOP10 cells (Invitrogen). The cells were electroporated and plated onto LB + kanamycin (50 µg/mL) selective plates. The plasmid was extracted from a single colony using a miniprep kit (Qiagen) and sequenced (Laragen) using the sequencing primers 1-4 listed in Table 3.1. The constructed pBad-His<sub>6</sub>-MBP-*uvrC* vector encodes for UvrC fused with an N-terminal hexahistidine affinity tag, followed by an MBP affinity tag. The gene is under control of an *ara* promoter. Expression of the UvrC fusion protein is driven by the addition of L-arabinose.

To express UvrC, six liters of LB, which had been inoculated with an overnight culture of TOP10 cells harboring the pBad-His<sub>6</sub>-MBP-*uvrC* vector, were shaken at 37 °C. After the cultures reached an O.D. of ~0.6-0.8, L-arabinose (Sigma Aldrich) was added to a concentration in each flask of 100 mg/L. The flasks were then returned to the incubator, which had been cooled to ~22 °C. After ~16 hours of induction at ~22 °C, the cells were collected by centrifugation at 5,500 rpm for 15 minutes. The cell pellets were frozen at -80 °C.

After 6 liters of LB, which had been inoculated with a starter culture of TOP10 cells containing pBad-MBP-*uvrC*, were shaken at 37 °C at 225 rpm and reached an O.D. of 1.0, enough (L)-arabinose was added to bring the concentration of arabinose to 100 mg/L. The flasks were then returned to the incubator, which was cooled to ~22 °C. After ~16 hours

of shaking at 150 rpm and 22° C, the cells were collected by centrifugation at 5,000 rpm for 15 minutes and frozen at -80 °C in 1 pellet.

The ~25 g pellet from 6 liters of culture that had been grown to express the protein, was resuspended in 300 mL of Buffer A (0.5M KCl, 1 mM DTT, 10% glycerol, 25 mM Tris-HCl, 7.5 pH at 25 °C), Complete protease inhibitor cocktail tablets (Roche), and DNase (15 kU). The resuspended cells were lysed by microfluidization. The lysate was cleared by centrifugation at 12,000 rpm for 45 minutes on the ultracentrifuge. The supernatant from the cell lysate was then passed through a 0.45 µm filter. Meanwhile, a 5 mL Histrap HP column (GE healthcare) was equilibrated with 5 column volumes (CV) of buffer A. The column was loaded with the cell lysate using a peristaltic pump (GE, set at a flow rate of 3.5 mL/min). The column was washed with ~4 CV of buffer A. The protein was eluted using a 15 CV gradient from 0-100 % buffer B (0.5 M KCl, 0.5 M imidazole, 20% glycerol, 25 mM Tris-HCl, 7.5 pH at 25 °C). All of the fractions from each column were pooled and directly loaded on to a 5 mL MBPTrap HP column (GE Healthcare) at a flow rate of ~2.0 mL/min. The column was then washed ~4 CV of buffer C (0.5 M KCl, 1 mM DTT, 20% glycerol, 25 mM Tris-HCl, 7.5 pH at 25 °C). The protein was then eluted off of the MBP column using a 10 CV 0-100% buffer D (0.5M KCl, 10 mM maltose, 1 mM DTT, 20% glycerol, 25 mM Tris-HCl, 7.5 pH at 25 °C) gradient. The majority of the protein eluted in one peak and was collected and loaded onto a Superdex 200 column (GE Healthcare), which was developed by passing 300 mL of buffer E (0.5 M KCl, 20% glycerol, 25 mM Tris-HCl, 7.5 pH at 25 °C) through the column, which had been pre-equilibrated with buffer E. Two major peaks eluted from the size exclusion column. One eluted at the void volume, which is likely denatured/aggregated protein. The

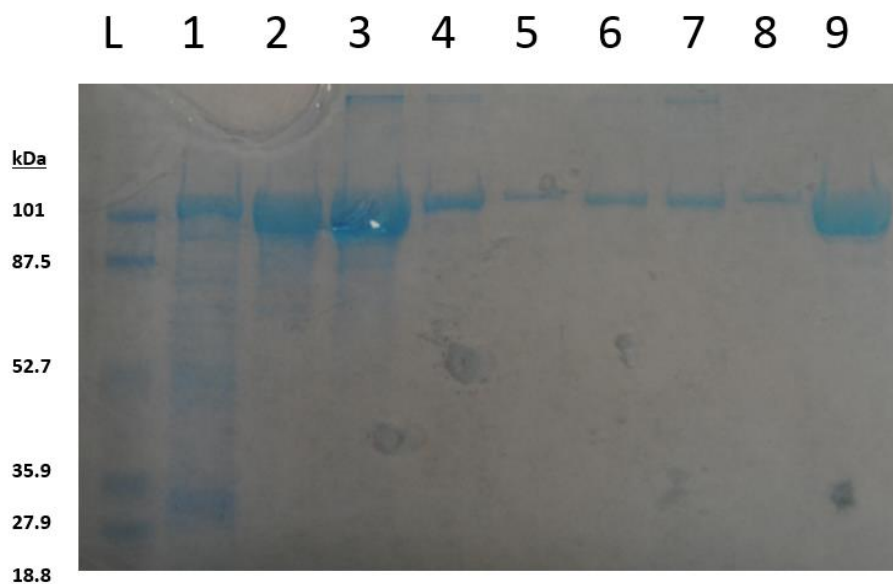


**Figure 3.1** SDS-PAGE of MBP-UvrC purification. Lane L = Molecular weight ladder, Lane 1 = MBP column flow-through, Lane 2 = MBP fraction 5 (F5), Lane 3 = MBP F9, Lane 4 = MBP F14 , Lane 5 = MBP F20, Lane 6 = Size exclusion column F5, Lane 7 = Size exclusion column F9, Lane 8 = Size exclusion column F15, Lane 9 = 5x-diluted stored protein.

second peak was collected. The purity of the gel was tracked using SDS-PAGE of sub-fractions (Figure 3.1). At each step, a protein band corresponding to ~105 kDa, the expected weight of the MBP-UvrC construct, was enriched. After the size exclusion column, this was the only major band observed, even after freeze-thaw and over-loading the gel lane. The identity of the purified protein was confirmed by protein mass-spec.

#### *Spectroscopic characterization of a 4Fe-4S cluster within UvrC*

A UV-visible absorbance spectrum was taken and was the first indication that the yellow-colored purified protein contained a 4Fe-4S cluster. X-band EPR spectra were collected with a Bruker EMX spectrometer. Samples were prepared by diluting flash-thawed 20  $\mu$ M MBP-UvrC 2-fold into 0.5 M KCl, 25 mM Tris-HCl, pH ~7.5, and 20% glycerol buffer that had been degassed with argon for over one hour, with or without 2 mM sodium ferricyanide or 2 mM sodium dithionite. All spectra were obtained at ~10 K, which was achieved using a helium cryostat. The microwave frequency used was 9.373 GHz with a power of 16.2 mW. The modulation amplitude was 10 gauss (G). The field was swept from 1000 to 4000 G. Samples without protein were used as blanks. Data were acquired using WinEPR software.

#### *DNA-modified UvrC Electrochemistry*

The DNA substrate used for the electrochemical characterization of DinG was either a well-matched 20-mer DNA oligomer or a 20-mer DNA oligomer containing an abasic site four base pairs from the bottom of the duplex (Table 3.1). A single-stranded 20-mer of DNA with a terminal thiol and 6-carbon linker at the 5' end of the strand was

annealed to an unmodified, single-stranded 20-mer of DNA to yield the electrochemical substrate. In the electrochemical cell, the DNA substrate is covalently tethered to the gold surface via a gold-thiol bond.

The thiol-modified strand was obtained by reducing with DTT a single-stranded 20-mer of DNA containing a disulfide bond six carbons from the terminus of the strand. The complementary strand was purchased from IDT. The thiol-modified and complementary strands were purified by HPLC using an analytical C-18 column (Agilent). DNA strands were characterized by MALDI mass-spectroscopy. The DNA was quantified by UV-Visible absorbance and equimolar amounts were annealed yielding either the well-matched DNA or DNA with an abasic site.

To prepare multiplexed DNA-modified gold electrodes, the chips were cleaned immediately before incubating them with DNA. The chip was rinsed and sonicated with acetone three times for 5 minutes, and once with isopropyl alcohol for 5 minutes. The gasket and clamp were washed and sonicated in 50% isopropanol/water for 5 minutes followed by 3 x 5 minute washes with water. All of the pieces were then dried with an argon gun. The chip was placed in an ozonator and was cleaned by ozonolysis for 15 minutes. The chip, gasket, and clamp were then assembled and 20 microliters of 25  $\mu$ M DNA were added to each quadrant of the multiplex chip as described previously.<sup>22,41</sup> Two of the four quadrants contained well-matched 20-mer DNA, one quadrant contained the same substrate with the exception of an abasic site placed incorporated 4 base pairs from the bottom of the duplex, and the last quadrant contained the single-stranded modified strand.

After overnight incubation with DNA at ambient temperature, the multiplex chip was rinsed five times with phosphate buffer (5 mM phosphate pH ~7.0, 50 mM NaCl) followed by two rinses with glycerol buffer (5% glycerol, 5 mM phosphate pH ~7.0, 50 mM NaCl). Each quadrant was then filled with 1 mM 6-mercaptohexanol, the backfilling agent, for ~45 minutes. Then the electrodes were rinsed ten times with the phosphate buffer. A platinum wire was used as the auxiliary electrode while a Ag/AgCl electrode was used as a reference electrode. After flash-freezing and dilution, 5  $\mu$ M UvrC in electrochemistry buffer (4 mM spermidine, 25 mM Tris-HCl, pH ~7.5, 250 mM KCl, 20% glycerol) was added to the entire chip as a common solution filling all four of the quadrants. Cyclic voltammetry scans were taken in air over the course of several hours. The scan rate used for these scans was 50 mV/s and the window was from -0.4 V to 0.2V vs. Ag/AgCl.

#### *Nucleotide Excision Repair UV sensitivity assay*

All mutant EndoIII plasmids, which were derived from pBBR1MCS-4, were constructed for previous studies with DinG.<sup>25</sup> The pBBR1MCS-4, pBBR1MCS-4-*nth*, The pBBR1MCS-4-*nth* D138A, and pBBR1MCS-4-*nth* Y82A plasmids encode and constitutively express no protein, WT EndoIII, EndoIII D138A, and EndoIII Y82A respectively. The pBBR1MCS-4 derived plasmids are referred to as p(empty), p(WT EndoIII), p(EndoIII D138A), and p(EndoIII Y82A), respectively, throughout the text as indicated in Table 3.2. WT MG1655 *E. coli* cells and WT  $\Delta$ *dinG::kan* strains were transformed by electroporation with the p(EndoIII D138A), p(empty), p(WT EndoIII), and p(EndoIII Y82A) plasmids (Table 3.2) and were selected for on LB + ampicillin (100  $\mu$ g/mL) agar plates. Plasmids from each of the newly generated strains were isolated and

sequenced (Laragen) using the forward and reverse pBBR1MCS-4-*nth* sequencing primers (Table 3.1) to verify that the plasmids were intact and contained the proper mutation within the *nth* gene in each plasmid.

The UV sensitivity assay was adapted from a previously published procedure.<sup>42</sup> The WT p(empty), WT p(WT EndoIII), WT p(EndoIII Y82A), and WT p(EndoIII D138A) in addition to  $\Delta$ *dinG* p(empty),  $\Delta$ *dinG* p(WT EndoIII),  $\Delta$ *dinG* p(EndoIII Y82A), and  $\Delta$ *dinG* p(EndoIII D138A) strains were grown to an O.D. of ~0.3 to 0.4 in LB + ampicillin (100  $\mu$ g/mL). They were then serially diluted and plated onto LB + ampicillin (100  $\mu$ g/mL) agar plates. After 30 minutes of incubation at 37 °C, the plates were irradiated with 0, 30, 60, or 90 J/m<sup>2</sup> of 254 nm UV light. They were then incubated overnight, at which points colonies were counted for each strain.

## Results and Discussion

### UvrC contains a 4Fe-4S cluster

It was predicted within our laboratory by Dr. Amie Boal that UvrC may contain a 4Fe-4S cluster from the analysis of its primary sequence. There are five well-conserved cysteines within the protein. These conserved residues are Cys 154, Cys 166, Cys 174, Cys 178, and Cys 265. Perhaps the most likely alternative to a 4Fe-4S cluster being ligated by four of these cysteine residues would be a zinc ion in the form of a zinc-finger; however, judging by primary sequence, the spacing of these residues does not match typical Zn-binding motifs.<sup>43</sup> To date, no full length crystal structures of bacterial UvrC have been reported, only N-terminal or C-terminal fragments.<sup>44-46</sup> In each case, the part of the protein containing the residues that putatively ligate the 4Fe-4S cluster, was not crystallized. Many

DNA-processing enzymes that contain 4Fe-4S clusters were only shown to have 4Fe-4S clusters upon re-examination of the proteins.

There appears to be a pattern emerging for the expression and purification conditions required for nucleic-acid processing enzymes to be purified with intact 4Fe-4S clusters. In many reports, DNA-binding proteins that contain 4Fe-4S clusters are best expressed using low concentrations of inducers and at incubation temperatures that are lower than room temperature.<sup>8-10,25,28</sup> Here we employed a similar expression strategy to obtain UvrC loaded with a 4Fe-4S cluster. We used a pBad vector in order to tightly control the expression of UvrC,<sup>47</sup> and we expressed the protein at 22 °C not 37 °C, as would be typical for the overexpression of recombinant proteins.

A UV-Visible absorbance spectrum of the stored protein (Figure 3.2) shows a clean 280 nm peak and a broad shoulder at 410 nm, which is what would be expected for a protein containing a 4Fe-4S. The expression and purification scheme used yields around 1.5 mL of ~15 micromolar cluster-loaded protein. Using an extinction coefficient for the MBP-UvrC fusion at 280 nm of ~0.91 M<sup>-1</sup> cm<sup>-1</sup> (estimated by the ExPASy ProtParam tool), and an extinction coefficient at 410 nm of ~ 17,000 M<sup>-1</sup> cm<sup>-1</sup> the loading of the 4Fe-4S cluster in the purified protein is ~70%.<sup>27</sup>

EPR spectroscopy of UvrC was used to further verify the presence of a 4Fe-4S cluster within the protein. The 4Fe-4S clusters have characteristic features that can be detected using EPR spectroscopy. When MBP-UvrC is treated with 2 mM sodium dithionite, an EPR spectrum expected for that of a [4Fe-4S]<sup>1+</sup> cluster is observed

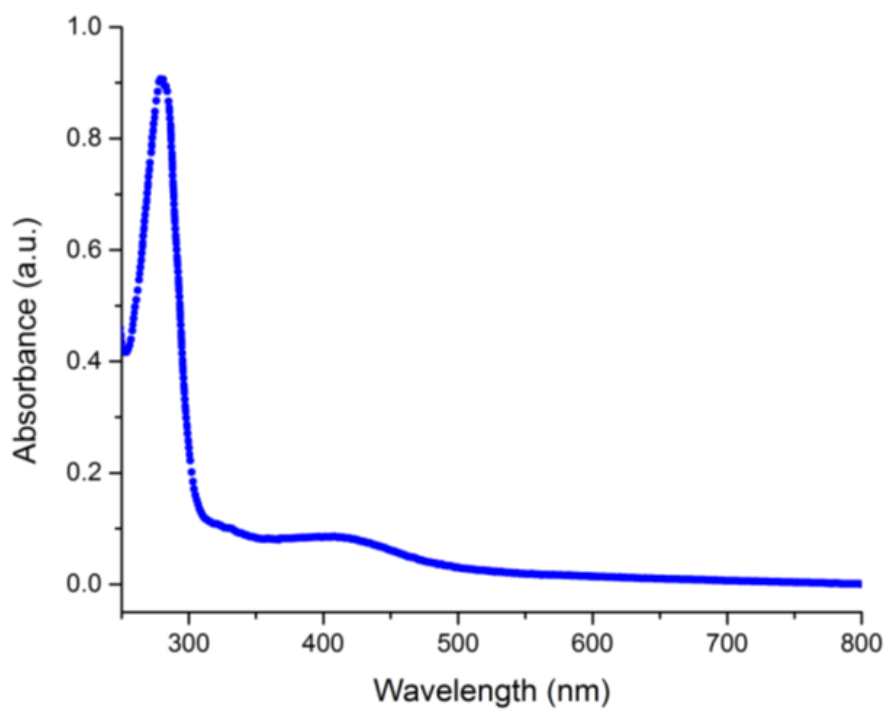


**Figure 3.2** UV-visible absorbance spectrum of MBP-UvrC. UvrC is in 0.5 M KCl, 20% glycerol, 25 mM Tris-HCl, 7.5 pH at 25 °C.

(Figure 3.3). This EPR spectrum contains a rhombic signal with g-values of ~2.04, 1.88, and 1.85, and resembles that of many proteins containing reduced 4Fe-4S clusters.<sup>13,48–50</sup> For untreated MBP-UvrC, a signal with a g-value of ~2.01 is present (Figure 3.4). We assign this to a  $[3\text{Fe-4S}]^{+1}$  species, which is a common oxidative degradation product of 4Fe-4S clusters, particularly upon freezing.<sup>13,24</sup> Once oxidized, one iron atom within the cluster becomes labile and can be lost. Without spin quantification, it is difficult to quantify the amount of UvrC that contains a 3Fe-4S cluster. The assignment of this signal to that of an organic radical was ruled out since the signal quickly broadens when warmed to temperatures of ~55 K. Interestingly, no EPR signals reminiscent of an iron-sulfur cluster are present in the EPR spectra after treatment with potassium ferricyanide, possibly due to complete degradation of the iron-sulfur cluster. This result could indicate that the iron-sulfur cluster of UvrC is particularly sensitive to oxidation. Since UvrC appears to contain a 4Fe-4S cluster, we sought to characterize the protein using DNA-modified electrochemistry to ascertain its redox properties when bound to DNA, as it would be within a cell.

### **UvrC is redox-active when bound to DNA and shares a redox potential with other DNA-processing enzymes that contain 4Fe-4S clusters**

With the knowledge that UvrC contains a 4Fe-4S cluster, the redox properties of the cluster were studied using DNA-modified electrochemistry. Cyclic voltammetry on multiplexed gold electrodes modified with a 20-mer DNA duplex reveals that UvrC has a DNA-bound redox potential of 80 mV vs. NHE (Figure 3.5). An array of

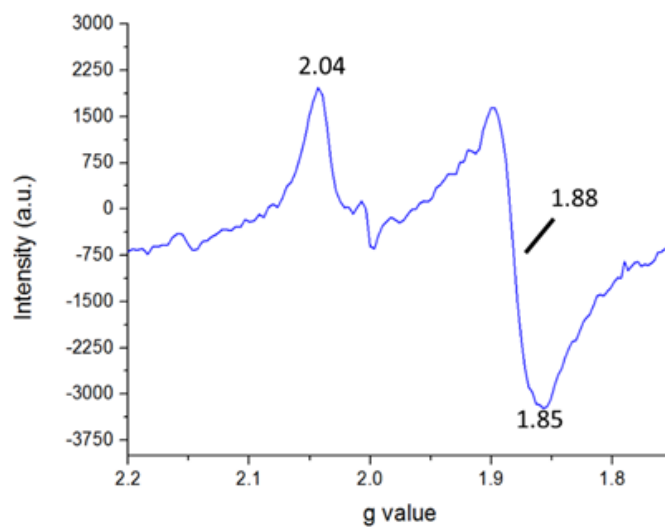


**Figure 3.3** EPR spectrum of MBP-UvrC and dithionite. EPR spectrum of 10  $\mu$ M MBP-UvrC + 2 mM dithionite in 0.5 M KCl, 25 mM Tris-HCl, pH  $\sim$ 7.5, and 20% glycerol buffer at 10 K.

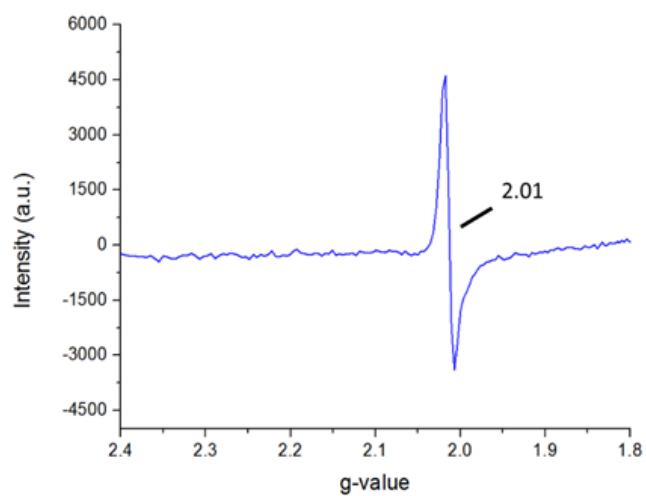


**Figure 3.4** EPR spectrum of MBP-UvrC. 10  $\mu$ M MBP-UvrC in 0.5 M KCl, 25 mM Tris-HCl, pH  $\sim$ 7.5, and 20% glycerol buffer at 10 K. There is one resonance at a g-value of  $\sim$ 2.01.

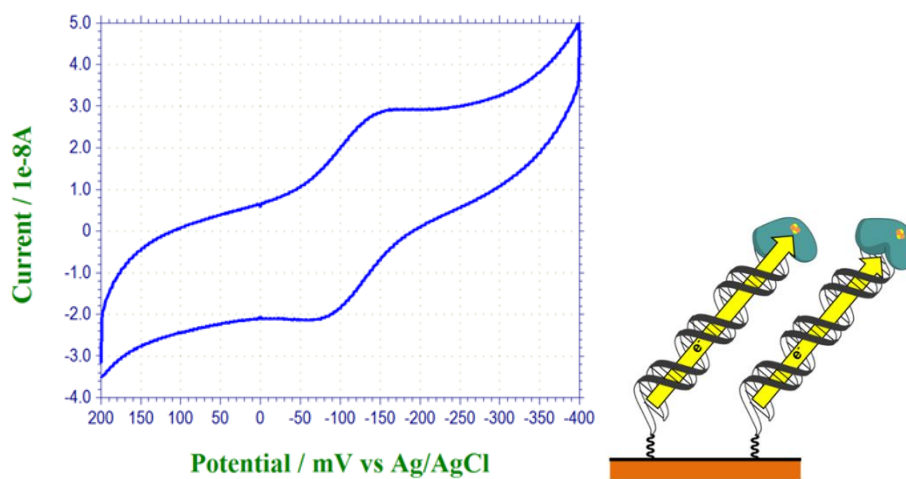


**Figure 3.5** (Left) Cyclic voltammetry of MBP-UvrC. 5  $\mu\text{M}$  UvrC is in 4 mM spermidine, 25 mM Tris-HCl, pH  $\sim 7.5$ , 250 mM KCl, and 20% glycerol on a multiplex chip modified with a 20-mer DNA duplex after 3 hours of incubation on the surface. A scan rate of 50 mV/s was used to obtain the spectrum. Note that the midpoint potential shown in the cyclic voltammogram is shifted compared to that we assign. This could be due to the reference electrode having a shifted potential. EndoIII was added to the electrode after UvrC and it was shown that they do in fact share a potential. (Right) Cartoon representation of DNA on the DNA-modified electrode.

DNA-processing enzymes containing 4Fe-4S clusters have been electrochemically characterized using DNA-modified electrodes.<sup>24-26</sup> When bound to DNA, *E. coli* EndoIII, MutY, and DinG all share a potential of ~80 mV vs. NHE, the same potential as that observed for UvrC here. For this class of enzymes, the DNA-bound potential is shifted compared to the potentials observed using redox mediators for the [4Fe-4S]<sup>2+/1+</sup> (<-350 mV vs. NHE) or the [4Fe-4S]<sup>3+/2+</sup> (>200 mV vs. NHE) redox couples when these proteins are freely diffusing in solution in the absence of DNA.<sup>4,48,51,52</sup> The redox signal observed at 80 mV vs. NHE couple has been assigned to that of the [4Fe-4S]<sup>3+/2+</sup> couple shifted negatively ~200 mV vs. NHE when bound to DNA.<sup>24</sup> Thermodynamically, this shift would correspond to a stabilization of the [4Fe-4S]<sup>3+</sup> state when bound to DNA, as would be expected due to electrostatic interactions of the cluster with the negatively charged, polyanionic backbone of DNA. Stabilization of the oxidized cluster would also correspond to an increase in the binding affinity of the protein for DNA of at least three orders of magnitude in the oxidized state compared to the reduced state.<sup>51</sup> Since these DNA-processing enzymes share a redox potential, they are competent to shuttle electrons between one another. Within our laboratory, we have considered how DNA-mediated CT may be used as a means of cooperative signaling by these proteins.<sup>20,53,54</sup> A body of evidence has now been accumulating that DinG, MutY, and EndoIII utilize DNA-mediated CT as a means of signaling to aid each of the proteins in locating and repairing target substrates in need of processing.<sup>25,27,29,54</sup> Given that UvrC shares a redox potential with these proteins, perhaps UvrC, too, may use DNA-mediated CT to scan the genome and locate damage that needs to be repaired by the nucleotide excision repair pathway.

### **DNA-mediated signaling within *E. coli* is required for efficient repair by UvrC**

A model for how DNA repair proteins with 4Fe-4S clusters utilize DNA-mediated CT chemistry as a means of signaling has been proposed by our lab.<sup>25,27,29,53,54</sup> Within this model, DNA-processing enzymes with 4Fe-4S clusters use DNA-mediated CT in order to scan the genome for damage and localize in the vicinity of damage. A depiction of the model is shown below in Figure 3.6. The model is based on four main postulates: i) DNA CT can occur over long molecular distances (>100 bp), ii) DNA damage attenuates DNA CT, iii) DNA-processing enzymes that share a redox potential can shuttle electrons between one another via DNA-CT, and iv) these enzymes have a higher binding affinity when the 4Fe-4S cluster is in the 3+ oxidation state vs. the 2+ oxidation state. It is hypothesized that if a protein with a 4Fe-4S cluster binds within CT distance of another protein that is oxidized, then it can shuttle an electron to the distally bound protein, so long as there is no intervening damage that would attenuate CT. The distally bound protein would then be reduced, promoting its dissociation from DNA, and signaling for it to search the genome elsewhere for damage. This acts as an effective scan of that segment of the genome. This process would continue until a protein binds in the vicinity of the damage, at which point the distally bound protein would stay bound and proceed to the site of damage to repair it. This mechanism is attractive since it would significantly speed up the search and repair process,<sup>27</sup> which is currently not well understood. Current models for how proteins like glycosylases, which are thought to be at low copy numbers within cells, locate damage within the time required by a cell before it divides do not take into account protein traffic.<sup>55-57</sup> DNA-mediated CT signaling would provide a mechanism for how proteins could bypass protein traffic, since CT can still occur through

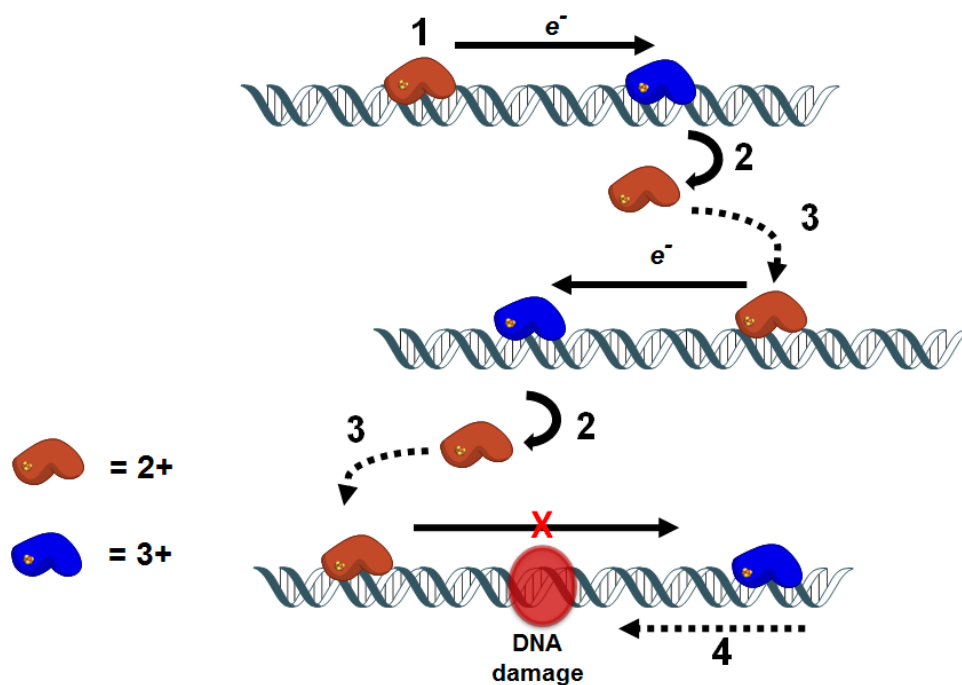


**Figure 3.6** Model for redistribution of DNA repair proteins to sites of damage. 1.) A DNA-processing enzyme with a 4Fe-4S cluster binds to DNA, shuttling an electron to an oxidized, distally bound protein. 2.) This reduction promotes the dissociation of the protein. 3.) The protein then takes advantage of 3-D diffusion to search the genome elsewhere. 4.) This process continues until the proteins locate damage, which attenuates DNA CT.

DNA that is bound by proteins. In fact the current models for repair and a DNA-mediated signaling mechanism are not mutually exclusive and would complement each other well; these proteins necessarily would need to utilize both hopping and facilitated 1-D diffusion to find and repair damage.

Since UvrC shares a midpoint redox potential with DinG, EndoIII, and MutY, we began investigations into whether DinG, EndoIII, and MutY could aid UvrC in locating and repairing its damage using DNA-mediated CT signaling, similar to what has been shown for signaling among DinG, EndoIII, and MutY (Figure 3.7). UvrC must locate the UvrB-DNA damage pre-incision complex to complete the repair of DNA damaged by UV. If DinG, EndoIII, and MutY assist UvrC using DNA-mediated signaling, one would expect that silencing these proteins within cells would make cells more susceptible to UV damage, which is repaired by UvrC, a lynchpin in the NER pathway. As illustrated in Figure 3.8, the UV sensitivity of a *dinG* knockout,  $\Delta dinG$ , does indeed have a 5-10 fold higher sensitivity to UV radiation than WT *E. coli* cells. This result establishes cross-talk between UvrC and DinG, but is this due to DNA-mediated signaling? If it is the 4Fe-4S cluster of these proteins that is required to facilitate the efficient repair of UV damage, then survival should be restored by complementing  $\Delta dinG$  with a protein that contains a 4Fe-4S cluster and is CT-proficient. We tested this by seeing if we could rescue  $\Delta dinG$  cells by complementing them with EndoIII D138A. EndoIII D138A, while catalytically inactive, can still bind DNA and can perform DNA CT comparably to WT EndoIII.<sup>27</sup> Indeed,  $\Delta dinG$  p(EndoIII D138A) is less sensitive to UV damage than  $\Delta dinG$ . Meanwhile, complementation with EndoIII Y82A, which is a mutant of EndoIII that is

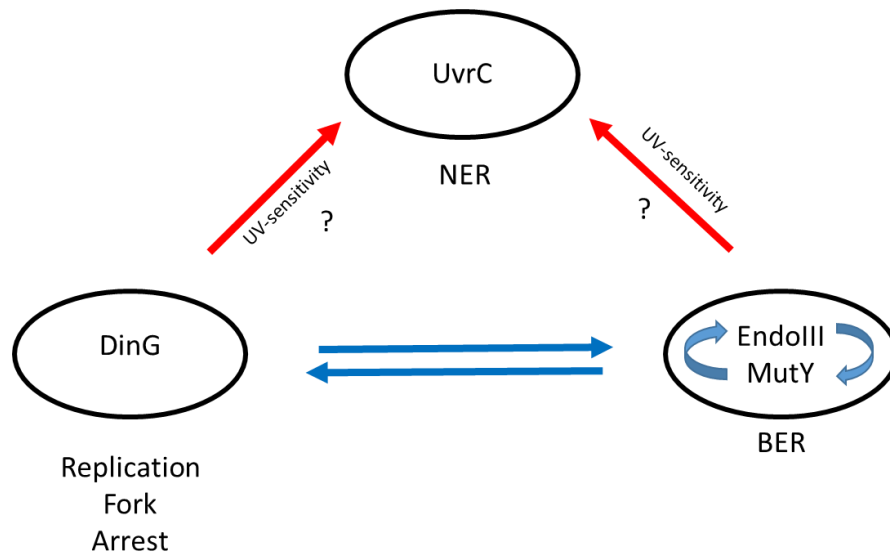


**Figure 3.7** Diagram depicting signaling among DNA repair proteins containing 4Fe-4S clusters. Evidence for DNA-mediated signaling among DinG, EndoIII, and MutY has been shown previously. Does similar signaling occur between these proteins and UvrC to facilitate NER?

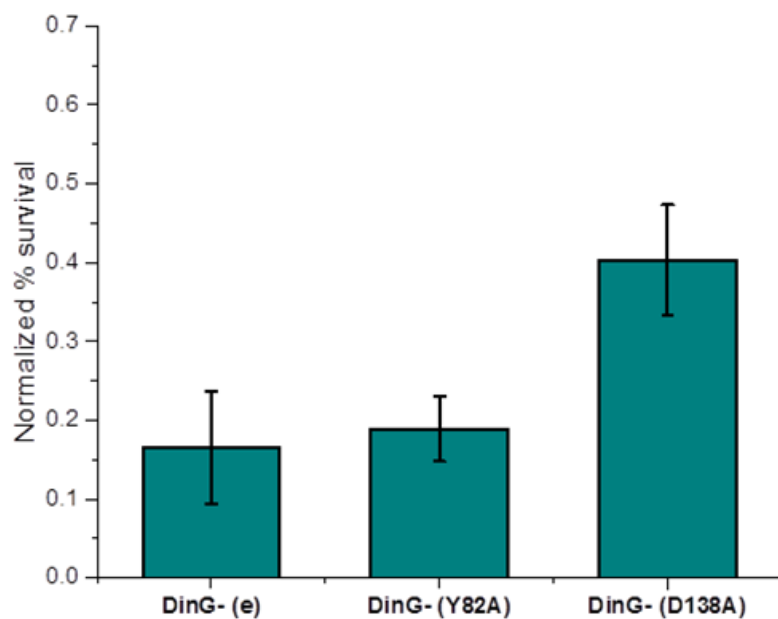


**Figure 3.8** UV-sensitivity assay. The survival of  $\Delta dinG$  cells transformed with an empty plasmid, a plasmid expressing EndoIII Y82A, or a plasmid expressing EndoIII D138A after irradiation with  $90 \text{ J/m}^2$  of UV light is shown. Note that % survival is normalized to the survival of WT *E. coli* cells transformed with an empty plasmid. Error represents SEM  $n \geq 3$ .

CT-deficient but catalytically active,<sup>27</sup> shows no rescue of repair activity (Figure 3.8). It appears, thus, that UvrC relies upon DNA-mediated signaling in order to efficiently repair UV damage. It must be stressed here that EndoIII and MutY are endonucleases within the base excision repair family, DinG is a helicase that unwinds R-loops at stalled replication forks, and UvrC is a dual-incision nuclease that is part of the nucleotide excision repair pathway. Despite the fact that these proteins are from different repair pathways, perform different catalytic functions, and repair different substrates, they all depend upon one another in order to facilitate their activities *in vivo*. What these proteins do have in common is that they all contain 4Fe-4S clusters that have similar redox potentials, and can all participate in long range redox reactions via DNA charge transport chemistry.

The question of how UvrC can locate UvrB bound to damage has been elusive. Our data supports a model in which UvrC utilizes DNA-mediated CT in order to localize to sites of damage, which would be bound by UvrB in the pre-incision complex. Previous work has been carried out observing single molecules of UvrA, UvrB, and UvrC that were each labeled with quantum dots by AFM.<sup>58</sup> Evidence was presented that UvrC can bind DNA independently but it has a long lifetime, on the order of tens of seconds. It would be interesting to know whether the UvrC used in these experiments was loaded with the 4Fe-4S cluster. If not, it would be tempting to propose that without a 4Fe-4S cluster, the protein is unable to efficiently scan DNA, as evidenced by the long lifetimes observed. DNA-binding with WT UvrC and UvrC mutants lacking the 4Fe-4S cluster needs to be tested.

## **Conclusion**

Taken together, these results provide even stronger evidence that DNA-mediated signaling is used as a *general* mechanism by which DNA repair proteins with 4Fe-4S clusters locate damage within *E. coli*. Here, upon spectroscopically showing that UvrC contains a 4Fe-4S cluster, DNA-modified electrochemistry was used to establish that UvrC shares a DNA-bound redox potential with MutY, EndoIII, and DinG. Previous work established that DNA-mediated signaling may be utilized by EndoIII, MutY, and DinG to coordinate the search and repair process. Here we show results that expand this putative DNA-mediated signaling network to include UvrC, the fourth DNA-processing enzyme shown to contain a 4Fe-4S cluster within *E. coli*. Regardless of the fact that the proteins within this network are from different repair pathways, target different substrates, and perform different catalytic functions, the proteins rely upon one another to maintain the fidelity of the genome, especially under stress. The unifying factor of this network of DNA-processing enzymes is that they contain 4Fe-4S clusters that share a redox potential. It will be of great interest to see if the trends observed in *E. coli* also hold true in higher organisms.

DNA-mediated charge transport chemistry offers an elegant mechanism to report on the integrity of the DNA duplex. DNA CT has been shown to travel long distances, is fast, and is highly sensitive to perturbations to base-stacking. This work adds to a growing body of evidence that indicates that proteins with 4Fe-4S cluster not only can participate in long-range redox reactions via DNA CT, but also use this chemistry as a means of cooperative signaling to coordinate the efficient repair and processing of DNA within cells.

## References

1. Wu, Y., Suhasini, A. N. & Jr, R. M. B. Welcome the Family of FANCI-like Helicases to the Block of Genome Stability Maintenance Proteins. *Cell. Mol. Life Sci.* **66**, 1209–1222 (2008).
2. Wu, Y. & Brosh, R. M. DNA helicase and helicase–nuclease enzymes with a conserved iron–sulfur cluster. *Nucleic Acids Res.* **40**, 4247–4260 (2012).
3. White, M. F. & Dillingham, M. S. Iron-sulphur clusters in nucleic acid processing enzymes. *Curr. Opin. Struct. Biol.* **22**, 94–100 (2012).
4. Cunningham, R. P. *et al.* Endonuclease III is an iron-sulfur protein. *Biochemistry* **28**, 4450–4455 (1989).
5. Kuo, C. F. *et al.* Atomic structure of the DNA repair [4Fe-4S] enzyme endonuclease III. *Science* **258**, 434–440 (1992).
6. Pokharel, S. & Campbell, J. L. Cross talk between the nuclease and helicase activities of Dna2: role of an essential iron–sulfur cluster domain. *Nucleic Acids Res.* **40**, 7821–7830 (2012).
7. Yeeles, J. T. P., Cammack, R. & Dillingham, M. S. An Iron-Sulfur Cluster Is Essential for the Binding of Broken DNA by AddAB-type Helicase-Nucleases. *J. Biol. Chem.* **284**, 7746–7755 (2009).
8. Saikrishnan, K. *et al.* Insights into Chi recognition from the structure of an AddAB-type helicase–nuclease complex. *EMBO J.* **31**, 1568–1578 (2012).
9. Fan, L. *et al.* XPD Helicase Structures and Activities: Insights into the Cancer and Aging Phenotypes from XPD Mutations. *Cell* **133**, 789–800 (2008).
10. Wolski, S. C. *et al.* Crystal Structure of the FeS Cluster–Containing Nucleotide Excision Repair Helicase XPD. *PLoS Biol* **6**, e149 (2008).

11. Liu, H. *et al.* Structure of the DNA Repair Helicase XPD. *Cell* **133**, 801–812 (2008).
12. Porello, S. L., Cannon, M. J. & David, S. S. A Substrate Recognition Role for the [4Fe-4S]<sub>2+</sub> Cluster of the DNA Repair Glycosylase MutY. *Biochemistry* **37**, 6465–6475 (1998).
13. Netz, D. J. A. *et al.* Eukaryotic DNA polymerases require an iron-sulfur cluster for the formation of active complexes. *Nat. Chem. Biol.* **8**, 125–132 (2012).
14. Weiner, B. E. *et al.* An Iron-Sulfur Cluster in the C-terminal Domain of the p58 Subunit of Human DNA Primase. *J. Biol. Chem.* **282**, 33444–33451 (2007).
15. Klinge, S., Hirst, J., Maman, J. D., Krude, T. & Pellegrini, L. An iron-sulfur domain of the eukaryotic primase is essential for RNA primer synthesis. *Nat. Struct. Mol. Biol.* **14**, 875–877 (2007).
16. Jain, R. *et al.* An Iron–Sulfur Cluster in the Polymerase Domain of Yeast DNA Polymerase  $\epsilon$ . *J. Mol. Biol.* **426**, 301–308 (2014).
17. Lessner, F. H., Jennings, M. E., Hirata, A., Duin, E. C. & Lessner, D. J. Subunit D of RNA Polymerase from *Methanosarcina acetivorans* Contains Two Oxygen-labile [4Fe-4S] Clusters IMPLICATIONS FOR OXIDANT-DEPENDENT REGULATION OF TRANSCRIPTION. *J. Biol. Chem.* **287**, 18510–18523 (2012).
18. Gari, K. *et al.* MMS19 Links Cytoplasmic Iron-Sulfur Cluster Assembly to DNA Metabolism. *Science* **337**, 243–245 (2012).
19. Stehling, O. *et al.* MMS19 Assembles Iron-Sulfur Proteins Required for DNA Metabolism and Genomic Integrity. *Science* **337**, 195–199 (2012).
20. Genereux, J. C., Boal, A. K. & Barton, J. K. DNA-Mediated Charge Transport in Redox Sensing and Signaling. *J. Am. Chem. Soc.* **132**, 891–905 (2010).

21. Genereux, J. C. & Barton, J. K. Mechanisms for DNA Charge Transport. *Chem. Rev.* **110**, 1642–1662 (2010).
22. Slinker, J. D., Muren, N. B., Gorodetsky, A. A. & Barton, J. K. Multiplexed DNA-Modified Electrodes. *J. Am. Chem. Soc.* **132**, 2769–2774 (2010).
23. Wan, C. *et al.* Femtosecond dynamics of DNA-mediated electron transfer. *Proc. Natl. Acad. Sci.* **96**, 6014–6019 (1999).
24. Boal, A. K. *et al.* DNA-Bound Redox Activity of DNA Repair Glycosylases Containing [4Fe-4S] Clusters†. *Biochemistry* **44**, 8397–8407 (2005).
25. Grodick, M. A., Segal, H. M., Zwang, T. J. & Barton, J. K. DNA-Mediated Signaling by Proteins with 4Fe–4S Clusters Is Necessary for Genomic Integrity. *J. Am. Chem. Soc.* **136**, 6470–6478 (2014).
26. Mui, T. P., Fuss, J. O., Ishida, J. P., Tainer, J. A. & Barton, J. K. ATP-Stimulated, DNA-Mediated Redox Signaling by XPD, a DNA Repair and Transcription Helicase. *J. Am. Chem. Soc.* **133**, 16378–16381 (2011).
27. Boal, A. K. *et al.* Redox signaling between DNA repair proteins for efficient lesion detection. *Proc. Natl. Acad. Sci.* **106**, 15237–15242 (2009).
28. Romano, C. A., Sontz, P. A. & Barton, J. K. Mutants of the Base Excision Repair Glycosylase, Endonuclease III: DNA Charge Transport as a First Step in Lesion Detection. *Biochemistry* **50**, 6133–6145 (2011).
29. Sontz, P. A., Mui, T. P., Fuss, J. O., Tainer, J. A. & Barton, J. K. DNA charge transport as a first step in coordinating the detection of lesions by repair proteins. *Proc. Natl. Acad. Sci.* **109**, 1856–1861 (2012).

30. Houten, B. V. Nucleotide excision repair in *Escherichia coli*. *Microbiol. Rev.* **54**, 18–51 (1990).
31. Goosen, N. & Moolenaar, G. F. Repair of UV damage in bacteria. *DNA Repair* **7**, 353–379 (2008).
32. Truglio, J. J., Croteau, D. L., Van Houten, B. & Kisker, C. Prokaryotic Nucleotide Excision Repair: The UvrABC System. *Chem. Rev.* **106**, 233–252 (2006).
33. Kad, N. M., Wang, H., Kennedy, G. G., Warshaw, D. M. & Van Houten, B. Collaborative Dynamic DNA Scanning by Nucleotide Excision Repair Proteins Investigated by Single- Molecule Imaging of Quantum-Dot-Labeled Proteins. *Mol. Cell* **37**, 702–713 (2010).
34. DellaVecchia, M. J. *et al.* Analyzing the Handoff of DNA from UvrA to UvrB Utilizing DNA-Protein Photoaffinity Labeling. *J. Biol. Chem.* **279**, 45245–45256 (2004).
35. Visse, R., King, A., Moolenaar, G. F., Goosen, N. & van de Putte, P. Protein-DNA interactions and alterations in the DNA structure upon UvrB-DNA preincision complex formation during nucleotide excision repair in *Escherichia coli*. *Biochemistry* **33**, 9881–9888 (1994).
36. Orren, D. K. & Sancar, A. The (A)BC excinuclease of *Escherichia coli* has only the UvrB and UvrC subunits in the incision complex. *Proc. Natl. Acad. Sci. U. S. A.* **86**, 5237–5241 (1989).
37. Orren, D. K. & Sancar, A. Formation and enzymatic properties of the UvrB.DNA complex. *J. Biol. Chem.* **265**, 15796–15803 (1990).

38. Verhoeven, E. E. A., Kesteren, M. van, Moolenaar, G. F., Visse, R. & Goosen, N. Catalytic Sites for 3' and 5' Incision of Escherichia coli Nucleotide Excision Repair Are Both Located in UvrC. *J. Biol. Chem.* **275**, 5120–5123 (2000).
39. Yoakum, G. H. & Grossman, L. Identification of E. coli uvrC protein. *Nature* **292**, 171–173 (1981).
40. Van Houten, B. & Kad, N. Investigation of bacterial nucleotide excision repair using single-molecule techniques. *DNA Repair* **20**, 41–48 (2014).
41. Pheaney, C. G., Arnold, A. R., Grodick, M. A. & Barton, J. K. Multiplexed Electrochemistry of DNA-Bound Metalloproteins. *J. Am. Chem. Soc.* **135**, 11869–11878 (2013).
42. Voloshin, O. N., Vanevski, F., Khil, P. P. & Camerini-Otero, R. D. Characterization of the DNA Damage-inducible Helicase DinG from Escherichia coli. *J. Biol. Chem.* **278**, 28284–28293 (2003).
43. Gamsjaeger, R., Liew, C. K., Loughlin, F. E., Crossley, M. & Mackay, J. P. Sticky fingers: zinc-fingers as protein-recognition motifs. *Trends Biochem. Sci.* **32**, 63–70 (2007).
44. Singh, S. *et al.* Solution structure and DNA-binding properties of the C-terminal domain of UvrC from E.coli. *EMBO J.* **21**, 6257–6266 (2002).
45. Truglio, J. J. *et al.* Structural insights into the first incision reaction during nucleotide excision repair. *EMBO J.* **24**, 885–894 (2005).
46. Karakas, E. *et al.* Structure of the C-terminal half of UvrC reveals an RNase H endonuclease domain with an Argonaute-like catalytic triad. *EMBO J.* **26**, 613–622 (2007).

47. Guzman, L. M., Belin, D., Carson, M. J. & Beckwith, J. Tight regulation, modulation, and high-level expression by vectors containing the arabinose PBAD promoter. *J. Bacteriol.* **177**, 4121–4130 (1995).
48. Ren, B., Duan, X. & Ding, H. Redox Control of the DNA Damage-inducible Protein DinG Helicase Activity via Its Iron-Sulfur Cluster. *J. Biol. Chem.* **284**, 4829–4835 (2009).
49. Gibney, B. R., Mulholland, S. E., Rabanal, F. & Dutton, P. L. Ferredoxin and ferredoxin–heme maquettes. *Proc. Natl. Acad. Sci.* **93**, 15041–15046 (1996).
50. McDevitt, C. A., Hanson, G. R., Noble, C. J., Cheesman, M. R. & McEwan, A. G. Characterization of the Redox Centers in Dimethyl Sulfide Dehydrogenase from *Rhodovulum sulfidophilum*†. *Biochemistry* **41**, 15234–15244 (2002).
51. Gorodetsky, A. A., Boal, A. K. & Barton, J. K. Direct Electrochemistry of Endonuclease III in the Presence and Absence of DNA. *J. Am. Chem. Soc.* **128**, 12082–12083 (2006).
52. Fu, W., O’Handley, S., Cunningham, R. P. & Johnson, M. K. The role of the iron-sulfur cluster in *Escherichia coli* endonuclease III. A resonance Raman study. *J. Biol. Chem.* **267**, 16135–16137 (1992).
53. Sontz, P. A., Muren, N. B. & Barton, J. K. DNA Charge Transport for Sensing and Signaling. *Acc. Chem. Res.* **45**, 1792–1800 (2012).
54. Grodick, M. A., Muren, N. B. & Barton, J. K. DNA Charge Transport within the Cell. *Biochemistry* **54**, 962–973 (2015).
55. Wallace, S. S. DNA glycosylases search for and remove oxidized DNA bases. *Environ. Mol. Mutagen.* **54**, 691–704 (2013).

56. Dunn, A. R., Kad, N. M., Nelson, S. R., Warshaw, D. M. & Wallace, S. S. Single Qdot-labeled glycosylase molecules use a wedge amino acid to probe for lesions while scanning along DNA. *Nucleic Acids Res.* **39**, 7487–7498 (2011).
57. Nelson, S. R., Dunn, A. R., Kathe, S. D., Warshaw, D. M. & Wallace, S. S. Two glycosylase families diffusively scan DNA using a wedge residue to probe for and identify oxidatively damaged bases. *Proc. Natl. Acad. Sci.* **111**, E2091–E2099 (2014).
58. Hughes, C. D. *et al.* Real-time single-molecule imaging reveals a direct interaction between UvrC and UvrB on DNA tightropes. *Nucleic Acids Res.* **41**, 4901–4912 (2013).

*Chapter 4*

## **Summary and perspectives**

The story of how the initial observations of DNA conducting charge led us to the point we are in studying possible applications for DNA CT within biological contexts is intriguing. It is an excellent example of how fundamental studies of the world around us have led to an entire branch of research, and one that may end up changing the paradigm for how we think about the processing and repair of DNA, which is arguably the most important biomacromolecule known to man. Many questions about how DNA CT may be utilized within biology have arisen. Do DNA repair proteins with redox-active moieties tap into the DNA helix and use it like a wire to perform DNA-mediated redox reactions from a distance? Does biology utilize the process of DNA CT? Specifically, do cells use DNA CT as a mechanism to interrogate the integrity of the DNA helix?

A number of DNA repair and DNA-processing enzymes are being found to contain 4Fe-4S clusters. These co-factors have been found in glycosylases, helicases, helicase-nucleases, and even enzymes such as DNA polymerase, RNA polymerase, and primase from organisms across the phylogeny. The role of these clusters in these enzymes has remained elusive. Generally, iron-sulfur clusters serve redox roles in nature since, formally, the cluster can exist in multiple oxidation states that can be accessed within a biological context. The 4Fe-4S clusters in DNA-processing enzymes were initially thought to serve solely a structural role, though, since the redox potentials for the clusters in proteins such as Endonuclease III (EndoIII) and DinG when freely diffusing lie outside the expected redox potentials within the cell. For these proteins, the  $[4\text{Fe-4S}]^{2+/1+}$  couple has a midpoint redox potential less than 400 mV vs. the normal hydrogen electrode (NHE) while the  $[4\text{Fe-4S}]^{3+/2+}$  couple has a midpoint redox potential of greater than 200 mV vs. NHE as measured using redox mediators and electrochemistry. It was previously shown using

DNA-modified electrodes, however, that EndoIII, MutY, afUDG, and SaXPD share a DNA-bound redox potential of 80 mV vs. NHE; by binding to DNA, the redox potentials move into the physiological range. Additionally, the ~200 mV negative shift of the potential of the  $[4\text{Fe-4S}]^{3+/2+}$  couple reflects an over three orders of magnitude increase in the DNA binding affinity of these proteins to in the oxidized state.

Taken together, these facts were used as a foundation for the hypothesis that DNA-binding proteins with 4Fe-4S clusters utilize DNA-mediated CT as a means to signal one another to scan the genome as a first step in locating the subtle damage that occurs within a sea of undamaged bases within cells, within the time constraints required by the cell. This mechanism would be of central importance, as it may explain how DNA repair proteins can search and repair damage before a cell divides. Indeed, it was previously shown using atomic force microscopy experiments examining EndoIII and SaXPD binding to well-matched vs. mismatched DNA that DNA-mediated CT can be used as a means of long range signaling to aid proteins with 4Fe-4S clusters in locating sites of damage. This DNA-mediated signaling was also tested within *E. coli* cells. It was shown using genetics experiments that EndoIII and MutY may utilize DNA-mediated signaling as a first step in recognizing damage within the genome. This work provided the first evidence that DNA-mediated CT may act as a signaling mechanism to coordinate DNA repair within the cell. But do other DNA repair proteins participate in this process, or is it exclusively used by base excision repair proteins? Is DNA-mediated signaling used globally by DNA-processing enzymes with 4Fe-4S clusters as a means to locate damage?

Herein we have described a role for 4Fe-4S clusters in DNA-mediated charge transport signaling among EndoIII, MutY, DinG, and UvrC, which appear to make up the

members of a network in *E. coli* that utilize this signaling as a means of coordinating the efficient repair of DNA. Using DNA-modified electrochemistry, we showed that when DinG is bound to a 20-mer duplex with a 15-mer 5' to 3' overhang, a substrate that DinG is competent to unwind in a helicase reaction, that DinG is redox-active at cellular potentials, and shares the 80 mV vs. NHE redox potential of EndoIII and MutY. When ATP, which activates the helicase activity of DinG, is added to solutions of DinG on these DNA-modified electrodes, the rate of growth of the electrochemical signal increased substantially.

We also explored if DinG cooperates with EndoIII or MutY using DNA-mediated CT as a means of signaling. Atomic force microscopy was used to directly visualize that DinG redistributes to sites of damage and that this redistribution is dependent on DNA-mediated CT. When DinG is mixed with strands of DNA that are well-matched and strands of DNA that contain a mismatch, the binding density ratio of DinG is greater on the mismatched strand. Signaling between EndoIII and DinG was established using the same assay. We also tested if DNA-mediated signaling with DinG could be observed within cells. Using a *lac*<sup>+</sup> reversion assay, it was found that knocking out DinG decreases MutY activity by ~2-fold. We showed that it is the iron-sulfur cluster and DNA-mediated CT by DinG that was responsible for this signaling; complementation with a different enzyme, EndoIII D138A, which is enzymatically inactive but CT-proficient, rescued the defect in MutY activity. EndoIII Y82A, which is enzymatically active but CT-deficient, led to no rescue in MutY activity. We showed that DinG can aid MutY in its activity, but does the same happen in reverse? Does MutY or EndoIII aid DinG in processing its substrate? Within InvA, a strain in which DinG is essential due to the need of DinG to unwind R-

loops, knocking out EndoIII led to a dramatic growth defect. Rescue was observed with RNaseH, which can act as a proxy for DinG since it can dismantle R-loops, establishing signaling between EndoIII and DinG. Additionally, WT EndoIII and EndoIII D138A rescued the growth defect, but EndoIII Y82A did not. Together, the experiments with DinG indicated that DNA-mediated signaling may be used by helicases in addition to glycosylases in order to facilitate enzymatic activity and that cross-talk can occur between two different repair pathways via a DNA-mediated mechanism.

In other work, it was shown herein that *E. coli* UvrC appears to contain a 4Fe-4S cluster. UV-visible absorbance was used to show that UvrC contains the characteristic broad peak at 410 nm attributed to a 4Fe-4S cluster. EPR spectroscopy revealed the signature features that would be expected for a 4Fe-4S cluster, specifically in the reduced state upon treatment with a chemical reductant. To further study the redox characteristics of UvrC, DNA-modified electrochemistry was used to show that UvrC shares a redox potential with EndoIII, MutY, and DinG. To probe whether UvrC depends upon DNA-mediated CT signaling in order to efficiently repair damage, a UV sensitivity assay was used to show that by knocking out DinG, cells are 5-10 fold more sensitive to UV light. This growth defect upon UV irradiation is again rescued by EndoIII D138A, but not EndoIII Y82A. Even though EndoIII, MutY, DinG, and UvrC are from different repair pathways and are responsible for processing different substrates, they all appear to use DNA-mediated CT as a means of signaling. What these enzymes have in common is the presence of a redox-active 4Fe-4S cluster that can participate in long range redox signaling. We believe we have now revealed a DNA-mediated signaling network that exists among DNA-processing enzymes that contain 4Fe-4S clusters within *E. coli*.

While only a handful of DNA-processing enzymes within *E. coli* have been shown to contain 4Fe-4S clusters, in higher organisms within the archaeal and eukaryotic domains of the phylogeny, these 4Fe-4S clusters have not only been maintained through evolution, but apparently became even more ubiquitous within DNA-processing enzymes. Multiple helicases, helicase-nucleases, and even DNA polymerases, RNA polymerase, and primase have now been shown to contain these inorganic cofactors in eukaryotes. Considering the energetic demands of synthesizing and delivering iron-sulfur clusters to proteins and the risk of bringing iron, which can severely damage DNA in the presence of reactive oxygen species, to DNA, it is curious that evolution held on to these 4Fe-4S clusters. This fact points to these clusters likely serving an important role within cells. Given the repertoire of structural building blocks that nature has at its disposal, it is unlikely that the primary role of these clusters is a structural one, though removing a cubane that resides near a protein's core still would disturb the local structure and could perturb DNA-binding, and thus enzymatic activity, since these 4Fe-4S clusters often reside near the protein-DNA binding interface. Herein, we have described how we believe that these 4Fe-4S clusters are utilized by DNA repair and DNA-processing enzymes within *E. coli*, but these studies must be extended to eukaryotic proteins and organisms. Given that enzymes involved in transcription and replication have been shown to contain 4Fe-4S clusters, it is tempting to propose that DNA CT may be used as a global mechanism to coordinate replication and transcription in addition to repair. Also, redox-dependent switching or tuning of enzymatic activity may occur within these enzymes. In conclusion, more and more evidence is emerging that there is a role for DNA CT within cells to coordinate the search and repair process, but a tremendous amount of information about this process is still unknown, and

more methods to study this phenomenon must be developed.

*APPENDIX I*

## **Multiplexed Electrochemistry of DNA-bound Metalloproteins**

Adapted from: Pheeny, C. G., Arnold, A. R., Grodick, M. A. & Barton, J. K. *J. Am. Chem. Soc.* **135**, 11869 (2013).

C. G. Pheeny developed, ran, and analyzed electrochemical experiments with the aid of A. R. Arnold and M. A. Grodick. A. R. Arnold expressed and purified EndoIII mutants and performed circular dichroism. M. A. Grodick purified wild type EndoIII.

## Introduction

Multiplexed electrodes are emerging as a powerful analytical tool particularly in the development of electrochemical diagnostics for the detection of pathogens and cancer markers.<sup>1-13</sup> Multiplexed DNA-modified electrodes have been developed to sense an extensive range of targets including small molecule,<sup>4,5,11</sup> DNA,<sup>6,10-12</sup> RNA,<sup>8-10</sup> and proteins.<sup>3,7,11-13</sup> These devices all strive to achieve the same goals of enhanced sensitivity, faster detection times, and tolerance to cell lysates.<sup>5,9,12</sup> Despite variety in the design of these multiplexed DNA-modified electrodes, they all possess the same intrinsic benefits of statistical comparisons and parallel experimentation; these advantages have proven to be essential for the electrochemical characterization of complex systems. Ultimately, these technologies possess ideal attributes for performing the next generation of fundamental electrochemical measurements as they have been optimized for low variability, real-time monitoring, and complex substrates.

The utility of multiplexed analysis for the fundamental studies of macromolecules was demonstrated in the characterization of charge transport through DNA.<sup>12-14</sup> One such case is the measurement of ground state DNA-mediated charge transport (DNA CT) through exceptionally long DNA distances up to 34 nm.<sup>14</sup> DNA CT is the process through which charge is conducted through the  $\pi$ -stack of the DNA base pairs.<sup>15-17</sup> Both the exquisite sensitivity of even a subtle perturbation in DNA stacking<sup>18,19</sup> and the shallow distance dependence<sup>14,15</sup> of DNA CT have been characterized using DNA-modified electrodes affixed with a redox-active moiety at the distal end of the duplex. Multiplexing these DNA-modified electrodes onto a single device was crucial in establishing that the

electrochemical signal was generated via DNA CT over such long molecular distances and that the  $\pi$ -stack of the DNA was well stacked and in a biologically relevant conformation.<sup>14</sup>

Here we utilize multiplexed technology to investigate the electrochemistry of DNA repair proteins containing [4Fe-4S] clusters (Figure A1.1). DNA-modified electrodes have become a necessary tool to investigate the electrochemistry of the iron-sulfur cofactor of many DNA repair proteins, including EndonucleaseIII (EndoIII), MutY, UDG, SoxR, and XPD, towards identifying the *in vivo* relevance for this redox activity.<sup>20-24</sup> Upon DNA-binding of EndoIII, the  $3^+/2^+$  redox couple of its [4Fe-4S] cluster has been shown to shift  $\sim -200$  mV compared to freely diffusing protein, to approximately 80 mV versus NHE.<sup>25</sup> Thus, binding of the DNA polyanion brings the  $3^+/2^+$  redox potential of the [4Fe-4S] cluster into a physiologically relevant range. Moreover, disease related mutants show deficiencies in DNA CT through their weaker electrochemical signals. Interestingly, DNA-binding proteins involved in genome maintenance have increasingly been found to contain [4Fe-4S] clusters.<sup>26-29</sup> We have proposed that the redox chemistry of these [4Fe-4S] clusters are critical as a first step in the search mechanism used by DNA repair proteins to redistribute to the vicinity of DNA damage.<sup>21,30</sup> The proposed model hinges on the ability of these [4Fe-4S] cluster proteins to electronically couple to the  $\pi$ -stack of DNA in order to perform efficient searching of the genome facilitated by DNA CT. This efficient DNA-mediated CT between repair proteins seems to depend on the similar reduction potentials of their clusters. The consistent DNA-bound midpoint potential of these various proteins containing [4Fe-4S] clusters has been of particular interest. In this work, we investigate

## Multiplexed [4Fe-4S] cluster protein electrochemistry

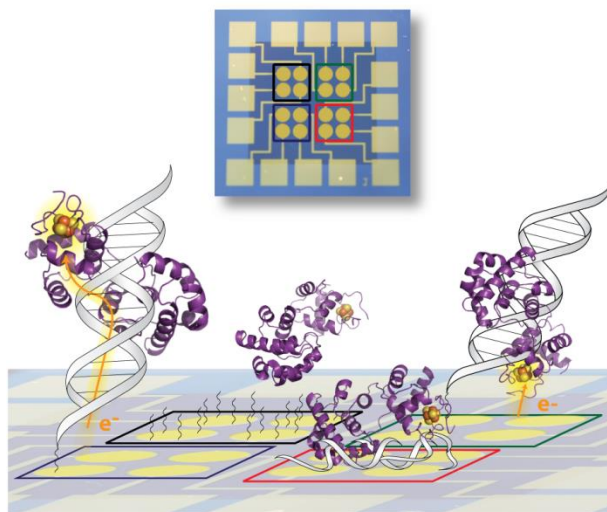


**Figure A1.1** Schematic depicting the versatility of multiplexed analysis for the investigation of metalloprotein electrochemistry. Our multiplexed devices are composed of 16 electrodes that are divisible into 4 separate quadrants of 4 electrodes, having the capability of producing 4 distinct experimental conditions on a single Au surface. This assembly allows for facile comparisons of the electrochemical signal from various DNA-bound proteins across varying DNA substrates and morphologies.

how the electrostatics of the protein fold, in addition to binding of the DNA polyanion, may tune the reduction potential of the cluster. Thus it becomes important to characterize the DNA-bound electrochemistry of these proteins containing [4Fe-4S] clusters in a quantitative manner that allows for direct side-by-side comparison of potentials and couplings through multiplexing.

## Materials and Methods

### *Oligonucleotide preparation*

All DNA substrates were synthesized on a 3400 Applied Biosystems DNA synthesizer with all phosphoramidites and reagents purchased from Glen Research. The sequences of the DNA substrates used were 5' - HS -C<sub>6</sub>- AGT ACA GTC ATC GCG - 3' for the thiol strand and 3' - TCA TGT CAG TAG CGC - 5' for the complement strand. Additional complements were prepared that yield either a TC mismatch or an abasic site at the position of the underlined adenine. Both the complement and thiol-modified DNA were purified through standard procedures as previously reported.<sup>13</sup> All single-stranded DNA was purified by high pressure liquid chromatography (HPLC) using a reverse phase PLRP-S column, purchased from Agilent. The identity of the oligonucleotides was confirmed by matrix-assisted laser-desorption ionization – time of flight (MALDI-TOF) mass spectrometry. The thiol-modified single stranded DNA was reduced with 100 mM dithiothreitol (Sigma) in Tris buffer (50 mM Tris HCl, 50 mM NaCl, pH 8.4) for 40 minutes and purified by size exclusion chromatography (Nap5 Sephadex G-25, GE Healthcare) as well as reverse phase HPLC. Single-stranded DNA stocks were then desalted by precipitation in ethanol and re-suspended in phosphate buffer (5.0 mM phosphate, 50 mM

NaCl, pH 7.0). Equimolar amounts of single-stranded stocks were combined based on quantification by UV-Visible spectroscopy. The extinction coefficients at 260 nm from the IDT SciTools were used for the quantification of the single-stranded DNA stocks. All DNA solutions were then thoroughly deoxygenated with argon and annealed by heating to 90 °C followed by a slow cooling to ambient temperature over 90 minutes.

#### *Site-Directed Mutagenesis*

E200K, Y205H, and K208E EndoIII mutants were prepared using a pET11 vector containing the *nth* gene with N-terminal ubiquitin and hexahistidine tags<sup>22</sup> and a Quikchange II-E Site-Directed Mutagenesis Kit (Stratagene). Y82A EndoIII was prepared previously.<sup>22</sup> Primers were purchased from Integrated DNA Technologies and primer sequences are provided in the Supporting Information (Table A1.1). All mutagenized plasmids were sequenced (Laragen) to confirm the desired sequences.

#### *Protein Overexpression and Purification*

A stock of BL21star-(DE3)pLysS containing a pET11-ubiquitin-His<sub>6</sub>-*nth* construct was used to inoculate a 100 mL culture of LB containing 100 µg/mL of ampicillin and 35 µg/mL of chloramphenicol. This culture was grown overnight at 37 °C with shaking. Then, 1 mL of the overnight culture was used to inoculate each of four 1L cultures of LB containing the same amount of ampicillin and chloramphenicol as the overnight culture. The 1L cultures were shaken at 37 °C until the OD<sub>600</sub> reached ~0.6-0.8. Enough isopropyl β-D-1-thiogalactopyranoside (IPTG) was then added to bring the

**Table A1.1** Primer Sequences for site-directed mutagenesis.

<b>Mutation</b>	<b>Primer</b>
Y205H	5'- TGT GAA <b>CAC</b> AAA GAG AAA GTT GAC ATC TGA GGA TCC GGC TGC TAA C -3' (Forward)
	5'- GTT AGC AGC CGG ATC CTC AGA TGT CAA CTT TCT CTT <b>TGT</b> <b>GTT</b> CAC A -3' (Reverse)
E200K	5'- GCC CCG CTG TGG CTC TTG TAT TAT <b>TAA</b> <b>AGA</b> TCT TTG TGA ATA C -3' (Forward)
	5'- GTA TTC ACA AAG ATC <b>TTT</b> AAT AAT ACA AGA GCC ACA GCG GGG C -3' (Reverse)
K208E	5'- GTG AAT ACA AAG <b>AGG</b> <b>AAG</b> TTG ACA TCT GAG GAT CCG GCT GCT AAC -3' (Forward)
	5'- GTT AGC AGC CGG ATC CTC AGA TGT CAA <b>CTT</b> <b>CCT</b> CTT TGT ATT CAC -3' (Reverse)

total concentration of IPTG to 300  $\mu\text{M}$ . The cultures were subsequently shaken at 150 rpm for ~3.5 hours at 30° C. The cells were collected by centrifugation at 5,500 rpm for 15 minutes, flash-frozen, and stored at -80 °C. All subsequent steps were carried out at 4 °C or on ice. On the day of the purification the pellet was resuspended in 250 mL of Buffer A (20 mM sodium phosphate, pH 7.4, 250 mM NaCl, 5 mM DTT, 5% glycerol, DNase (Roche), RNase (Roche), and EDTA-free protease inhibitor cocktail tablets (Roche)). The resuspended cells were lysed via microfluidization. The cell lysate was clarified by centrifugation at 17,000  $g$  for 30 minutes. Enough NaCl was added to the resulting supernatant to bring the NaCl concentration to 500 mM. The supernatant was then loaded onto a Histrap HP column (GE Healthcare) that had been equilibrated with buffer B (20 mM sodium phosphate, pH 7.4, 500 mM NaCl, 1 mM DTT). After washing with buffer B, EndoIII was eluted using a gradient from 0-100% buffer C (20 mM sodium phosphate, pH 7.4, 500 mM NaCl, 500 mM imidazole, 1 mM DTT) over 20 column volumes. A yellow band that eluted at ~100 mM imidazole was collected. This imidazole-containing buffer was then immediately exchanged into buffer D (20 mM sodium phosphate, pH 7.4, 500 mM NaCl, 0.5 mM EDTA, and 20 % glycerol) using a HiPrep 26/10 desalting column (GE Healthcare). The protein solution, now in buffer D, was concentrated down to ~5 mL using 10,000 MWCO Amicon Ultra-15 centrifugation filter units (Millipore) and was loaded onto a HiLoad Superdex 16/600 75  $\mu\text{g}$  size exclusion column (GE Healthcare) that had been equilibrated with the protein storage buffer (20 mM sodium phosphate, pH 7.4, 100 mM NaCl, 0.5 mM EDTA, 20 % glycerol). A clean peak that eluted after approximately 50-55 mL of buffer had passed through the column was collected and concentrated to achieve a final concentration of ~ 100  $\mu\text{M}$  as quantified using an  $\epsilon_{410}$  of 17,000  $\text{M}^{-1}\text{cm}^{-1}$ .<sup>30</sup>

The protein was then aliquoted, flash-frozen in liquid nitrogen and stored at -80 °C. The approximate yield was 6 mg/L. The purity of the protein was determined to be >95% as analyzed by SDS-PAGE (data not shown).

#### *Glycosylase activity assay*

Glycosylase activity was determined for each mutant (Y205H, K208E, and E200K) compared to wild type EndoIII based on previously established methods.<sup>22</sup> For this assay, protein samples (1  $\mu$ M) were incubated for 15 min at 37 °C with 5'-<sup>32</sup>P-radiolabeled 35-mer duplex DNA (100 nM) modified with 5-hydroxy uracil, a substrate for EndoIII, in 10 mM Tris HCl, 1 mM EDTA, 50 mM NaCl, pH 7.6. Reactions were then quenched by adding of 1 M NaOH to a final concentration of 100 mM NaOH, dried, and electrophoresed through 20% denaturing PAGE at 90 W for 1.5 hours (Figure A1.2). The glycosylase activity was determined as the fraction of 14-mer product observed relative to the total quantity of DNA.

*Multiplexed Chip Fabrication* Multiplexed chips consisting of 16 gold electrodes were prepared using standard photolithography techniques as adapted from previously established protocols.<sup>13</sup> Photoresist was used to pattern nine 1 inch by 1 inch chips on 525  $\mu$ m thick silicon wafers (SiliconQuest) that had a thermal oxide layer grown to a thickness of roughly 4,000 Å to insulate the wafer. A titanium adhesion layer (3 nm) followed by a gold layer (100 nm) was deposited using an electron beam evaporator without breaking the vacuum between depositions. The metal lift-off was performed directly after metal deposition using Remover PG (MicroChem) heated to 60 °C for one

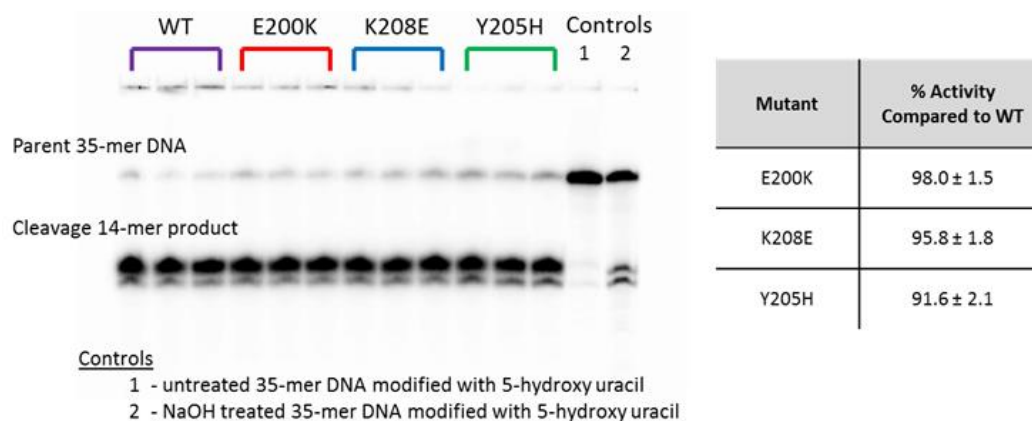


**Figure A1.2** Enzymatic assay for EndoIII glycosylase activity. Glycosylase activity was determined for each mutant (Y205H, K208E, and E200K) compared to wild type EndoIII based on previously established methods (22). For this assay, protein samples (1  $\mu$ M) were incubated for 15 min at 37 °C with 5'-<sup>32</sup>P-radiolabeled 35-mer duplex DNA (100 nM) modified with 5-hydroxy uracil, a substrate for EndoIII, in 10 mM Tris HCl, 1 mM EDTA, 50 mM NaCl, pH 7.6. Reactions were then quenched by adding of 1 M NaOH to a final concentration of 100 mM NaOH, dried, and electrophoresed through 20% denaturing PAGE at 90 W for 1.5 hours. Glycosylase activity of EndoIII results in the appearance of the 14-mer cleavage product in the denaturing gel. The glycosylase activity was determined as the fraction of 14-mer product observed relative to the total quantity of DNA and the percent activity compared to WT (purple) was then calculated for Y205H (green), K208E (blue), and E200K (red). Two control lanes containing the 35-mer duplexed DNA, yet lacking the enzymatic protein, were either untreated or treated with the 1 M NaOH.

hour. The wafers were then dehydrated by baking at 180 °C for at least 2 hours and an insulating SU8 layer (3  $\mu$ m) was coated on the wafer. This SU8 layer was patterned such

that the working electrodes and contact pads were left exposed yet the connective wires were covered to define a controlled working electrode area ( $2 \text{ mm}^2$ ). The SU8 was cured with a final hard bake at  $150 \text{ }^\circ\text{C}$  for 15 minutes. The wafer was then cleaved into individual chips (Dynatex Scriber/Braker) to prevent any scratching of the exposed working electrode surfaces.

#### *DNA-modified Electrode Assembly*

Single electrode experiments were performed with a low-volume constrained Au(111) on mica surface (Molecular Imaging), as previously established.<sup>20</sup> Multiplexed electrode experiments were performed with the 16 electrode chips divided into four quadrants of four electrodes each.<sup>13</sup> Multiplexed chips were cleaned in acetone and isopropanol as well as ozone-cleaned for 5 minutes at 20 mW immediately prior to the assembly into a holder and the exposure to thiol-modified DNA. The cleaned chip was then assembled in a polycarbonate holder used to position the chip. A rubber gasket and acrylic clamp are used to define the four quadrants and create a common central well. The rubber Buna N gasket (0.020" thick, unless otherwise indicated) and clamp are manufactured by SAS Industries and Xcentric, respectively. A fresh gasket and clamp are used for each experiment to prevent any cross contamination between experiments.

Duplex DNA (20  $\mu\text{l}$  of 25  $\mu\text{M}$ ) was placed in each quadrant of a multiplexed chip and left to self-assemble overnight (16-24 hours) in a humid environment. To ensure efficient monolayer formation, thiol-modified DNA was used within two weeks of the dithiothreitol reduction. Loosely packed DNA films were assembled in the absence of  $\text{MgCl}_2$  while closely packed DNA films were assembled with the addition of 100 mM

MgCl<sub>2</sub>. Once DNA films were assembled and thoroughly washed with phosphate buffer, the electrodes were backfilled with 1 mM 6-mercaptohexanol (MCH) for 45 min in phosphate buffer with 5 % glycerol. Background scans were acquired with common running buffers exposed to the electrodes. An initial background scan is acquired in phosphate buffer (5 mM phosphate, 50 mM NaCl, pH 7.0) followed by a subsequent scan in spermidine buffer (5 mM phosphate, 50 mM NaCl, 40 mM MgCl<sub>2</sub>, 5 mM spermidine, pH 7.0).

#### *Protein Electrochemical Measurements*

Electrochemical measurements were performed with a CHI620D Electrochemical Analyzer and a 16-channel multiplexer from CH Instruments. A three-electrode setup was used with a common Pt auxiliary and a quasi Ag/AgCl reference electrode (Cypress Systems) placed in the central well of the clamp. Cyclic voltammetry data were collected at 100 mV/s over a window of 0.1 mV to -0.4 mV versus Ag/AgCl unless otherwise indicated. After background scans, EndoIII samples in phosphate buffer (20 mM sodium phosphate, 100 mM NaCl, 0.5 mM EDTA, 20 % glycerol, pH 7.4) were added to the central well or separated quadrants (120  $\mu$ L total for the four quadrants), ranging in concentrations from 30 – 90  $\mu$ M quantified using the absorbance of the [4Fe-4S] cluster at 410 nm ( $\epsilon = 17,000 \text{ M}^{-1}\text{cm}^{-1}$ ).<sup>31</sup> EndoIII was allowed to incubate on the multiplexed chip for up to 12 hours and monitored over time. The chip was stored in a humid environment between subsequent scans to prevent solution evaporation and hold the concentration constant over time.

### *Circular Dichroism Thermal Denaturation*

For protein samples (5  $\mu\text{M}$ ), the ellipticity at 223 nm (the largest difference between native and denatured protein) was measured as a function of increasing temperature (20  $^{\circ}\text{C}$  to 60  $^{\circ}\text{C}$ ) using a Model 62A DS circular dichroism spectrometer (AVIV). All data shown are the average of at least duplicate measurements. Measured ellipticity was converted to fractional change in ellipticity by assigning the native protein a value of 0 and the fully denatured protein a value of 1. In order to extract melting temperature values, data were fit using a non-linear least-squares regression to a simple two-state unfolding model.<sup>32</sup> Reported errors in  $T_m$  values are derived from this fitting.

## **Results**

### **Multiplexed electrochemistry of EndoIII**

The electrochemical behavior of the [4Fe-4S] cluster of EndoIII incubated on loosely packed DNA films, assembled in the absence of  $\text{MgCl}_2$ , was first compared between individual and multiplexed electrode assemblies. A reversible signal for the [4Fe-4S]-cluster of EndoIII, with the ratio of the reduction and oxidation currents being near unity, at a mid-point potential of  $80 \pm 3$  mV vs. NHE was observed on both single electrode and multiplexed assemblies (Figure A1.3).

The signal size for the redox couple of EndoIII depended on incubation time and concentration on both assemblies; this behavior as well as the mid-point potential is consistent with previously established results for EndoIII on DNA-modified electrodes.<sup>22</sup> The consistency across all 16 multiplexed electrodes was comparable to that seen with previous multiplexed DNA-modified electrodes and showed at most a 3.5 % deviation in

signal size (Figure A1.3).<sup>13</sup> The analogous experiment run on individual single electrodes would yield dramatically higher variability on the order of 20-40 %.<sup>22</sup>

Due to the modular nature of the multiplexed electrode assembly, the thickness of the rubber gasket used to seal the central well was varied to increase accessibility to the electrodes. Background scans and EndoIII signal sizes were compared for gaskets 0.064", 0.032", and 0.020" thick. Oxygen contributions in the background scans, likely caused by trapped oxygen in close proximity to the electrode surface, were decreased drastically with the use of the thinner gaskets yielding much more uniform CVs and increased EndoIII signal size (Figure A1.4). Overall, the most exposed electrodes produced featureless background scan resulting in a 0.020" thick Buna N gasket being utilized for all subsequent experiments.

### **EndoIII on differing DNA monolayers**

The effect of DNA substrates and film morphology on the EndoIII signal was next investigated. Allowing the self-assembly of DNA monolayers to form in the presence of  $\text{MgCl}_2$  dramatically affects the film packing and ultimately the density of the DNA monolayer formed.<sup>33</sup> In the presence of  $\text{MgCl}_2$ , the negative charge of the DNA phosphate backbone is screened, allowing neighboring duplexes to more closely associate and self-assemble into a tightly packed DNA monolayer. Incubation of EndoIII on DNA-modified electrodes assembled with duplex DNA (dsDNA) was found to produce a redox couple with the same mid-point potential as previously described ( $80 \pm 3$  mV vs. NHE)

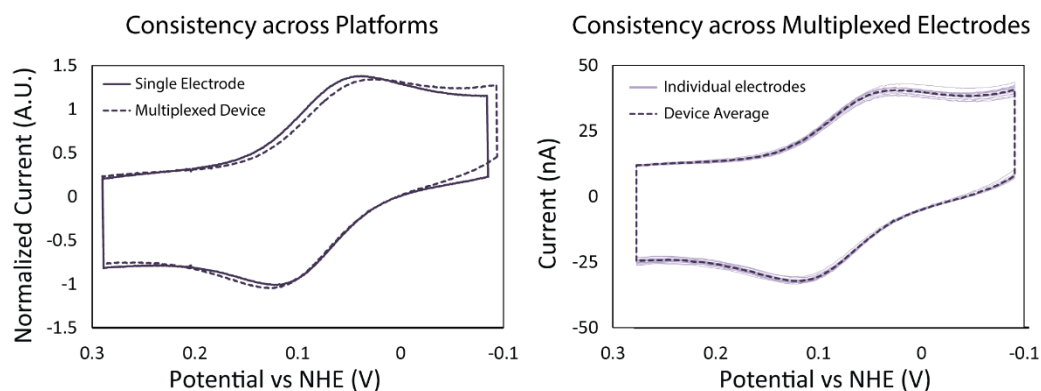


**Figure A1.3** Consistency of DNA-modified electrodes. (*Left*) The signals generated after incubation of loosely packed DNA-modified electrodes with EndoIII (30  $\mu\text{M}$ ) in phosphate buffer (20 mM sodium phosphate, 100 mM NaCl, 0.5 mM EDTA, 20 % glycerol, pH 7.4) were used to directly compared the single (solid) and multiplexed (dashed) electrochemical assemblies. The cyclic voltammetry (scan rate = 100 mV/s) was normalized, based on the capacitance at 0.3 mV vs NHE, so relative signal sizes could be compared across platforms. (*Right*) The variability of the EndoIII signal, under the same conditions, across all 16 electrodes (light solid line) of a single multiplexed device was within 3.5% of the average CV for the device (dark dashed line).

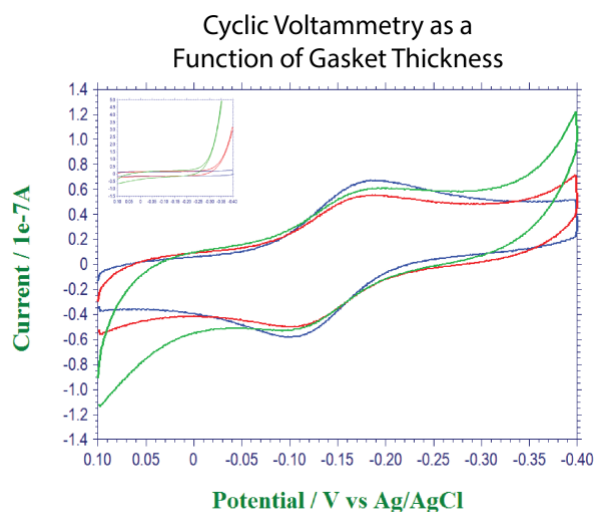


**Figure A1.4** Cyclic voltammetry (scan rate = 100 mV/s) of EndoIII (30  $\mu$ M) incubated on closely packed well-matched duplex DNA monolayers acquired in phosphate buffer (20 mM sodium phosphate, 100 mM NaCl, 0.5 mM EDTA, 20 % glycerol, pH 7.4) are presented. Three different thicknesses for the Buna N gasket, utilized during the multiplexed chip assembly, were tested: 0.064" (green), 0.032" (red), and 0.020" (red). With decreasing gasket thickness the signal generated from EndoIII is shown to increase while the background contributions decrease. *Inset*: Background signals acquired prior to the addition of EndoIII in spermidine buffer (5 mM phosphate, 50 mM NaCl, 40 mM  $\text{MgCl}_2$ , 5 mM spermidine, pH 7.0).

regardless of DNA film morphology, while single-stranded DNA (ssDNA) monolayers showed cyclic voltammograms that were relatively featureless compared to background scans, even after 8 hours of protein incubation (Figure A1.5). As both the underlying gold surface and the protein solution were common across all electrodes, this appearance of a reversible redox couple from EndoIII on the dsDNA monolayers but not on the ssDNA films indicates that the signal generated from EndoIII is dependent on binding to duplex DNA. Moreover, since the DNA-bound redox potential for EndoIII is not observed on these ssDNA-modified electrodes, these ssDNA-modified electrodes provide a useful control against surface contaminants.

The DNA-bound signal of EndoIII was then compared on DNA-modified electrodes assembled with different morphologies. The peak splitting for the  $3^{+}/2^{+}$  redox couple of the [4Fe-4S] cluster of EndoIII was found to be dependent on monolayer morphology, while the mid-point potential remained unaltered. The consistency of the mid-point potentials between the surface morphologies indicates that EndoIII is in the same electrostatic environment, bound to duplex DNA, regardless of the monolayer morphology. The closely and loosely packed DNA monolayers show peak splittings of  $88 \pm 4$  mV and  $64 \pm 2$  mV, respectively (Figure A1.5). In addition to the increase in peak splitting, there is also a broadening of the signal observed upon switching to the more closely packed DNA films. Increases in the peak splitting and broadening of the redox couple are both indicative of decreases in the rate of electron transfer and the homogeneity of the electrochemical process.<sup>34</sup> These two characteristics, an increase in peak splitting and heterogeneity, have previously been seen as characteristics of a redox-active moiety on DNA-modified electrodes being reduced by DNA CT.<sup>35</sup>

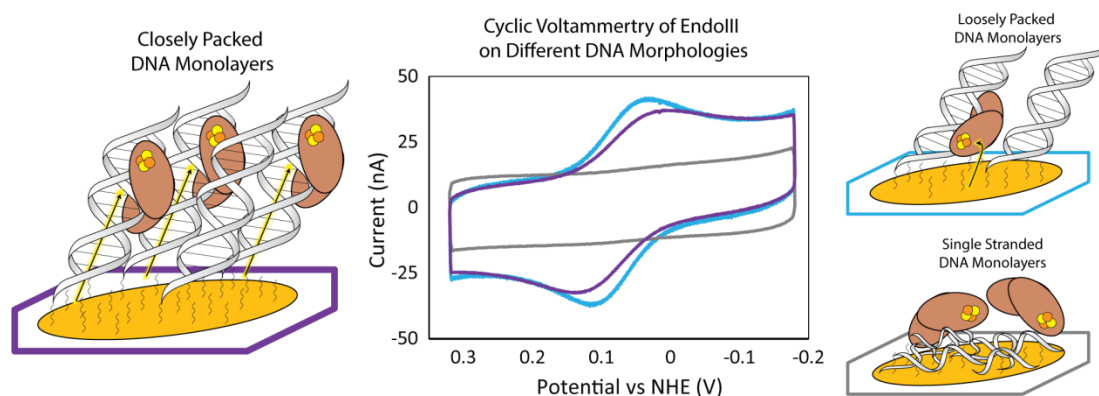


**Figure A1.5** The electrochemistry of EndoIII on DNA-modified electrodes was determined as a function of the underlying DNA film morphology. DNA monolayers were allowed to self-assemble over 16-24 hours either with or without 100 mM  $\text{MgCl}_2$  to form either closely (purple) or loosely (blue) packed DNA monolayers. All morphologies were directly compared on the same multiplexed device so the differences in the EndoIII (60  $\mu\text{M}$ ) redox signal could be resolved. Cyclic voltammetry scans (scan rate = 100 mV/s) were compared in phosphate buffer (20 mM sodium phosphate, 100 mM NaCl, 0.5 mM EDTA, 20 % glycerol, pH 7.4) and the peak splitting and signal size were both quantified. Single-stranded DNA monolayers (grey) were prepared and shown to not produce a DNA-bound EndoIII signal.

### DNA-mediated electrochemistry of EndoIII

The mechanism of electron transfer to the [4Fe-4S] cluster in EndoIII was next investigated on both loosely and closely packed dsDNA-modified electrodes. DNA-mediated reduction is exceptionally sensitive to even subtle perturbations to the intervening  $\pi$ -stack.<sup>18,19</sup> Therefore, the yield of [4Fe-4S] cluster reduction was examined after introducing a single perturbation site into the DNA duplexes self-assembled on the electrodes. Either a single thymine-cytosine mismatch (TC) or an abasic site (Ab) were incorporated into thiol-modified dsDNA near the electrode surface to prevent EndoIII binding to the  $\pi$ -stack below the perturbation site, as EndoIII binds non-specifically to non-substrate DNA. The dsDNA stocks for the well-matched (WM), TC, and Ab sequences were all quantified and annealed using the same thiol-modified ssDNA stock. This consistency of the thiol strand avoids any variability caused by the efficiency of monolayer formation due to the reactivity of the thiol-modifier. These dsDNA sequences, as well as a ssDNA control, were then assembled on a multiplexed chip.

The reduction signal for the [4Fe-4S] cluster of EndoIII was characterized across these different DNA substrates on both loosely and closely packed films (Figure A1.6). When these DNA substrates were assembled in the presence of MgCl<sub>2</sub>, producing closely packed DNA monolayers, the reduction signal of EndoIII was attenuated upon introducing single base pair lesions. The WM, TC, and Ab dsDNA monolayers gave signal sizes of  $56 \pm 1$  nA,  $42 \pm 1$  nA, and  $41 \pm 4$  nA respectively after EndoIII incubation (60  $\mu$ M for 8 hours), resulting in an average signal attenuation of  $24 \pm 1\%$  and  $26 \pm 2\%$  upon incorporating a TC mismatch or an abasic site, respectively (Figure A1.6). This attenuation in the reduction signal due to the incorporation of perturbations to the  $\pi$ -stack

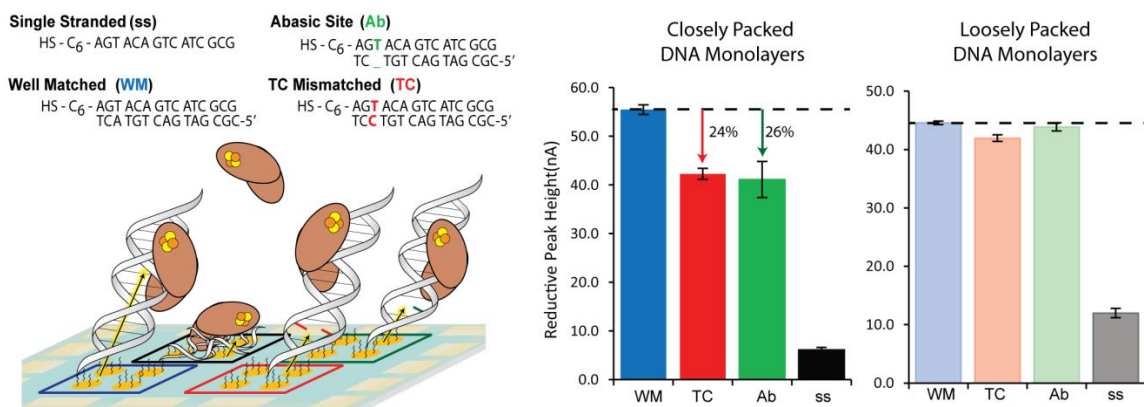


**Figure A1.6** The degree of signal attenuation induced by a single perturbation to the  $\pi$ -stack, for both closely and loosely packed DNA monolayers was investigated. (Left) Schematic of multiplexed devices prepared with well-matched (blue), TC mismatched (red), and abasic site (green) duplex DNA, and a single-stranded control (black). The sequences are indicated above. (Right) The reductive signals from DNA-bound EndoIII in phosphate buffer (20 mM sodium phosphate, 100 mM NaCl, 0.5 mM EDTA, 20 % glycerol, pH 7.4) were quantified for DNA monolayers assembled in both the presence (dark) and absence (light) of 100 mM MgCl<sub>2</sub> yielding closely and loosely packed DNA, respectively. The percent signal attenuations of the TC mismatch and abasic site were determined based on the average signal size, across all four electrodes in a quadrant, compared to that of well-matched DNA. The signals generated from closely packed DNA-films displayed distinct attenuation upon introducing either a mismatch or abasic site, while the signals from loosely packed DNA-films did not display this sequence dependence.

support the assignment of the electrochemical signal from EndoIII observed on closely packed DNA films being mediated by DNA CT. Conversely, when the same set of DNA substrates was compared using loosely packed DNA monolayers, there was no significant difference in the reduction signal observed with the introduction of these perturbations. The loosely packed DNA monolayers of WM, TC mismatched, and Ab DNA produced signal sizes of  $45 \pm 0.3$  nA,  $42 \pm 1$  nA, and  $44 \pm 1$  nA, respectively, which yield a p-value  $> 0.05$  when compared using a one-tailed t-test, do not display statistically significant signal attenuation as compared to EndoIII bound to the closely packed DNA monolayer. This lack of signal attenuation with the incorporation of perturbation to the  $\pi$ -stack indicates that the DNA-bound signal of EndoIII is not mediated by electron transfer through the  $\pi$ -stack, in loosely packed DNA monolayers.

### **Kinetics of EndoIII reduction**

The kinetics of EndoIII reduction was assessed on these two different dsDNA morphologies to explore further the mechanistic differences in the electron transfer pathways. In addition to the peak splitting, the EndoIII reduction on loosely and closely packed DNA monolayers was found to differ in the signal accumulation both as a function of scan rate as well as incubation time. For a diffusion rate-limited process this signal accumulation increases linearly as a function of the square root of the scan rate.<sup>34</sup> The [4Fe-4S] cluster signal of EndoIII was measured over 10 different scan rates ranging from 10 mV/s to 200 mV/s on both loosely and closely packed dsDNA films and plotted as a function of the square root of the scan rate,  $v^{1/2}$  (Figure A1.7). In the case of loosely packed dsDNA films, the current was found to be linear with respect to  $v^{1/2}$ , as previously

Scan Rate Dependence of EndoIII Reduction Signal

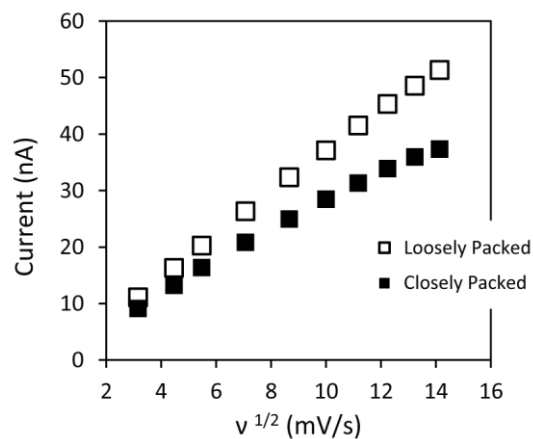


**Figure A1.7** Kinetic analysis of the signal generated from EndoIII on differing DNA film morphologies is indicated. Cyclic voltammetry (scan rates ranging from 10 mV/s to 200 mV/s) of EndoIII were obtained in phosphate buffer (20 mM sodium phosphate, 100 mM NaCl, 0.5 mM EDTA, 20 % glycerol, pH 7.4) for both closely (solid) and loosely (outlined) packed DNA monolayers. The reductive peak height for both morphologies, on the same multiplexed device, was quantified and plotted as a function of the square root of the scan rate,  $v^{1/2}$ . The non-linearity of the signal from closely packed DNA films indicates that the signal is not diffusion rate limited.

established for the diffusion rate-limited reduction of DNA-bound [4Fe-4S] cluster proteins on this dsDNA film morphology.<sup>24</sup> The same protein solution, on the same multiplexed chip, displayed nonlinear behavior on closely packed dsDNA films. More quantitative approaches for determining the rate of electron transfer, such as the Laviron analysis, were not possible due to the degree of heterogeneity of the observed electrochemical signals. However, the total signal accumulation for the reduction of EndoIII as a function of time on both these dsDNA film morphologies displayed the same trend; loosely versus closely packed dsDNA films accumulated signal linearly and nonlinearly respectively, over time (Figure A1.8). This further supports the finding that only the signal observed on the loosely packed dsDNA films is limited by diffusion.

### **Multiplexed characterization of DNA CT proficiency**

Since the electrochemical signal for the [4Fe-4S] cluster of EndoIII is generated primarily via DNA CT on closely packed dsDNA films, the DNA CT proficiency of a known disease-related mutant, Y82A, was compared to that of wild type EndoIII using this morphology. The Y82A mutant of EndoIII has previously been shown to be DNA CT deficient compared to wild type EndoIII using individual DNA-modified electrodes.<sup>21,22</sup> The DNA CT deficiency has been attributed to disruptions in the electron transport pathway from the DNA  $\pi$ -stack to the [4Fe-4S] cluster due to mutation of the aromatic tyrosine residue, located in close proximity to the  $\pi$ -stack based on the crystal structure of the wild type protein bound to DNA.<sup>36</sup> The quantification of the extent of DNA CT proficiency for [4Fe-4S] cluster proteins has proven to be challenging due to the variability between individual DNA-modified electrodes.

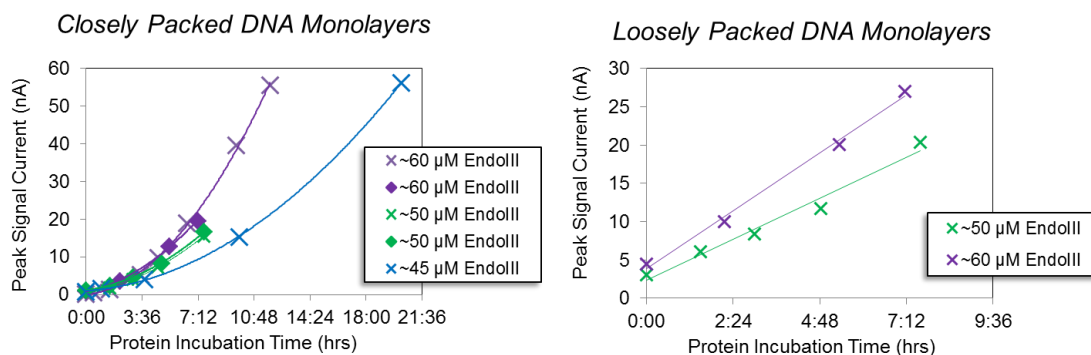


**Figure A1.8** Signal accumulation of EndoIII as a function of time at various concentrations on both closely and loosely packed dsDNA monolayers formed in the presence and absence of 100 mM MgCl<sub>2</sub> during assembly, respectively. The peak signal current was quantified based on the reductive signal of EndoIII in the cyclic voltammogram (scan rate = 100 mV/s) acquired in phosphate buffer (20 mM sodium phosphate, 100 mM NaCl, 0.5 mM EDTA, 20 % glycerol, pH 7.4).

Multiplexed characterization of the wild type (WT) and Y82A mutant EndoIII allows for a more quantitative comparison of the extent of coupling with the DNA-modified electrode. Multiplexed chips were assembled with half well-matched and half TC-mismatched closely packed dsDNA films. Orthogonally, WT and Y82A EndoIII were added to two quadrants each, such that each protein was incubated on both well matched and TC-mismatch DNA-modified electrodes (Figure A1.9). Samples of equal protein concentration were prepared based on the absorption at 410 nm, reflecting the [4Fe-4S] cluster concentration for each protein ( $\sim 70 \mu\text{M}$ ). Using this multiplexed configuration, the reduction of the [4Fe-4S] cluster in both WT and Y82A mutant EndoIII, was confirmed to have been generated via DNA CT, since both proteins displayed signal attenuation ( $23 \pm 3 \%$ ) upon introducing a TC mismatch. Furthermore, the signal from Y82A was  $72 \pm 5 \%$  attenuated compared to that of wild type EndoIII. Taken together with the attenuation upon mismatch incorporation, the observation of decreased DNA-mediated signal intensity verifies that the Y82A mutation results in a deficiency in DNA CT. Circular dichroism (CD) thermal denaturation confirmed that the stability of the protein fold was relatively unaltered upon introducing the Y82A mutation (Figure A1.9). Upon fitting the thermal denaturation curves to a 2-state unfolding model,<sup>32</sup> melting temperatures for Y82A and WT EndoIII were found to be  $49.2 \pm 0.3 \text{ }^\circ\text{C}$  and  $48.5 \pm 0.3 \text{ }^\circ\text{C}$ , respectively.

### **Direct comparison of electrostatic EndoIII mutants**

Finally, the multiplexed DNA-modified electrodes were harnessed for the characterization of a new family of EndoIII mutants relative to wild type protein. In

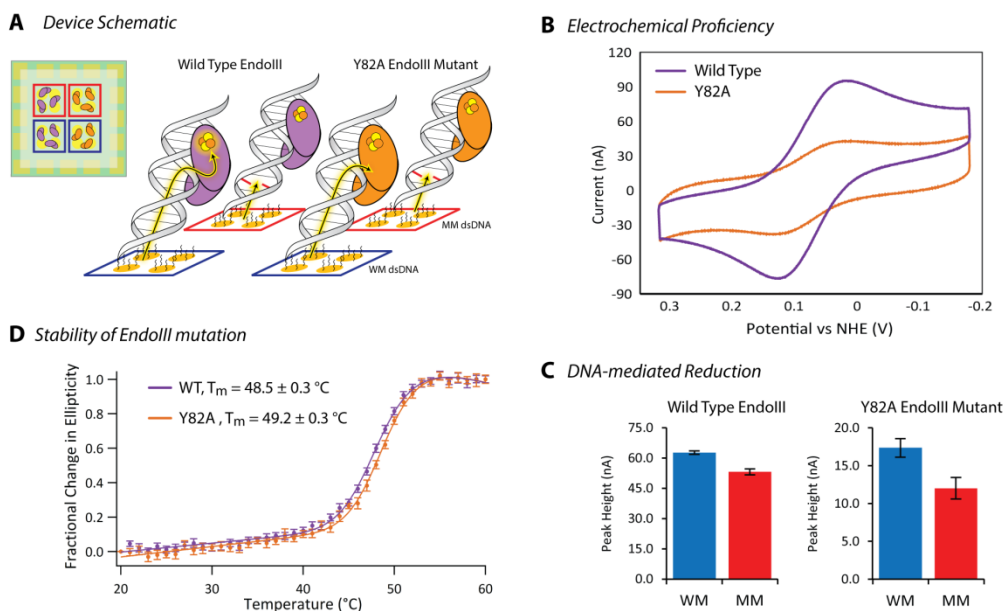


**Figure A1.9** Comparison of the electrochemical properties and stability of wild type EndoIII and a Y82A mutant. (A) Multiplexed electrode assembly schematic where electrodes are assembled with 100 mM  $\text{MgCl}_2$ , with either well-matched (blue) or TC mismatched (red) duplex DNA, and then incubated with either wild type (purple) or Y82A (orange) EndoIII (90  $\mu\text{M}$ , based on absorbance at 410 nm). (B) Cyclic voltammetry (scan rate = 100 mV/s) in phosphate buffer (20 mM sodium phosphate, 100 mM NaCl, 0.5 mM EDTA, 20 % glycerol, pH 7.4) are indicated for both wild type and Y82A EndoIII on closely packed, well-matched DNA monolayers. (C) The reductive signal upon introducing a TC mismatch (red) compared to well-matched (blue) validates the mechanism of reduction to be DNA-mediated for both proteins. (D) Circular dichroism thermal denaturation (5  $\mu\text{M}$  protein) validates that the Y82A mutation does not significantly alter the stability of the protein.

designing this new family of EndoIII mutants, only residues that were unlikely to cause significant changes in the DNA-binding affinity of EndoIII were chosen.<sup>37</sup> The glycosylase activity of these mutants was verified to be equal to that of wild type protein (Figure A1.2), so that the observed electrochemical differences cannot be attributed to deficiencies in DNA binding. The Y205H, K208E, and E200K EndoIII mutations investigated were originally designed to explore a possible shift in the mid-point potential of the [4Fe-4S] cluster, since these mutations alter the electrostatics surrounding the cluster. However, as can be seen in Figure A1.10, when compared in parallel on a single multiplexed chip on a closely packed dsDNA film, the mid-point potential of all the mutants are not found to be statistically different,  $\pm 10$  mV of the WT protein (Figure A1.10). Likely, the electrostatic effects of the DNA polyanion along with the associated counter ions mitigate any effects of local electrostatic changes of nearby peptides.

Interestingly, despite the lack of difference in mid-point potential, large differences in signal intensity between the mutants relative to WT were observed when the electrochemistry of the proteins was assayed at equivalent concentrations based on the absorbance of the [4Fe-4S] cluster at 410 nm, which are statistically significant with 95% confidence based on a two-tailed t-test. E200K yields a reductive current of  $14.8 \pm 0.3$  nA in the cyclic voltammogram, and is seen to be CT-deficient relative to WT EndoIII which displays a current intensity of  $24.4 \pm 0.8$  nA. In contrast, K208E and Y205H exhibit significantly larger signals,  $56.5 \pm 2$  nA and  $118 \pm 6$  nA, respectively, relative to the WT protein.

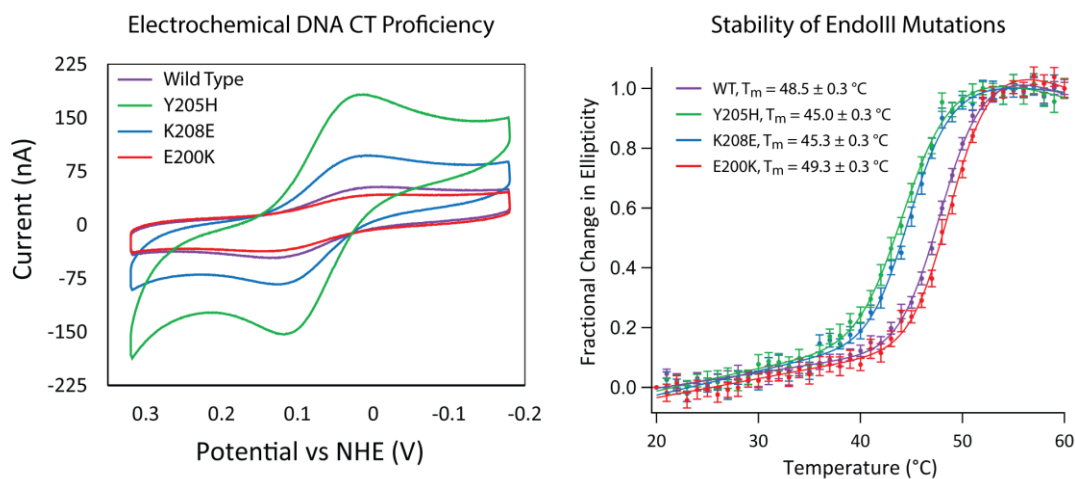


**Figure A1.10** Electrochemical and stability comparison of a new family of electrostatic EndoIII mutations, Y205H (green), K208E (blue), and E200K (red), with wild type EndoIII (purple). (*Left*) Cyclic voltammetry (scan rate = 100 mV/s) in phosphate buffer (20 mM sodium phosphate, 100 mM NaCl, 0.5 mM EDTA, 20 % glycerol, pH 7.4) is displayed for all four proteins on closely packed, (assembled with 100 mM Mg Cl<sub>2</sub>) well-matched DNA monolayers. Protein samples had equivalent concentrations of [4Fe-4S] (70  $\mu$ M based on the 410 nm absorbance). (*Right*) Circular dichroism thermal denaturation (5  $\mu$ M protein) was performed to correlate the altered electronic coupling of these mutations in close proximity of the [4Fe-4S] cluster with the differential stability of the proteins.

To explore these significant differences, CD thermal denaturation experiments were performed. The melting temperature for the Y205H, K208E, and E200K EndoIII as well as wild type protein (5  $\mu$ M) are  $45.0 \pm 0.3$  °C,  $45.3 \pm 0.3$ °C,  $49.3 \pm 0.3$  °C, and  $48.5 \pm 0.3$ °C respectively (Figure A1.10). The denaturation temperature of these EndoIII mutants correlates with the electrochemical signal size. Those that show a thermal stability that is reduced relative to the wild type protein show a significantly higher signal size electrochemically. Conversely, E200K is slightly stabilized relative to the wild type protein, and displays an attenuated electrochemical signal. For all proteins, the signal initially grows with time and subsequently diminishes over extended incubation times. This signal decrease with time correlates with the thermal stability of the proteins; those proteins that are thermal destabilized diminish faster, while the signal persists for more stable proteins (Figure A1.11). Notably, the Y205H mutation, which is involved in hydrogen bonding to the [4Fe-4S] cluster, is found to be the most proficient in DNA CT, with a 5-fold larger signal than wild type, and the least stable mutant by both electrochemical measurements and CD thermal denaturation.

## **Discussion**

### **Multiplexed electrochemical analysis of EndoIII**

In this study, the redox activity of the [4Fe-4S] cluster of EndoIII upon DNA binding was investigated using multiplexed DNA-modified electrodes. The utility of multiplexed analysis has previously been illustrated in using DNA-modified electrodes for the detection of biomarkers<sup>3-11</sup> as well as in performing sensitive measurements of DNA CT on long DNA duplexes.<sup>14</sup> As there is growing interest in understanding of the

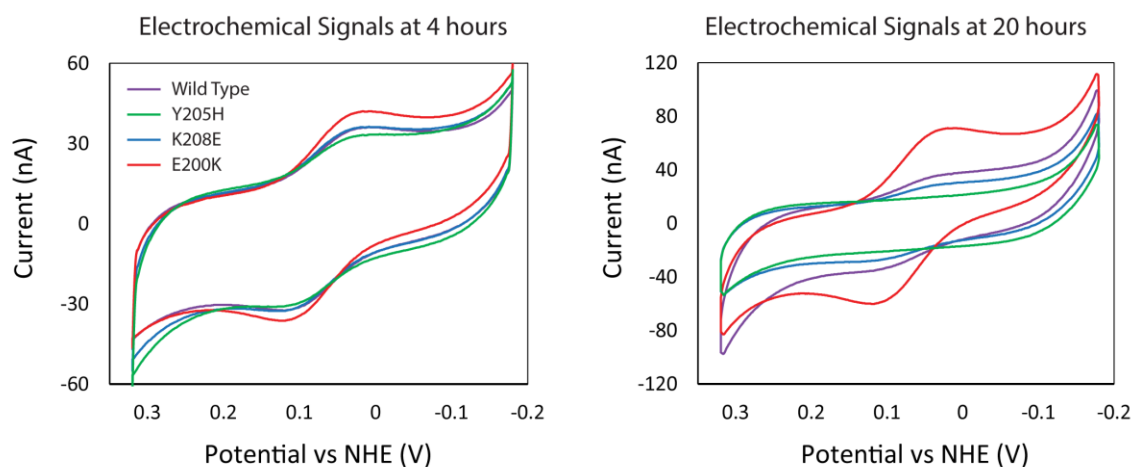


**Figure A1.11** Electrochemical stability of EndoIII mutants. (*Left*) Protein concentrations were normalized for electrochemistry coupling to yield approximately equivalent signal sizes at early time points (~ 4 hours). Cyclic voltammetry (scan rate =100 mV/s) acquired in phosphate buffer (20 mM sodium phosphate, 100 mM NaCl, 0.5 mM EDTA, 20 % glycerol, pH 7.4) for wild type (purple), Y205H (green), K208E (blue), and E200K (red) EndoIII are presented. (*Right*) After extended incubation (~20 hours) on the multiplexed chip, the electrochemical signal from the electrostatic EndoIII mutants and wild type protein diminished based on their CVs. The degree of signal loss directly correlates with the stability and DNA CT proficiency of the proteins, with the remaining signal size decreasing in the following order: E200K (red), wild type (purple), K208E (blue), and finally Y205H (green), which had no discernible signal remaining.

redox properties of proteins containing [4Fe-4S] clusters that are involved in genome maintenance, the extension of multiplexed analysis has become essential to investigate these complex proteins and their subtle differences in redox behavior.

The electrochemical signal of EndoIII obtained using multiplexed DNA-modified electrodes was shown to be comparable to that seen using individual DNA-modified electrodes.<sup>20-22</sup> Differences in peak potential and signal size are difficult to compare on individual electrodes given the variability in DNA-modified surfaces among experiments. The complexity of protein samples further amplifies this variability. Multiplexing removes the variability associated with protein preparation and surface modification. Specifically, multiplexing allows, with confidence, for a given protein to be examined in parallel across different DNA substrates or for many proteins to be compared on a given DNA-substrate. Thus, by harnessing this ability to probe in parallel for subtle differences in the electrochemical signal of EndoIII, effects of DNA substrate and morphology can be elucidated.

### **Mechanistic insights into EndoIII electrochemistry.**

Multiplexed analysis of the  $3^{+}/2^{+}$  redox couple of EndoIII on differing DNA morphologies show subtle differences in the DNA-bound electrochemical signals. These differences in electrochemistry result from differences in electron transfer pathways between the electrode and DNA-bound EndoIII that vary as a function of DNA film morphology. DNA-modified electrodes with single-stranded DNA, firstly, are found to function as an ideal control. Since EndoIII does not bind single-stranded DNA with high affinity, the single-stranded DNA does not serve as a means to increase the local

concentration of EndoIII at the electrode surface. Moreover it appears that the negatively charged signal-stranded DNA serves as an effective passivation layer, preventing protein denaturation on the gold surface, a common occurrence for protein electrochemistry.<sup>38</sup> Instead EndoIII appears to be electrochemically silent on these electrodes modified with single stranded DNA.

Secondly, the duplex DNA film morphology, established during electrode assembly, is demonstrated to be critical in dictating the predominant electron transfer pathway between the electrode surface and the [4Fe-4S] cluster of DNA-bound EndoIII. Differing electron transfer pathways to a single DNA-bound redox active moiety were previously characterized using DNA-modified electrodes with covalent redox active reporters.<sup>14,35</sup> In the case of a DNA-bound redox-active reporter, such as DNA-tethered methylene blue, it has been shown that the accessibility of the redox-active moiety to the electrode surface determines whether the predominant reduction mechanism is DNA CT or direct reduction by the surface of the electrode.<sup>35</sup> In the case of the DNA-mediated reduction, we have established that the rate limiting step for the DNA-mediated reduction of distally bound redox active species is not DNA CT itself, but tunneling through the alkane thiol linkage to the electrode.<sup>39</sup> The lateral charge diffusion through these DNA-modified films has also been established to be quite slow, negating the possibility of cross-talk throughout these films.<sup>40</sup> The redox activity of EndoIII on DNA-modified electrodes assembled with closely packed DNA monolayers, with limited surface accessibility, display all the previously established hallmarks of a DNA-mediated reduction pathway, including increased peak splitting, signal broadening, sensitivity to perturbations, and non-diffusion rate limited kinetics. Conversely, the DNA-bound electrochemical signal from

EndoIII on loosely packed DNA films, which have enhanced surface accessibility, display the opposite electrochemical behaviors that are characteristic of an electron transfer pathway that is not DNA-mediated. As both these signals involve reduction of *DNA-bound* EndoIII, the signals display only subtle differences. Only by using multiplexed analysis to investigate the electrochemistry of a single protein solution in parallel across differing DNA-modified electrodes are these two different electron transfer pathways cleanly distinguishable.

### **Electron transfer in EndoIII Mutants**

Multiplexed analysis was demonstrated to be useful not only in the characterization of different electron transfer pathways from the electrode surface to the DNA-bound EndoIII, but also in comparing directly the electron transfer efficiencies of different EndoIII mutants. As proof-of-principle, the DNA CT proficiency of a known disease-related EndoIII mutant, Y82A, was electrochemically compared to wild type EndoIII. It has previously been established that introducing the Y82A mutation into EndoIII yields a functionally active protein that is DNA CT-deficient.<sup>21</sup> Due to the proximity of this aromatic tyrosine residue to the DNA  $\pi$ -stack, the deficiencies in the electrochemical signal have been attributed to disrupting the electron transfer pathway between the DNA and [4Fe-4S] cluster.<sup>21</sup> Our multiplexed experiment allowed for the validation of this result along with a more quantitative assessment of CT deficiency.

The mechanism of reduction for both wild type and Y82A EndoIII was shown to be DNA-mediated on the closely packed DNA films, since both proteins display the

characteristic sensitivity to single base pair perturbations. The inherent DNA CT-deficiency of Y82A was characterized in parallel so that the difference in electrochemical efficiency of Y82A bound to DNA compared to wild type can be conclusively attributed to decreased DNA CT proficiency. The degree of DNA CT deficiency quantified for this mutant was found to be twice as pronounced compared to previous measurements, given the overall decreased variability of the DNA-modified electrodes and, importantly, the decreased contributions from surface reduction of the [4Fe-4S] cluster due to the optimized DNA morphology.

Moreover, this multiplexed technology is sufficiently reliable to permit characterization of the effects on the electron transfer pathway of a new family of EndoIII mutations. This family was found to show significant differences in DNA CT efficiency, while displaying very similar DNA-bound reduction potentials for the  $3^+/2^+$  redox couple of the [4Fe-4S]. Key to conclusively attributing differences, or lack thereof, observed in the mutant electrochemistry to changes in the electron transfer pathway through EndoIII was the ability to perform this comparison on identical gold surfaces, allowing for the geometry of electron transfer between the electrode and EndoIII to be held constant.

Previous work by Burgess and co-workers that focused on changing the electrostatics in *Azotobacter vinelandii* ferredoxin I resulted in large potential shifts; a single phenylalanine to histidine mutation caused a shift of over 200 mV for the [4Fe-4S] cluster while leaving overall protein structure unaffected.<sup>41</sup> With the same aims, EndoIII mutations were prepared that invert the electrostatics of three residues within 4 Å of the [4Fe-4S] cluster that are oriented on the opposite face of the cluster relative to the DNA. Multiplexed analysis of these three different EndoIII mutants allowed for their

simultaneous comparison to wild type EndoIII. The lack of distinguishable differences of the DNA-bound midpoint potentials for these electrostatic EndoIII mutants likely reflects the overwhelming contribution of polyanionic DNA, as DNA binding has already negatively shifts the reduction potential of EndoIII by approximately 200 mV.<sup>25</sup> The strict consistency of the measured DNA-bound midpoint potentials likely further derives from the screening effect of counter-ions associated with the DNA, as well as from the broad, heterogeneous nature of the observed DNA-mediated signals.

As mentioned above, we have proposed a model where DNA repair proteins containing [4Fe-4S] clusters utilize DNA CT as a first step to localize to the vicinity of DNA damage.<sup>21</sup> All of the proteins that we have investigated thus far have similar DNA-bound reduction potentials of approximately 80 mV vs. NHE.<sup>20</sup> These results suggest that DNA-binding could be a mechanism that standardizes the reduction potentials of iron-sulfur cluster-containing DNA repair proteins once bound to DNA, allowing for efficient DNA-mediated electron self-exchange between repair proteins.

Unlike the Y82A mutation, these mutations were specifically designed to affect residues in close proximity to the [4Fe-4S] cluster but presumably without affecting the pathway for DNA-mediated electron transfer (Figure A1.12). Nonetheless, as seen in Figure A.10, these changes unambiguously result in significant changes in the DNA CT efficiency. Multiplexed electrochemical characterization in conjunction with thermal denaturation circular dichroism experiments indicates that the differences in DNA CT efficiencies of these mutants are most likely caused by changes in the stability and solvent accessibility of the [4Fe-4S] cluster. Those proteins with decreased thermal stability show increased DNA CT yield compared to WT. Structured water molecules

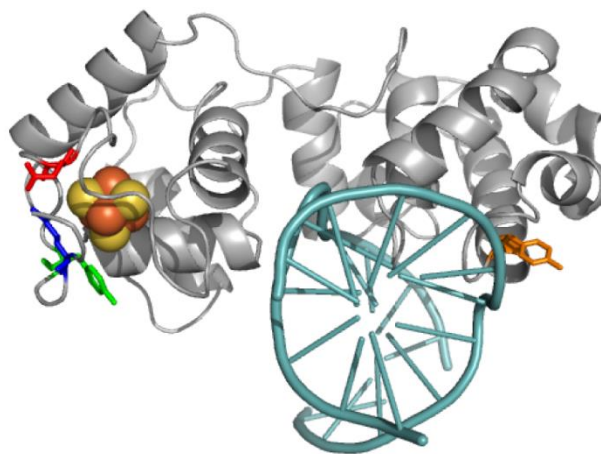


**Figure A1.12** Crystal structure of EndoIII with the location of mutations shown relative to the DNA (cyan) and [4Fe-4S] cluster: Y205 (green), K208 (blue), E200 (red), and Y82 (orange). PDB: 2ABK with DNA from 1ORN.

have been proposed to mediate efficient biological electron transfer in several intra- and intermolecular protein systems,<sup>42-46</sup> generally by forming robust hydrogen-bonding pathways that increase electronic coupling between the donor and acceptor.<sup>47</sup>

We hypothesize that the destabilization we observe in Y205H and K208E EndoIII may result in the formation of a water pocket in EndoIII that would facilitate ET, as we have suggested previously for other destabilizing EndoIII mutations.<sup>22</sup> In the case of E200K, which is slightly stabilized relative to wild type, substitution for a larger lysine residue along the face of the cluster may instead screen the cluster from solvent and contribute to the observed CT deficiency. While the Y82A mutant is marginally stabilized compared to WT EndoIII, it is more significantly defective in DNA CT proficiency compared to E200K. Therefore, the extent the DNA CT deficiency of Y82A cannot be fully attributed to the change in stability and is thought to originate from directly disrupting the electron transfer pathway. Overall, it appears that differences in DNA CT proficiency can be caused both by altering the electron transfer pathway by removing aromatics and also by more indirectly modulating the electronic coupling of the cluster by changing protein stability and presumably solvent accessibility.

## **Conclusion**

Multiplexed characterization of the DNA repair protein EndoIII bound to DNA provides new insights into the DNA-mediated reduction of this metalloprotein and the resolution of subtle electrochemical variations associated with DNA substrate and surface morphology. Multiplexed analysis leads to more reliable statistics as well as decreased surface variability and background contribution. The reduction of EndoIII is seen to be

DNA-dependent, yet once bound to duplex DNA, there are two different pathways through which the electron transfer proceeds. The predominant mechanism for the reduction of the [4Fe-4S] cluster of EndoIII is shown to correlate with the surface accessibility of the protein, resulting in DNA-mediated reduction being observed only with closely packed DNA films. In addition to the electron transfer pathway between the electrode surface and EndoIII being characterized, the use of multiplexed analysis also allowed for the direct comparison of electron transfer pathways through the protein itself. The electrochemistry and stability of various EndoIII mutants was characterized, including a new family of mutations introducing electrostatic changes in close proximity to the [4Fe-4S] cluster. The stability of a given mutation was shown to correlate with the electrochemical yield, leading to the hypothesis that mutations not directly on the electron transfer pathway through the protein can alter the rate of electron transfer by affecting the solvation surrounding the [4Fe-4S] cluster. Most interestingly, this side-by-side quantitative comparison of varying electrostatics in the protein fold provides a demonstration of the dominance that DNA-binding elicits on the reduction potential of DNA repair proteins.

These multiplexed chips provide the needed flexibility and robustness to characterize the redox activity of emerging [4Fe-4S]-containing proteins that bind DNA. Multiplexed analysis will be integral in relating the function and redox activity of these DNA-binding proteins in order to establish roles for these critical redox active co-factors *in vivo*.

## References

1. Zheng, G., Patolsky, F., Cui, Y., Wang, W. U. & Lieber, C. M. Multiplexed electrical detection of cancer markers with nanowire sensor arrays. *Nat. Biotechnol.* **23**, 1294–1301 (2005).
2. Morrow, T. J., Li, M., Kim, J., Mayer, T. S. & Keating, C. D. Programmed Assembly of DNA-Coated Nanowire Devices. *Science* **323**, 352–352 (2009).
3. Swensen, J. S. *et al.* Continuous, Real-Time Monitoring of Cocaine in Undiluted Blood Serum via a Microfluidic, Electrochemical Aptamer-Based Sensor. *J. Am. Chem. Soc.* **131**, 4262–4266 (2009).
4. Plaxco, K. W. & Soh, H. T. Switch-based biosensors: a new approach towards real-time, in vivo molecular detection. *Trends Biotechnol.* **29**, 1–5 (2011).
5. Bonham, A. J. *et al.* Quantification of Transcription Factor Binding in Cell Extracts Using an Electrochemical, Structure-Switching Biosensor. *J. Am. Chem. Soc.* **134**, 3346–3348 (2012).
6. White, R. J. *et al.* Wash-free, Electrochemical Platform for the Quantitative, Multiplexed Detection of Specific Antibodies. *Anal. Chem.* **84**, 1098–1103 (2012).
7. Hsieh, K., Patterson, A. S., Ferguson, B. S., Plaxco, K. W. & Soh, H. T. Rapid, Sensitive, and Quantitative Detection of Pathogenic DNA at the Point of Care through Microfluidic Electrochemical Quantitative Loop-Mediated Isothermal Amplification. *Angew. Chem. Int. Ed.* **51**, 4896–4900 (2012).
8. Fang, Z. *et al.* Direct Profiling of Cancer Biomarkers in Tumor Tissue Using a Multiplexed Nanostructured Microelectrode Integrated Circuit. *ACS Nano* **3**, 3207–3213 (2009).

9. Vasilyeva, E. *et al.* Direct Genetic Analysis of Ten Cancer Cells: Tuning Sensor Structure and Molecular Probe Design for Efficient mRNA Capture. *Angew. Chem. Int. Ed.* **50**, 4137–4141 (2011).
10. Lam, B., Fang, Z., Sargent, E. H. & Kelley, S. O. Polymerase Chain Reaction-Free, Sample-to-Answer Bacterial Detection in 30 Minutes with Integrated Cell Lysis. *Anal. Chem.* **84**, 21–25 (2012).
11. Das, J. *et al.* An ultrasensitive universal detector based on neutralizer displacement. *Nat. Chem.* **4**, 642–648 (2012).
12. Pheaney, C. G., Guerra, L. F. & Barton, J. K. DNA sensing by electrocatalysis with hemoglobin. *Proc. Natl. Acad. Sci.* **109**, 11528–11533 (2012).
13. Slinker, J. D., Muren, N. B., Gorodetsky, A. A. & Barton, J. K. Multiplexed DNA-Modified Electrodes. *J. Am. Chem. Soc.* **132**, 2769–2774 (2010).
14. Slinker, J. D., Muren, N. B., Renfrew, S. E. & Barton, J. K. DNA charge transport over 34 nm. *Nat. Chem.* **3**, 228–233 (2011).
15. Genereux, J. C. & Barton, J. K. Mechanisms for DNA Charge Transport. *Chem. Rev.* **110**, 1642–1662 (2010).
16. Murphy, C. J. *et al.* Long-range photoinduced electron transfer through a DNA helix. *Science* **262**, 1025–1029 (1993).
17. Wagenknecht, H.-A. in *Charge Transfer in DNA* (ed. Wagenknecht, P. H.-A.) 1–26 (Wiley-VCH Verlag GmbH & Co. KGaA, 2005).  
<<http://onlinelibrary.wiley.com/doi/10.1002/3527606629.ch1/summary>>

18. Boon, E. M., Ceres, D. M., Drummond, T. G., Hill, M. G. & Barton, J. K. Mutation detection by electrocatalysis at DNA-modified electrodes. *Nat. Biotechnol.* **18**, 1096–1100 (2000).
19. Boal, A. K. & Barton, J. K. Electrochemical Detection of Lesions in DNA. *Bioconjug. Chem.* **16**, 312–321 (2005).
20. Boal, A. K. *et al.* DNA-Bound Redox Activity of DNA Repair Glycosylases Containing [4Fe-4S] Clusters<sup>†</sup>. *Biochemistry* **44**, 8397–8407 (2005).
21. Boal, A. K. *et al.* Redox signaling between DNA repair proteins for efficient lesion detection. *Proc. Natl. Acad. Sci.* **106**, 15237–15242 (2009).
22. Romano, C. A., Sontz, P. A. & Barton, J. K. Mutants of the Base Excision Repair Glycosylase, Endonuclease III: DNA Charge Transport as a First Step in Lesion Detection. *Biochemistry* **50**, 6133–6145 (2011).
23. Lee, P. E., Demple, B. & Barton, J. K. DNA-mediated redox signaling for transcriptional activation of SoxR. *Proc. Natl. Acad. Sci. U. S. A.* **106**, 13164–13168 (2009).
24. Mui, T. P., Fuss, J. O., Ishida, J. P., Tainer, J. A. & Barton, J. K. ATP-Stimulated, DNA-Mediated Redox Signaling by XPD, a DNA Repair and Transcription Helicase. *J. Am. Chem. Soc.* **133**, 16378–16381 (2011).
25. Gorodetsky, A. A., Boal, A. K. & Barton, J. K. Direct Electrochemistry of Endonuclease III in the Presence and Absence of DNA. *J. Am. Chem. Soc.* **128**, 12082–12083 (2006).

26. Wu, Y., Suhasini, A. N. & Jr, R. M. B. Welcome the Family of FANCI-like Helicases to the Block of Genome Stability Maintenance Proteins. *Cell. Mol. Life Sci.* **66**, 1209–1222 (2008).
27. Vaithiyalingam, S., Warren, E. M., Eichman, B. F. & Chazin, W. J. Insights into eukaryotic DNA priming from the structure and functional interactions of the 4Fe-4S cluster domain of human DNA primase. *Proc. Natl. Acad. Sci.* **107**, 13684–13689 (2010).
28. White, M. F. & Dillingham, M. S. Iron-sulphur clusters in nucleic acid processing enzymes. *Curr. Opin. Struct. Biol.* **22**, 94–100 (2012).
29. Wu, Y. & Brosh, R. M. DNA helicase and helicase–nuclease enzymes with a conserved iron–sulfur cluster. *Nucleic Acids Res.* **40**, 4247–4260 (2012).
30. Sontz, P. A., Mui, T. P., Fuss, J. O., Tainer, J. A. & Barton, J. K. DNA charge transport as a first step in coordinating the detection of lesions by repair proteins. *Proc. Natl. Acad. Sci.* **109**, 1856–1861 (2012).
31. Cunningham, R. P. *et al.* Endonuclease III is an iron-sulfur protein. *Biochemistry* **28**, 4450–4455 (1989).
32. Koepf, E. K., Petrassi, H. M., Sudol, M. & Kelly, J. W. WW: An isolated three-stranded antiparallel  $\beta$ -sheet domain that unfolds and refolds reversibly; evidence for a structured hydrophobic cluster in urea and GdnHCl and a disordered thermal unfolded state. *Protein Sci.* **8**, 841–853 (1999).
33. Lapierre, M. A., O’Keefe, M., Taft, B. J. & Kelley, S. O. Electrocatalytic Detection of Pathogenic DNA Sequences and Antibiotic Resistance Markers. *Anal. Chem.* **75**, 6327–6333 (2003).

34. Wiley: Electrochemical Methods: Fundamentals and Applications, 2nd Edition - Allen J. Bard, Larry R. Faulkner.  
<<http://www.wiley.com/WileyCDA/WileyTitle/productCd-0471043729.html>>
35. Pheaney, C. G. & Barton, J. K. DNA Electrochemistry with Tethered Methylene Blue. *Langmuir* **28**, 7063–7070 (2012).
36. Fromme, J. C. & Verdine, G. L. Structure of a trapped endonuclease III–DNA covalent intermediate. *EMBO J.* **22**, 3461–3471 (2003).
37. Thayer, M. M., Ahern, H., Xing, D., Cunningham, R. P. & Tainer, J. A. Novel DNA binding motifs in the DNA repair enzyme endonuclease III crystal structure. *EMBO J.* **14**, 4108–4120 (1995).
38. Zhang, J. *et al.* Interfacial electrochemical electron transfer in biology – Towards the level of the single molecule. *FEBS Lett.* **586**, 526–535 (2012).
39. Drummond, T. G., Hill, M. G. & Barton, J. K. Electron Transfer Rates in DNA Films as a Function of Tether Length. *J. Am. Chem. Soc.* **126**, 15010–15011 (2004).
40. Kelley, S. O., Jackson, N. M., Hill, M. G. & Barton, J. K. Long-Range Electron Transfer through DNA Films. *Angew. Chem. Int. Ed.* **38**, 941–945 (1999).
41. Chen, K. *et al.* Crystal structures of ferredoxin variants exhibiting large changes in [Fe|ndash]|S] reduction potential. *Nat. Struct. Mol. Biol.* **9**, 188–192 (2002).
42. Francisco, W. A., Wille, G., Smith, A. J., Merkler, D. J. & Klinman, J. P. Investigation of the Pathway for Inter-Copper Electron Transfer in Peptidylglycine  $\alpha$ -Amidating Monooxygenase. *J. Am. Chem. Soc.* **126**, 13168–13169 (2004).

43. Casimiro, D. R., Richards, J. H., Winkler, J. R. & Gray, H. B. Electron transfer in ruthenium-modified cytochromes c.  $\sigma$ -tunneling pathways through aromatic residues. *J. Phys. Chem.* **97**, 13073–13077 (1993).
44. Tezcan, F. A., Crane, B. R., Winkler, J. R. & Gray, H. B. Electron tunneling in protein crystals. *Proc. Natl. Acad. Sci.* **98**, 5002–5006 (2001).
45. Van Amsterdam, I. M. C. *et al.* Dramatic modulation of electron transfer in protein complexes by crosslinking. *Nat. Struct. Mol. Biol.* **9**, 48–52 (2002).
46. Miyashita, O., Okamura, M. Y. & Onuchic, J. N. Interprotein electron transfer from cytochrome c2 to photosynthetic reaction center: Tunneling across an aqueous interface. *Proc. Natl. Acad. Sci. U. S. A.* **102**, 3558–3563 (2005).
47. Lin, J., Balabin, I. A. & Beratan, D. N. The Nature of Aqueous Tunneling Pathways Between Electron-Transfer Proteins. *Science* **310**, 1311–1313 (2005).